Notice 1

Notice 2

ERRATA

p. vii line 3 from bottom: "to" for "too".

Throughout this thesis, when an equation is followed by the word "Where", this should be replaced by "where".

The use of the word "mechanic", particularly in chapter 4, should be replaced by "mechanism".

Throughout the thesis, the term "mode" is used when sometimes "vibrational transition" would be more appropriate.

p. v 3rd para line 2: "Strong coupling mechanics" is defined as a coupling mechanism where the affect on the spectra is highly significant.

p. 3 lines 5-7: "possible allowed modes" are usually referred too as the "normal modes of vibration".

p. 8 line 5: "the S-reduction" should read "the matrix elements of the S-reduction"

p. 8: The A-reduction is considered superior for very asymmetric molecules.

Pg.15, line 11: "net change in the electric polarization" should be replaced by "net change in the electric dipole moment".

Table 1.2. Higher order transitions can also occur but are less probable. Transitions with $\Delta J = \pm l$, $\Delta K_a = \pm m$ and $\Delta K_c = \pm n$ are also allowed to exhibit the selection rules of $\Delta J = \pm (l + 2)$, $\Delta K_a = \pm (m + 2)$ and $\Delta K_c = \pm (n + 2)$.

p. 19 last line: "transition" for "transitions".

p. 20 2nd last line: "differences in the transition dipole moments" for "differences in the dipole moments".

p. 32 line 1: "Third" for "3rd".

p. 33 line 9: "from that" for "to that".

p. 35 line 2: "unapodized" for "unapodised".

p. 39 line 5: "were on" for "were of".

p. 42 line 7: "following" for "proceeding".

p. 47 line 3: "within a given sub-band" for "in a given sub-band".

p. 51: It should be made clearer that the software minimizes the sum of the squares of the deviations between observed and simulated spectra.

Far-infrared ro-vibrational spectroscopy of Coriolis coupled molecules of interstellar importance.

Michael Kenneth Bane, BSc. (Hons.)

School of Chemistry, Monash University

Submitted August 24th 2012

Table of Contents

Abstract

One of the fundamental limiting factors in ro-vibrational spectroscopy has been the lack of high brilliance sources in the far-infrared region of the electromagnetic spectrum. Synchrotron sources are somewhat able to fill this gap, and spectroscopy of the usually weak lowest energy vibrational modes is becoming more accessible. A detailed knowledge of the molecular parameters of low energy vibrational modes is important for interstellar detection, since it is these modes that are most likely to be thermally populated in these systems.

The first chapter of this thesis outlines the fundamental theory associated with the high-resolution vibration-rotation spectroscopy of molecules. Firstly, a theory of the allowable energies of molecules is presented, with careful consideration of the quantum mechanical nature of the entity. Secondly, a theory of the interaction with light is discussed, which relates to the observable absorbance and selection rules. Finally, the theory of the Fourier transform is discussed in relation to the collection and attributes of the recorded spectra.

The second chapter discusses the instrumentation and analytical basics of the project. Detailed aspects of the synchrotron source and spectrometer are first outlined and give insight into the experimental work done during this project. For context, a discussion of complementary high-resolution techniques is included regarding the recording of both pure rotational and ro-vibrational spectra. The majority of this project involved detailed

spectral analysis, and thus an explanation of the most useful tools and techniques is included. Finally a section justifying the selection of ketenimine, 1-phosphapropyne, thiirane and chlorodifluoromethane as target molecules is included. This also serves as a summary of the work done on each molecule, and elaborates slightly on what is presented in the publications.

Chapter 3 contains the work published during this project. This work mainly relates to the analysis of high-resolution far-infrared spectra of molecules which are either predicted to be, or have been detected as, a part of the interstellar medium. Chapter 4 discusses the implications of this research, and suggests possible future extension.

A major theme of this project is the de-perturbation of modes which exhibit strong coupling mechanics, highlighted by the characterization of an intensity stealing mechanism which allows effectively infrared inactive modes to be enhanced and become observable. This effect was found, by chance, to be crucial in explaining the spectra of two of the three molecules studied in this thesis. This leads to the tantalizing prospect that perhaps this mechanism may be important in the study of the ro-vibrational spectra of other molecules.

PART A: General Declaration

Monash University
Monash Research Graduate School

Declaration for thesis based or partially based on conjointly published or unpublished work

General Declaration

In accordance with Monash University Doctorate Regulation 17/ Doctor of Philosophy and Master of Philosophy (MPhil) regulations the following declarations are made:

I hereby declare that this thesis contains no material which has been accepted for the award of any other degree or diploma at any university or equivalent institution and that, to the best of my knowledge and belief, this thesis contains no material previously published or written by another person, except where due reference is made in the text of the thesis.

This thesis includes 5 original papers published in peer reviewed journals and 1 unpublished publications. The core theme of the thesis is ro-vibrational spectroscopy. The ideas, development and writing up of all the papers in the thesis were the principal responsibility of myself, the candidate, working within the school of chemistry under the supervision of Prof. Don McNaughton and Dr Christopher Thompson.

The inclusion of co-authors reflects the fact that the work came from active collaboration between researchers and acknowledges input into team-based research.

In the case of chapter 3 my contribution to the work involved the following:

Thesis chapter	Publication title	Publication status	Nature and extent of candidate's contribution
3.1	High-resolution FTIR spectroscopy of the v_8 and Coriolis perturbation allowed v_{12} bands of ketenimine	Published	Initiation, key ideas, development, writing up (80%)
3.2	High-resolution Fourier-transform infrared spectroscopy of the Coriolis coupled ground state and v_7 mode of ketenimine	Published	Initiation, key ideas, development, writing up (80%)
3.3	High-resolution Fourier-transform infrared spectroscopy of the v_6 and Coriolis perturbation allowed v_{10} modes of ketenimine	Published	Initiation, key ideas, development, writing up (80%)
3.4	High-resolution FTIR spectroscopy of the v_7 and v_8 bands of 1-phosphapropyne	Published	Initiation, key ideas, development, writing up (80%)
3.5	Synchrotron far infrared spectroscopy of the ground, v_5 and v_{15} states of Thiirane	Accepted	Initiation, key ideas, development, writing up (80%)
3.6	Overview of High-Resolution Infrared Measurement and Analysis for Atmospheric Monitoring of Halocarbons	Published	Key ideas, development (15%)

I have not renumbered sections of submitted or published papers.

Signed: ....

Date: ....

Acknowledgements

First and foremost I would like to thank my two supervisors, Don and Chris. Without Don's unwavering persistence that I go the extra mile (for example finding those damn ^{34}S transitions!) and my uplifting consultations with Chris, particularly during the tough ketenimine years, the project would not be half what it is.

I would also like to thank Evan for your willingness to help me sort out the toughest of perturbations. And to Dom, thanks for teaching me about the experimentation (and turning up at all hours when I screwed them up) and for supporting me on multiple occasions in obtaining funding and grants.

Thanks to the Biospec group, Danielle, Ruth and particularly my office mates Mot, Chris, Andy and David. I couldn't imagine a better group of guys to spend every day with and I wish you all the best in your future careers. To all my mates outside of uni, thanks for a lot of great times. No matter how stressed I got at uni, it was nice to know that come friday night there was always a good time just around the corner.

To my Mum and Dad and extended family, I thank you for instilling in me that I can achieve in life whatever I set my mind too, which is a true gift that I am thankful for every day. Also thanks for not killing me during my teenage years, which obviously would have been detrimental to me achieving this PhD. To Lachlan, thanks for just being

a great bro and my best mate. To Michael, Debbie and Brad thanks for the hot Tuesday night dinners, which were quite often a sight for sore eyes and gave me the energy to keep going for another week!

Finally to the one who has sacrificed the most for me over the last 3.5 years, Nicole. Thanks for living a no frills life in a crappy 1 bedroom flat so that I could achieve my dreams, thanks for making me happy every day within 5 minutes of getting home, and thanks for never doubting I was doing the right thing. Couldn't have done it without you.

"Everything should be made as simple as possible, but not simpler."

- Albert Einstein

Chapter 1

Fundamental Theory

1.1 Molecular Energy

1.1.1 Separation of vibration and rotation

The Born-Oppenheimer approximation[1] is essentially the assumption that molecular rotations, vibrations and the dynamics of electrons can be treated separately, and their influence on each other is negligible. Under this approximation, the total wave function, Ψ, can be presented in terms of independent factors and the molecular Hamiltonian, $\hat{H}$, can be broken into parts which only act on a single factor:

$$\Psi = \phi_{elec}\phi_{vib}\phi_{rot}$$

$$\hat{H}\Psi = (\hat{H}_{elec} + \hat{H}_{vib} + \hat{H}_{rot})\phi_{elec}\phi_{vib}\phi_{rot}$$
$$= (E_{elec} + E_{vib} + E_{rot})\phi_{elec}\phi_{vib}\phi_{rot}$$

Ro-vibrational spectroscopy is concerned only with the vibrational and rotational energies of molecules, and thus the electronic wave-function is not required.

1.1.2 Vibration

The oscillations of the atomic nuclei (molecular vibrations) are governed by the Schrödinger equation in a harmonic potential. A more complex Morse potential[2] can be employed for higher accuracy however for small oscillations the harmonic approximation

is adequate. This is a well studied system (see for example Sakurai[3] of Messiah[4]) which gives the following result:

$$\hat{H}_{vib}\left|n\right\rangle = \hbar\omega(n + \tfrac{1}{2})\left|n\right\rangle \equiv v_0\left|n\right\rangle$$

where $\hbar$ is the reduced Plank's constant, ω is the angular frequency of vibration and $\left|n\right\rangle$ is an eigenstate of the vibrational Hamiltonian. A molecule will in general have $3N - 5$, where N is the number of atoms, solutions to the Schrodinger equation corresponding to the possible allowed vibrational modes ($3N - 6$ for linear molecules). Each of these modes can be exited to states of different n quantum number, which allows for the observation of "overtones" and "hot-bands" (see figure 1.1).
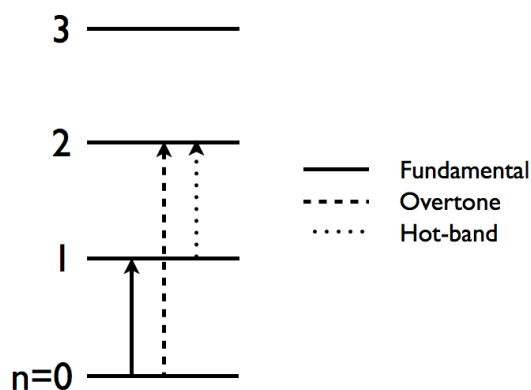
Figure 1.1: Illustration of fundamental, overtone and hot-band transition.

The types of transitions which are studied in this project are ro-vibrational in nature and each vibrational transition is accompanied by a lower energy rotational transition. The

main contribution of the vibrational energy is to simply add a constant energy, v_0, to the much richer rotational structure. If we make the assumption vibration is completely independent of rotation (which can be a poor one), this is the only contribution from vibration we need to consider during an analysis. Although ro-vibrational spectroscopy can determine very accurate values for v_0, most of the important information which can be obtained by this technique relates to the rotational characteristics of the molecule in question.

1.1.3 Rotation

The Hamiltonian of the rigid rotor is derived by canonical quantization of the classical expression for the energy of a rotating body. This derivation of the dominant terms in the molecular Hamiltonian is based heavily on that presented in Allen & Cross[5]:

$$\hat{H}_{rot} = \frac{\hat{J}^2}{2I} = \frac{\hat{J}_x^2}{2I_x} + \frac{\hat{J}_y^2}{2I_y} + \frac{\hat{J}_z^2}{2I_z}$$

where $\hat{J}$ is the total angular momentum operator, $\hat{J}_i$ is the component of angular momentum in the spatial direction i and I is the rotational moment of inertia. The non-zero matrix elements of the $\hat{J}$ and $\hat{J}_z$ operators are determined as (see Refs [3,4]):

$$\langle J, K | \hat{J} | J, K \rangle = \sqrt{J(J+1)}\hbar$$
$$\langle J, K | \hat{J}_z | J, K \rangle = \hbar K$$

Where *J* and *K* are the quantum numbers associated with the total and *z*-component of angular momentum respectively. These elements easily allows for actions of the $\hat{J}^2$ and $\hat{J}_z^2$ operator to be determined (see below). The matrix elements relating to $\hat{J}_x^2$ and $\hat{J}_y^2$ are more complex to derive since the components of angular momentum do not commute and cannot be simultaneously determined:

$$[\hat{J}_x, \hat{J}_y] = i\hbar\hat{J}_z \neq 0$$

where $[A, B] \equiv AB - BA$. $\hat{J}_x$ and $\hat{J}_y$ can be evaluated by studying the action of a complex superposition of the two operators on the wavefunctions. The following observation is useful:

$$\hat{J}_z(\hat{J}_y \pm i\hat{J}_x)|J, K\rangle = (\hat{J}_y \pm i\hat{J}_x)(\hat{J}_z \pm \hbar)|J, K\rangle$$
$$= \hbar(K \pm 1)(\hat{J}_y \pm i\hat{J}_x)|J, K\rangle$$

The action of the $\hat{J}_z(\hat{J}_y \pm i\hat{J}_x)$ operator is identical to that of the $\hat{J}_z$ operator on a wave-function with *K* = *K* ±1, and thus the action of the complex superposition of $\hat{J}_x$ and $\hat{J}_y$ can be redefined as:

$$(\hat{J}_y \pm i\hat{J}_x)|J, K\rangle \equiv \hat{J}_\pm|J, K\rangle = n_\pm|J, K \pm 1\rangle$$

Where $n_\pm$ is a normalizing constant with value $\hbar[(J \mp K)(J \pm K + 1)]^{\frac{1}{2}}$. $\hat{J}_y$ is the real part,

$\Re$, of the $\hat{J}_+$ operator:

$$\Re(\hat{J}_y + i\hat{J}_x) = \tfrac{1}{2}(\hat{J}_y + i\hat{J}_x) + \tfrac{1}{2}(\hat{J}_y + i\hat{J}_x)^* = \tfrac{1}{2}(\hat{J}_y + i\hat{J}_x) + \tfrac{1}{2}(\hat{J}_y - i\hat{J}_x)$$

Thus the non zero matrix elements of $\hat{J}_y$ are determined as;

$$\langle J, K \pm 1 | \hat{J}_y | J, K \rangle = \tfrac{1}{2}\langle J, K \pm 1 | \hat{J}_+ | J, K \rangle + \tfrac{1}{2}\langle J, K \pm 1 | \hat{J}_- | J, K \rangle$$
$$= {n_\pm}\big/{2}$$

Similar logic allows for the calculation of the matrix elements of $\hat{J}_x$

$$\langle J, K \pm 1 | \hat{J}_x | J, K \rangle = \mp {in_\pm}\big/{2}$$

The rotational Hamiltonian contains squared operators, which act twice on the state vectors. It is readily obtainable using logic already presented that the matrix elements of the squared operators are;

$$\langle J,K|\hat{J}_z^2|J,K\rangle = \hbar^2 K^2$$

$$\langle J,K|\hat{J}_y^2|J,K\rangle = \langle J,K|\hat{J}_x^2|J,K\rangle = \tfrac{1}{2}\langle J,K|(\hat{J}^2 - \hat{J}_z^2)|J,K\rangle$$
$$= \tfrac{\hbar^2}{2}[J(J+1) - K^2]$$

$$\langle J,K\pm 2|\hat{J}_y^2|J,K\rangle = -\langle J,K\pm 2|\hat{J}_x^2|J,K\rangle$$
$$= \tfrac{\hbar^2}{4}[(J \mp K)(J \pm K + 1)(J \mp K - 1)(J \pm K + 2)]^{\frac{1}{2}}$$

The total matrix elements of the Hamiltonian, $\hat{H}_{rot}$, can now be evaluated:

$$\langle J,K|\hat{H}_{rot}|J,K\rangle = \tfrac{1}{2}(B + C)[J(J+1) - K^2] + AK^2$$

$$\langle J,K+2|\hat{H}_{rot}|J,K\rangle = -\langle J,K|\hat{H}_{rot}|J,K+2\rangle$$
$$= \tfrac{1}{4}(C - B)[(J - K)(J - K - 1)(J + K + 1)(J + K + 2)]^{\frac{1}{2}}$$

where $A = \tfrac{\hbar^2}{2I_z}$, $B = \tfrac{\hbar^2}{2I_x}$ and $C = \tfrac{\hbar^2}{2I_y}$ (I^r representation). A, B and C are known

as the rotational constants and are identified with the spatial dimensions x, y and z such

the $A > B > C$, with the common labeling scheme of various identifications shown in

table 1.1.

Table 1.1: Identification of x, y and z spatial dimensions with A, B and C

	I^r	II^r	III^r	I^l	II^l	III^l
x	B	C	A	C	A	B
y	C	A	B	B	C	A
z	A	B	C	A	B	C

When analyzing high-resolution spectra obtained through experiment, the rigid rotor approximation is not sufficient. Adjustments to the rotational Hamiltonian must be made to account for the centrifugal distortion of the rotating molecule, which will in general be J and K dependant. The derivation of these terms will not be presented here, however the S-reduction of the Hamiltonian derived by Watson[6] which includes centrifugal distortion terms is shown below to order 6:

$$\langle n, J, K | \hat{H} | n, J, K \rangle = v_0 + \frac{1}{2}(B + C)[J(J+1) - K^2] + AK^2 - D_J[J(J+1)]^2 - D_{JK}[J(J+1)]K^2$$
$$- D_K K^4 + H_{JJJ}[J(J+1)]^3 + H_{JJK}[J(J+1)]^2 K^2 + H_{JKK}[J(J+1)]K^4 + H_{KKK}K^6 + ...$$
$$\langle n, J, K+2 | \hat{H} | n, J, K \rangle = -\langle J, K | \hat{H} | J, K+2 \rangle$$
$$= \frac{1}{4}(C - B) + d_1[J(J+1)] + h_1[J(J+1)]^2$$
$$\langle n, J, K+4 | \hat{H} | n, J, K \rangle = -\langle J, K | \hat{H} | J, K+4 \rangle$$
$$= d_2 + h_2[J(J+1)]$$
$$\langle n, J, K+6 | \hat{H} | n, J, K \rangle = -\langle J, K | \hat{H} | J, K+6 \rangle$$
$$= h_3$$

Where the factors of $n_\pm$ and $\hbar$ are absorbed into the distortion parameters. Note that the vibrational contribution to the molecular energy, v_0, is included. This reduction is generally considered superior to the A-reduced Hamiltonian also derived by Watson, and

was used throughout this project. The time-independent Schrödinger equation determines the energies of the ro-vibrational states according to:

$$\hat{H}|n,J,K\rangle = E_{n,J,K}|n,J,K\rangle$$

This Hamiltonian is diagonalised numerically, which yields the energy eigenvalues of the states $|n,J,K\rangle$ as the diagonal elements. This process can be greatly simplified for the case of symmetric molecules, where $B - C = 0$. If we ignore off diagonal distortion terms, the matrix can be re-written explicitly as an equation:

$$\begin{aligned}
E = \nu_0 &+ BJ(J+1) + (A-B)K^2 - D_J[J(J+1)]^2 - D_{JK}[J(J+1)]K^2 \\
&- D_K K^4 + H_{JJJ}[J(J+1)]^3 + H_{JJK}[J(J+1)]^2 K^2 \\
&+ H_{JKK}[J(J+1)]K^4 + H_{KKK}K^6 + ...
\end{aligned}$$

1.1.4   Vibration-rotation (Coriolis) interactions

Coriolis interactions represent a breakdown of the Born-Oppenheimer approximation, which assumes the vibration and rotation of the molecule can be treated independently. A rotating frame is an example of a non-inertial (or accelerating) frame, for which Newton's equation of motion, $F = ma$, is not sufficient. In this reference frame, an extra term must be included of the form;

$$\vec{F}_{Coriolis} = -2m\vec{\rho} \times \vec{s}$$

Since the molecule is rotating with angular velocity $\vec{\rho}$ and the nuclei of mass m are vibrating with some linear velocity $\vec{s}$ a Coriolis force is apparent within the rotating frame of the vibrating molecule. This force can act to simultaneously excite another vibration, and one cannot speak of individual and separate modes but only the coupled system involving both. Quantum mechanically, this is described by a superposition of states as presented in Mills[7]

$$\left| v_A^p \right\rangle = a_k \left| v_A \right\rangle - i\sigma b_k \left| v_B \right\rangle \tag{1.1.1}$$

$$\left| v_B^p \right\rangle = a_k \left| v_B \right\rangle + i\sigma b_k \left| v_A \right\rangle \tag{1.1.2}$$

Where

$$a_k^2 = [(\Delta_k + \delta)/2\Delta_k] \tag{1.1.3}$$

$$b_k^2 = [(\Delta_k - \delta)/2\Delta_k] \tag{1.1.4}$$

$$\Delta_k^2 = \delta^2 + 16A_e^2 k^2 \zeta_{A,B}^2 \Omega_{A,B}^2 \tag{1.1.5}$$

$$\Omega_{A,B} = (v_A + v_B)(v_A v_B)^{-1/2} \tag{1.1.6}$$

$$\delta = v_B - v_A \tag{1.1.7}$$

Where $|k| \equiv K$ and $\sigma^2 = 1$. Note: The vibrational energy, v, is labeled as ω in chapter 3. This is merely a change of notation.

The strength of the interaction is characterized by the Coriolis coupling constant, ζ, which can take values between zero and one. The modulus squared of the inner products of the basis vectors with the coupled superposition determine the probability of observation of a specific state if a measurement is made;

$$\left| \left\langle V_A \middle| V_A^p \right\rangle \right|^2 = \left| \left\langle V_B \middle| V_B^p \right\rangle \right|^2 = a_k^2$$

$$\left| \left\langle V_B \middle| V_A^p \right\rangle \right|^2 = \left| \left\langle V_A \middle| V_B^p \right\rangle \right|^2 = b_k^2$$

This result shows us that when modes are coupled, there will be a non-zero probability of them being observed in either state A or B. This is consistent with the idea that coupled modes can no longer be treated separately.

The Coriolis interaction also introduces new terms into the rotational Hamiltonian as derived by Nakagawa & Morino[8]:

a-axis

$$\langle n, J, K | \hat{H} | n', J, K \rangle = \{\zeta_{n'n}^{a} + \eta_{n'n}^{aJ} J(J+1) + \eta_{n'n}^{aK} K^{2}\}K$$

$$\langle n, J, K | \hat{H} | n', J, K \pm 2 \rangle = \{\mp \tfrac{1}{2}\eta_{n'n}^{bc} + \eta^{a}(K \pm 1)\}F_{\pm}(J,K)F_{\pm}(J,K \pm 1)$$

b-axis

$$\langle n, J, K | \hat{H} | n', J, K \pm 1 \rangle = -\tfrac{1}{2}\{\zeta_{n'n}^{b} + \eta_{n'n}^{bJ} J(J+1) + \eta_{n'n}^{bK} K^{2} - (\pm 2K + 1)\eta_{n'n}^{ac}\}F_{\pm}(J,K)$$

c-axis

$$\langle n, J, K | \hat{H} | n', J, K \pm 1 \rangle = -\tfrac{1}{2}\{\zeta_{n'n}^{c} + \eta_{n'n}^{cJ} J(J+1) + \eta_{n'n}^{cK} K^{2} - (\pm 2K + 1)\eta_{n'n}^{ab}\}F_{\pm}(J,K)$$

Where $F_{\pm}(J,K) \equiv \{J(J+1) - K(K \pm 1)\}^{1/2}$ and η are the second order Coriolis interaction parameters. The addition of these off-diagonal terms to the Hamiltonian act to make the ro-vibrational structure much more complex, and much harder to predict. The size of these terms can cause the effects to be local or global, and the distinction between these is generally not well defined. Treating energy perturbations is by far the most difficult and unpredictable aspect of the analysis of high-resolution spectra.

1.2 Transition probability

1.2.1 The transition dipole moment

The following derivations are taken from teaching material prepared by Paganin[9], which are largely based on Sakurai[3]. Due to the wave-like nature of the Schrodinger equation, the total wave function of the molecule, $|\Psi\rangle$, can be represented as a superposition of simpler waves:

$$|\Psi\rangle = \sum_{n,J,K} c_{n,J,K}(t)|n,J,K\rangle$$

where $c(t)$ represents the time dependant probability amplitude for observing the molecule in the eigenstate $|n,J,K\rangle$. When an interaction between a molecule, described by $|\Psi\rangle$, and light occurs the molecular Hamiltonian is slightly perturbed. The new Hamiltonian can be written as the sum of the unperturbed Hamiltonian, $\hat{H}$, and a new "interaction Hamiltonian", $\hat{H}_i$, which is small compared to $\hat{H}$. The new time-dependant Schrodinger equation under this scheme becomes:

$$(\hat{H} + \hat{H}_i)|\Psi\rangle = i\hbar \frac{d}{dt}|\Psi\rangle$$

The detailed derivation of the transition probabilities for each state will not be provided, however by working to first order time-dependant perturbation theory these are calculated as:

$$\left| c_{n,J,K}(t) \right|^2 / t = \frac{2\pi}{\hbar} \left| \langle n',J',K' | \hat{H}_i | n,J,K \rangle \right|^2 \delta(E_{n',J',K'} - E_{n,J,K} - \hbar\omega)$$

Where δ denotes the delta function. So the probability per unit time of finding $|\Psi\rangle$ in energy eigenstate $|n',J',K'\rangle$ after initially being in state $|n,J,K\rangle$ after the perturbation has been "switched on" is dependant on the right hand side of this equation. This equation not only states $E_{n',J',K'} - E_{n,J,K} - \hbar\omega = 0$ (conservation of energy) for a transition to have non-zero probability of occurring but that the matrix element $\langle n',J',K' | \hat{H}_i | n,J,K \rangle$ should also be non-zero.

$\hat{H}_i$ is made up of a number of terms, however if we only consider those which correspond to single photon absorption, and make the approximation that the wavelength of the absorbing photon is large compared to the absorbing molecule (i.e. the dipole approximation, which is particularly applicable for infrared photons) then this matrix element becomes:

$$\left| \langle n',J',K' | H_i | n,J,K \rangle \right|^2 \approx \left| \langle n',J',K' | \sum_i q_i \hat{r}_i | n,J,K \rangle \right|^2 \equiv \left| \langle n',J',K' | \mu | n,J,K \rangle \right|^2$$

Where q is the electric charge, r is the position in space of the nuclei (μ represents the spatial distribution of charge of the molecule). The quantity $\langle n', J', K' | \mu | n, J, K \rangle$ is commonly referred to as the transition dipole moment (TDM) and can be seen as an operation on the initial state $| n, J, K \rangle$. This quantity can be expanded as a Taylor series:

$$\left| \langle n', J', K' | \mu | n, J, K \rangle \right|^2 \approx \left| \langle n', J', K' | \mu_0 | n, J, K \rangle \right|^2 + \left| \langle n', J', K' | r d\mu / dr | n, J, K \rangle \right|^2$$

For reasons which will not be derived here (see for example Grinter[10]) if a change in the vibrational quanta, n, occurs then only the second term can be non-zero and if there is no change in n only the first term can be non-zero. The result is that for pure rotational transitions to be observed, the molecule must possess a permanent electric dipole moment ($\mu_0 \neq 0$) and for ro-vibrational transitions to occur the net change in the electric polarization as the molecule vibrates must be non-zero ($d\mu / dr \neq 0$). The selection rules are derived from the symmetries of the quantities that make up the TDM. To illustrate this, the TDM is re-expressed in terms of functions rather than vectors:

$$\langle n', J', K' | \mu | n, J, K \rangle \equiv \int_{-\infty}^{\infty} dr \Phi(r)_{n',J',K'} \mu \Phi^*(r)_{n,J,K}$$

Since the transition dipole moment can be interpreted as an integral, it can only have a non-zero value if the function of three factors being integrated over is symmetric (anti-symmetric functions always give zero when integrated over the whole function). For fundamental modes, the ground state (G. S.) has symmetric character, implying that the

15

TDM and upper state should have the same character (either both symmetric or anti-symmetric) for transitions have a probability of occurring.

The selection rules are dependant on the point group of the molecule in question. For the asymmetric rotor and the C_{3v} symmetric rotor (which are the subjects of this thesis) the selection rules for rotational transitions are as follows:

Table 1.2: Selection rules of the asymmetric rotor.

Mode type	Selection rules
A	$\Delta J = 0,\pm 1$ $\quad \Delta K_a = 0$ $\quad \Delta K_c = \pm 1$
B	$\Delta J = 0$ $\quad\quad \Delta K_a = \pm 1$ $\quad \Delta K_c = \pm 1$
C	$\Delta J = 0,\pm 1$ $\quad \Delta K_a = \pm 1$ $\quad \Delta K_c = 0$

Table 1.3: Selection rules of the C_{3v} symmetric rotor.

Mode type	Selection rules
A_1 (parallel)	$\Delta J = 0,\pm 1$ $\quad \Delta K = 0$
E (perpendicular)	$\Delta J = 0,\pm 1$ $\quad \Delta K = \pm 1$

One final note is that the initial population distribution in the lower state follows a Boltzmann distribution,

$$\frac{N_i}{N} = \frac{d_i}{Z} \exp(-\frac{E_i}{k_B T})$$

Where N_i, d_i and E_i are the population, degeneracy and energy respectively of the ith state, Z is the associated partition function, k_B is the Boltzmann constant and T is temperature. For a transition to occur, there must first be some population in the lower state, and the distribution of intensities in observed spectra reflects this. Spectral simplification or amplification can be achieved by manipulation of the initial population by variation of the temperature of the molecules to be analyzed.

1.2.2 Intensity perturbations

One of the major outcomes of this work is the identification and treatment of a novel intensity stealing effect which is a manifestation of the Coriolis coupling. First we need to look at the TDM "operation" applied to a superposition of coupled states (as derived by Mills[7]).

$$\langle G.S.|\mu_x \mp i\mu_y|v_A^p\rangle = \langle G.S.|\mu_x \mp i\mu_y\{a_k|v_A\rangle - i\sigma b_k|v_B\rangle\}$$
$$= a_k M_A \mp b_k M_B$$

$$\langle G.S.|\mu_x \mp i\mu_y|v_B^p\rangle = \langle G.S.|\mu_x \mp i\mu_y\{a_k|v_B\rangle + i\sigma b_k|v_A\rangle\}$$
$$= -ib_k M_A \mp ia_k M_B$$

This result assumes that the TDM of modes A and B are only in the x and y directions respectively (i.e. $\langle G.S.|\mu_x|v_B\rangle = \langle G.S.|\mu_y|v_A\rangle = 0$). The line strength, S, is proportional to the modulus squared of these equations.

$$S_A = a_k^2 M_A^2 + b_k^2 M_B^2 \mp 2a_k b_k M_A M_B \qquad (1.2.1)$$

$$S_B = b_k^2 M_A^2 + a_k^2 M_B^2 \pm 2a_k b_k M_A M_B \qquad (1.2.2)$$

Where the sign of the interference term is dependant on whether the J quantum number is increasing or decreasing (denoted as P- and R-branch transitions respectively) over the transition and the notations $\langle G.S.|\mu_x|\nu_A \rangle \equiv M_A$ and $\langle G.S.|\mu_y|\nu_B \rangle \equiv M_B$ are employed. As can be seen from equations 1.1, as the product $A_e^2 k^2 \zeta_{A,B}^2 \Omega_{A,B}^2$ increases, $\Delta \gg \delta$ and the values of both a_k^2 and b_k^2 approach the value of ½ (shown graphically in figure 1.2). Under these conditions, the intensities of both modes will be exactly the same, even if they were initially different, which can be interpreted as a weaker mode stealing intensity away from a stronger mode.

A major result of this project is the identification and characterization of systems where the expected (a.k.a. natural) TDM is either zero or small enough to be neglected given noise, which are enhanced via this mechanism and become analyzable.

1.2.3   Examples of intensity stealing

The first case to be discussed is the case where the approximation $M_A \approx 0$ can be made. Under this assumption, both the natural contribution to the line strength, governed by the $a_k^2 M_A^2$ term and the interference term $\mp 2a_k b_k M_A M_B$ can be neglected and the intensity is purely dependant on the stealing term $b_k^2 M_B^2$.
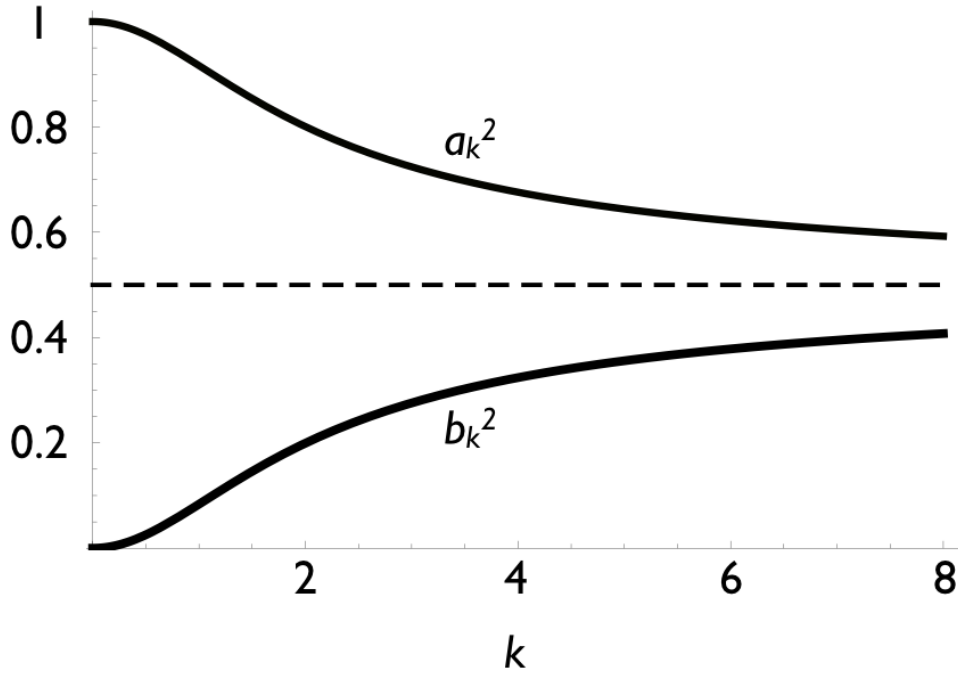
Figure 1.2: Example taken from a real world system (ketenimine v_8 and v_{12}) of how given the right conditions, b_k^2 can approach its maximum value of ½ even at observable k values.

If b_k is appreciable at sufficiently low k, mode A can gain intensity from the $b_k^2 M_B^2$ term which is essentially stolen from the intensity of the mode which it is coupled to since its intensity is also diminished. Under this scheme, the intensity of both modes is dependant on the transitions dipole moment of a single mode

$$S_A \approx b_k^2 M_B^2$$

$$S_B \approx a_k^2 M_B^2$$

One consequence of this type of coupling is that the dipole moment essentially becomes k-dependant, and the distribution of intensities is shifted toward higher k than is normally observed assuming a standard Boltzmann distribution. Under this mechanic the $k = 0$ transitions have no intensity, which is contrary to what would be expected assuming a standard TDM for which $k = 0$ transitions generally have very high relative intensity. Secondly, the selection rules for transitions enhanced by this mechanism are an amalgamation between the rules of the dipole moment being stolen and the selection rules for the coupling, as summarized in table 1.4

Table 1.4: Selection rules for modes whose intensity is dependant on intensity derived from a stolen TDM. Dipole moment of mode being stolen and axis of interaction are labeled on the horizontal and vertical respectively.

	A-type	B-type	C-type
a-axis	$\Delta K_a = 0$ $\Delta K_c = 0, \pm 2$	$\Delta K_a = \pm 1$ $\Delta K_c = 0, \pm 2$	$\Delta K_a = \pm 1$ $\Delta K_c = \pm 1$
b-axis	$\Delta K_a = \pm 1$ $\Delta K_c = 0, \pm 2$	$\Delta K_a = 0, \pm 2$ $\Delta K_c = 0, \pm 2$	$\Delta K_a = 0, \pm 2$ $\Delta K_c = \pm 1$
c-axis	$\Delta K_a = \pm 1$ $\Delta K_c = \pm 1$	$\Delta K_a = 0, \pm 2$ $\Delta K_c = \pm 1$	$\Delta K_a = 0, \pm 2$ $\Delta K_c = 0$

Another situation that can arise is when M_A is small enough to be neglected, but the product $M_A M_B$ is large enough that a similar assumption may not be valid. This situation can occur if there is a very large difference in the dipole moments of the modes which are coupled:

$$S_A \approx b_k^2 M_B^2 \mp 2 a_k b_k M_A M_B$$

$$S_B \approx a_k^2 M_B^2 \pm 2a_k b_k M_A M_B$$

Under this scheme, the intensities of the *P-* and *R*-branch transitions will have high asymmetry due to the interference term $\mp 2a_k b_k M_A M_B$. Since these terms are still highly dependant on *k*, intensity is still shifted to unexpected values of *k* as is summarized in figure 1.3.
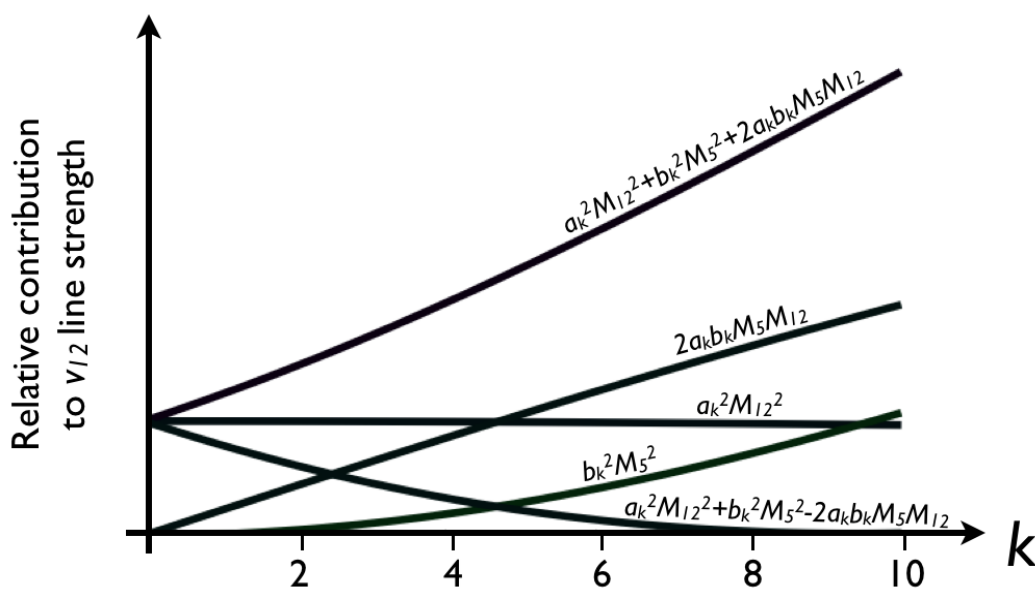
Figure 1.3: Example taken from a real world system (thiirane v_5 and v_{12}) of how various terms in equations 1.2 can contribute to the line strengths. This figure shows particularly the large difference in the predicted *P-* and *R*-branch intensity.

One final note is for the case where $M_A = M_B \equiv M$ and $\delta = 0$ (which implies $a_k^2 = b_k^2 = 1/2$ for $k > 0$) which is the case for a degenerate vibration of a symmetric rotor. Under this scheme equations 1.2 becomes:

$$S_A = \tfrac{1}{2}M^2 + \tfrac{1}{2}M^2 \mp M^2 = M^2 \mp M^2$$
$$S_B = \tfrac{1}{2}M^2 + \tfrac{1}{2}M^2 \pm M^2 = M^2 \pm M^2$$

The *P*-branch will be completely suppressed for one of the degenerate modes and the *R*-branch will have double intensity. The opposite is true for the other degenerate mode, and overall the mode appears the same as what would be expected if the two modes were simply superimposed with symmetric intensity between branches.

1.3 Interferometry

1.3.1 The role of the Fourier transform

A simplified schematic of the Michelson interferometer, made famous for its negative result for the determination of the velocity of the earth with respect to the "ether"[11], is shown in figure 1.4. The Fourier transform[12] (FT) essentially utilizes the fact that any function can be represented by a sum of simpler basis functions, and that a description of how these are summed is equivalent to the original description.
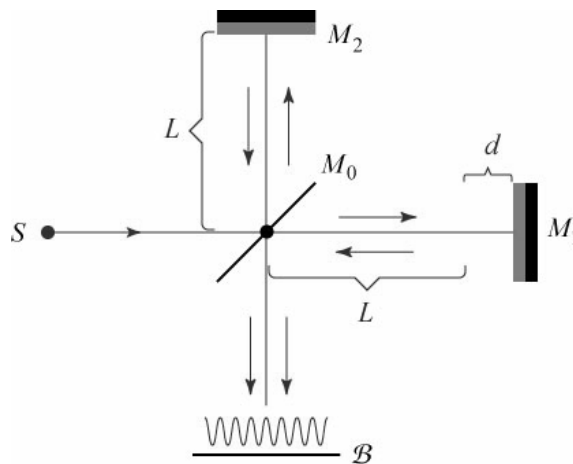
Figure 1.4: Simplified schematic of a Michelson interferometer. A source of radiation is incident on a beam splitter which ideally reflects 50 % of the radiation while allowing 50% to be transmitted. The two beams are recombined by reflection from the mirrors and the intensity is measured at a detector.

By varying the path difference between the split beams (by varying the length *d*) an interferogram can be collected by measuring intensity as a function of path difference. When monochromatic light illuminates the detector the interferogram, *I*(*x*), oscillates between 0 and $2S_0$ according to,

$$I(x) = S_k[1 + \cos(2\pi xk)]$$

Where S_k relates to how much light is absorbed at the frequency of the incident radiation and $k = 1/wavelength$. If we then generalize to a polychromatic incident beam of radiation,

$$I(x) = 2\int_0^\infty S(k)[1 + \cos(2\pi xk)]dk = 2\int_0^\infty S(k)\cos(2\pi xk)dk + 2\int_0^\infty S(k)dk$$

where *S*(*k*) is the FT of *I*(*x*), and is physically interpreted as the absorbance as a function of wavelength (a.k.a. a spectrum). The second term has no *x* dependence and has little significance in the spectra. The inverse FT yields the spectrum.

$$S(k) = 2\int_0^\infty I(x)\cos(2\pi xk)dx$$

Under theoretically ideal conditions, the form of $S(k)$ can be approximated by a sum of Dirac delta functions[13]. A delta function is defined as:

$$\delta(k) = \lim_{a \to \infty}[\{ \begin{matrix} a & -1/a \leq x \leq 1/a \\ 0 & -1/a > x > 1/a \end{matrix}]$$

As a approaches ∞, the function becomes infinitely thin and sharp. Since transitions only occur at discrete, well defined energies (k_1, k_2,...k_N), these can be summed to describe the allowable energies of an entire spectrum,

$$S_\infty(k) = \delta(k - k_1) + \delta(k - k_2) + ... + \delta(k - k_N) \qquad (1.3)$$

In reality, the spectra obtained are always of finite path difference, and the obtained interferograms are always of the form.

$$I(x) = I_\infty(x) * B(x)$$
$$B(x) = \{ \begin{matrix} 1 & x \leq d \\ 0 & x > d \end{matrix}$$

Where d is the extent that the interferogram is sampled over. Since the FT is actually performed on what is essentially a product, the convolution theorem becomes relevant:

$$\Im\{f.g\} = \Im\{f\} \otimes \Im\{g\}$$

Where $\Im$ denotes the FT and $\otimes$ is defined as the convolution operation. Since the FT of the "infinite" interferogram is stated explicitly in equation 1.3 (an ideal spectrum), and the second quantity in the product is simply $B(x)$, a description of the spectrum of allowable energies can be written as:

$$
\begin{aligned}
\Im\{I(x)*B(x)\} &= S_\infty(k) \otimes \Im\{B(x)\} \\
&= [\delta(k-k_1) + \delta(k-k_2) + ... + \delta(k-k_N)] \otimes [(\sin(\pi KL)/\pi k] \\
&= \sin(\pi[k-k_1]L)/\pi k + \sin(\pi[k-k_2]L)/\pi k + ... + \sin(\pi[k-k_N]L)/\pi k
\end{aligned}
$$

where in the third line we make use of the translational property of convolutions involving delta functions. Note this only describes the energies and does not consider intensities. This result allows us to study two important aspects of FT spectroscopy, resolution and apodization.

By investigating the behavior of a single peak as measured by an instrument with finite path difference (as all real spectrometers are) we can gain an insight as to how the spectrum differs from the ideal. Figure 1.5 depicts the quantity $\sin(\pi kL)/k$ for two differing values of d.

26
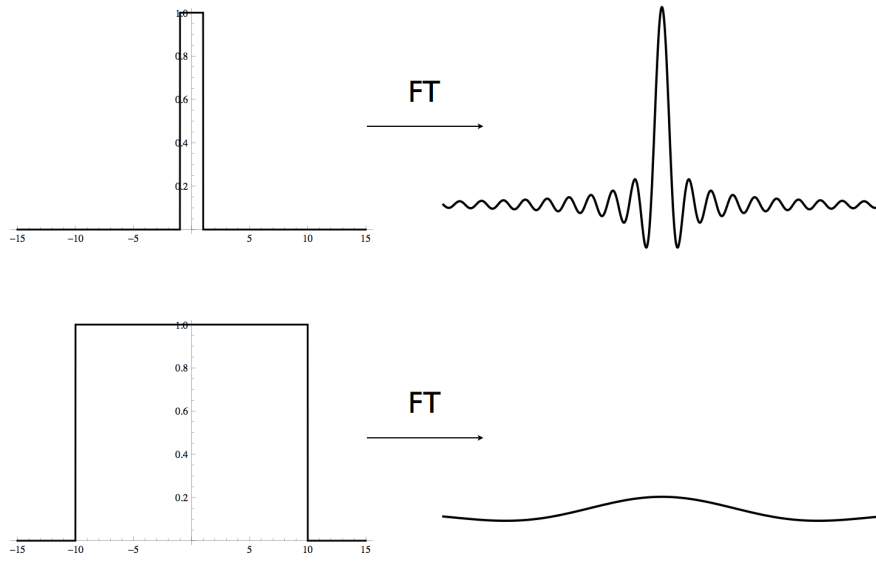
Figure 1.5: Comparison of FT of two $B(x)$ functions differing by the distance d.
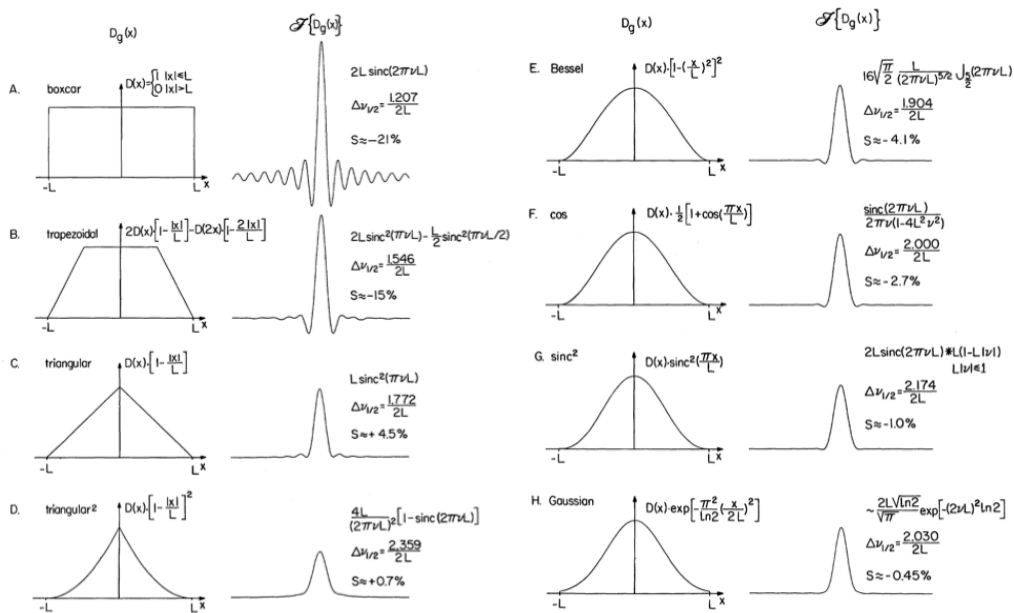

Figure 1.6: Examples of some common apodization functions and their Fourier transform. Taken from Kauppinen et. al.[14]. Δv relates to the resolution achievable and S relates to the size of the "feet" compared to that of the major peak.

This figure shows that the more of the interferogram collected, the better defined the peak. Since the peaks are more like the ideal delta function when d is large, peaks which are close in energy are more easily distinguished, and we can say that the resolution or resolving power is greater. The major difference between the instrument used in this study and an average table-top FTIR spectrometer (except for the source), is that our maximum path-difference is approximately 10 m, which is far greater than table-top devices (usually only a few centimeters). This allows us to resolve rotational transitions which are far closer in energy than vibrational transitions.

Although the peaks are much more like ideal delta-functions, they still retain a remnant of $B(x)$ in the form of small oscillations or "feet" near the base of the peak. This effect can be seen as a leakage of intensity out of the peak, which is undesirable and can actually mask weaker features. In order to limit this leakage, a process of apodization (which literally means "to remove feet") can be applied to the interferogram by simply multiplying it by an "apodization function". The oscillations observed in figure 1.5 are purely the result of the FT of $B(x)$ being of the form $\sin(k)/k$, and if a different function is chosen, the peaks will have a different shape. These apodization functions effectively "soften" the abruptly ending $B(x)$, and aim to strike more of a balance between resolution and leakage. In this work, high resolution is extremely important so this balance is highly skewed toward increased resolution, and the apodization function does not differ too greatly from $B(x)$. Some examples of apodization functions and their effect on the line shape is shown in figure 1.6.

Another process that is generally applied to the interferogram is post-zero filling. Since the interferogram is collected at discrete points, a discrete FT is used, resulting in a discrete spectrum (i.e. $x \to n*\Delta x$, $k \to m*\Delta k$).

$$S(m*\Delta k) = \sum_{n=0}^{N-1} I(n*\Delta x) * e^{i2\pi nm/N}$$

Zero's can be added to the spectra, to effectively make $n*\Delta x$ appear greater (since there are apparently more points sampled in the interferogram). There is no new information added upon inclusion of zeros, however it does make the spectrum appear more continuous. This process can be considered an extrapolation in Fourier space, which simply makes peaks appear smoother (Δk is effectively reduced) and can result in slightly more precision in determining the peak positions of spectral features.

It is also of note that in general the output of this discrete form of the FT will be complex, and the interferogram picks up a complex phase. The modulus, A, can be retrieved by a phase correction known as the Mertz method, by taking the real component of the product of the FT output and the complex conjugate of the phase:

$$\Im\{I(n*\Delta x)\} = A(m*\Delta k)e^{i\phi(m*\Delta k)}$$
$$A(m*\Delta k) = \text{Re}[\Im\{I(n*\Delta x)\}e^{-i\phi(m*\Delta k)}]$$

29

References

[1]   M. Born and R. Oppenheimer, AdP. **389** (20), 457 (1927).

[2]   P. M. Morse, Phys. Rev. **34** (1), 57 (1929).

[3]   J. J. Sakurai, *Advanced Quantum Mechanics*. (Addison-Wiley Reading, 1967).

[4]   A. Messiah, *Quantum Mechanics, Two Volumes Bound as One*. (Dover Publications, 1999).

[5]   H. C. Allen and P. D. Cross, *Molecular Vib-rotors: The Theory and Interpretation of High Resolution Infrared Spectra*. (John Wiley & Sons Inc, 1963).

[6]   J. K. G. Watson, in *Vibrational Spectra an Structure*, (Elsevier scientific publishing company, 1977), Vol. 6.

[7]   I. M. Mills, Pure Appl. Chem. **11** (3-4), 325 (1965).

[8]   T. Nakagawa and Y. Morino, J. Mol. Spec. **38** (1), 84 (1971).

[9]   D. Paganin, *PHS4200: "Advanced Quantum Mechanics" 2008 [DP's Section]*. (Monash University School of Physics, 2008).

[10]   R. Grinter, *The Quantum in Chemistry: An Experimentalist's View*. (Wiley: Chichester, 2005).

[11]   A. Michelson, Phil. Mag. Series 5 **34** (280), 280 (1892).

[12]   J. Fourier, *The Analytical Theory of Heat*. (Cambridge University Press, 1878).

[13]   P. Dirac, *Principles of quantum mechanics*, 4th ed. (Oxford at the Clarendon Press, 1958).

[14]   J. Kauppinen, T. Kärkköinen, and E. Kyrö, Appl. Opt. **17** (10), 1587 (1978).

Chapter 2

Instrumentation and

Analysis

2.1 High-resolution synchrotron FTIR

2.1.1 The synchrotron source

3rd generation synchrotron light sources such the Australian synchrotron (AS) consist of an initial linear accelerator (LINAC) followed by an inner booster ring in which electrons are accelerated to close to the speed of light corresponding to, in the case of the AS, an energy of 3 GeV. These electrons are then injected into a larger storage ring where they are held in a kind of "discrete" circular trajectory. This orbit is achieved using bending magnets which impart a Lorentz force to the electrons causing them to deviate and emit electro-magnetic radiation. This radiation is collected at various points around the ring, and harnessed for experimentation.

The beam-line utilized in these experiments is the far-infrared (FIR) beamline at the AS. One of the defining characteristics of this beamline is that the optics have a relatively large angle of acceptance for the emitted synchrotron light, which allows for the collection of the longest wavelength radiation from the bending magnets. Both edge[1] and bending magnet radiation are collected at the beamline, which is separated by optics and directed to two separate workstations (for detailed schematic see Creagh *et. al.*[2]). The FIR beamline mostly receives the longer wavelength edge radiation whereas an IR microscopy beamline receives mostly bending magnet radiation.

An advantage of synchrotron radiation comes from the fact that it is effectively emitted from a point source (electron-beam diameter approx. 350 μm), implying that the optics can theoretically achieve an almost perfectly collimated beam. This is an advantage, since apertures are generally not required, implying less light is wasted. Small apertures are required when recording high-resolution spectra, which can reduce the Jacquinot advantage (see below). The high collimation somewhat reclaims this advantage, since the role of apertures becomes less important.

Another advantage is that the mechanism of synchrotron emission is completely different to that of laboratory IR sources (which are dependant on thermal black body emission) and thus the emission profile is different. The detectable intensity of the synchrotron setup compared to internal sources is shown in figure 2.1.

It can be seen from this figure that there is a greater flux from the synchrotron source in the FIR region between 10 and 1000 cm^{-1}. The high FIR flux ensures that sensitivity is high enough that modes in this region may be observed and analyzed. This region is particularly important since many molecules of astrophysical importance have modes of energy <1000 cm^{-1}, which are the most likely to be populated in astrophysical (cold) environments. High flux in this region also allows for the observation of high quantum number pure rotational data, which generally appears below 100 cm^{-1}, and is also important for astrophysical detection.
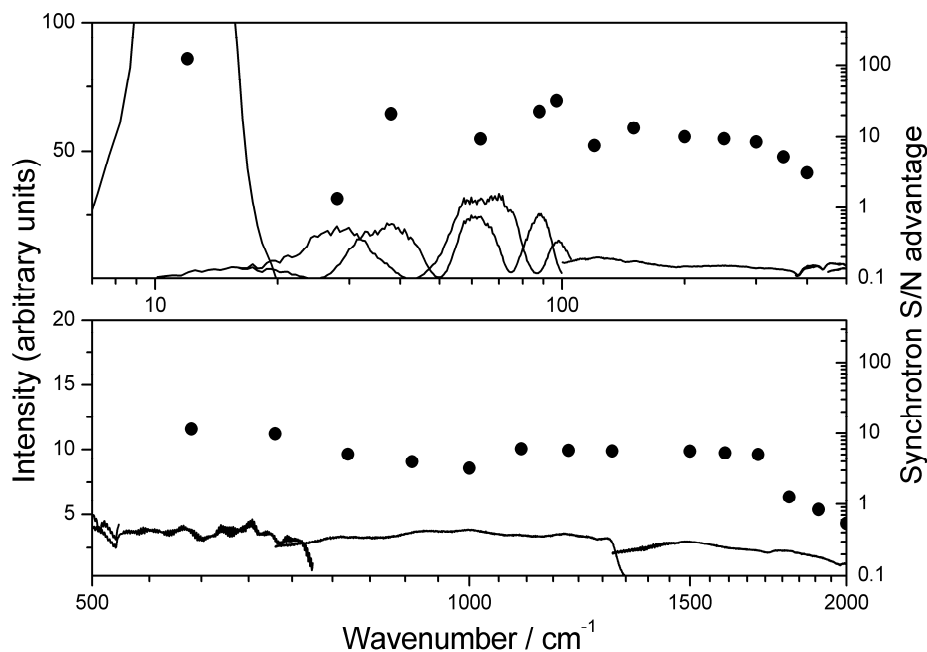
Figure 2.1: Detectable FIR flux for the synchrotron source[3]. The lowest energy trace which cuts off at approximately 20 cm^{-1} was recorded using CSR emission (see section 2.1.3). This figure does not show the pure emission spectrum of the synchrotron, rather it shows our experimentally determined ability to detect signal as a function of wavelength using appropriate optics and detectors. Dots represent the improvement of the synchrotron source compared to internal sources (not shown explicitly).

2.1.2 The spectrometer

During the work presented in this thesis, the commercially available Bruker IFS125HR Fourier Transform Infrared (FTIR) spectrometer shown in figures 2.2 and 2.3 was used to obtain high-resolution spectra. This spectrometer is located at the FIR beamline at the AS, and utilizes the high FIR flux of the synchrotron light. This particular spectrometer

34

can achieve a maximum path difference of approximately 10 m, allowing it to achieve an unapodised resolution of 0.00096 cm^{-1}.

The spectrometer can be fitted with a range of apertures, beam splitters, detectors, windows and filters depending on the desired spectral region. The spectrometer is kept under high vacuum to reduce contaminant absorbance from IR active molecules in the atmosphere such as H_2O and CO_2.
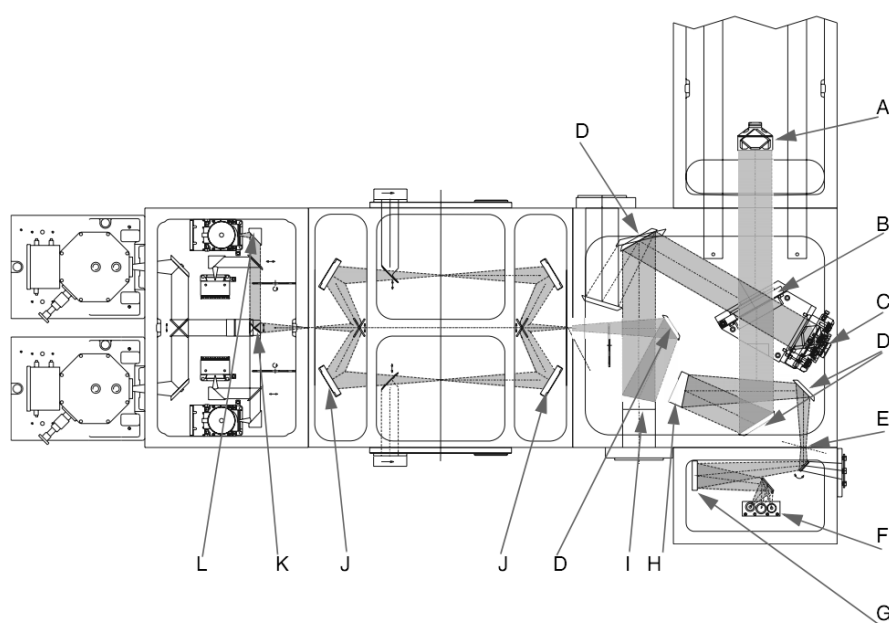
Figure 2.2: Schematic diagram of the Bruker IFS125HR FTIR spectrometer[4]. A) Scanning (moveable) mirror, B) beam-splitter, C) stationary retro-reflecting mirror, D) folding mirror, E) source aperture, F) sources, G) spherical mirror, H) collimating parabolic mirror, I) focusing parabolic mirror, J) toroidal mirror, K) collimating parabolic mirror, L) focusing parabolic mirror. In our study, the instrument is coupled to a synchrotron source which is not shown. Figure re-printed with permission of Bruker Biosciences Pty. Ltd.

Figure 2.3: Picture of the Bruker IFS125HR spectrometer located at the FIR beamline of the AS with emphasis on the scanner arm. The 10 m path difference the scanning mirror is able to achieve allows for the collection of high-resolution spectra.

The instrument is also fitted with internal sources which cover the very FIR (Hg lamp), far- and mid-IR (Globar source, 100-5000 cm^{-1}), near-IR (tungsten lamp, 3000-25000 cm^{-1} and UV/Vis (xenon-lamp, 10000-42000 cm^{-1}). The Globar source was the only internal source used in this work, and spectra over 1000 cm^{-1} were recorded using this as a source. Since internal sources were useable during synchrotron down time, they were often used for diagnosis to locate known intense mid-IR bands to confirm the presence of target molecules in preparation for our limited synchrotron beam-time.

The spectrometer is a Fourier transform based instrument, as opposed to a dispersion based instrument, which has the following major advantages:

- The multiplex advantage[5]. Since all wavelengths are collected simultaneously, data is collected significantly faster compared to a dispersive instrument. This allows for more data to be collected and a higher amount of averaging to be allowed (which increases signal/noise since noise is random and should cancel). This also reduces the chance of undesired variation of experimental conditions over the course of the measurement. This is also commonly referred to as the Fellget advantage.

- The Connes Advantage[6]. The mirror is tracked by comparison with the interference pattern of a HeNe laser, with each zero-point in the lasers interference pattern corresponding to an increment of the interferogram. This laser is highly monochromatic allowing for extremely precise calibration.

- The Jacquinot advantage[7]. FTIR spectrometer uses circular apertures, as opposed to the slits found in dispersion based instruments, which let through significantly more light. This is most important when internal sources are used.
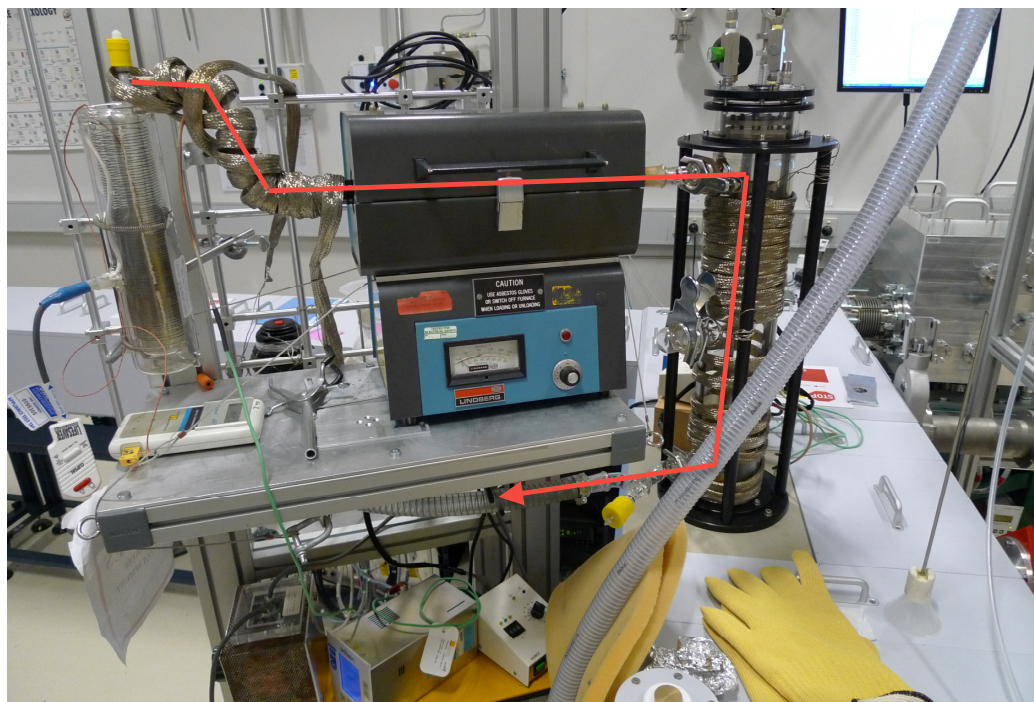
Figure 2.4: Illustration of the cell and flow through pyrolysis setup attached to the spectrometer. Liquid sample is stored and the vapor is pumped through the furnace and cell and exhausted or trapped. Sample concentrations and flow rates could be controlled by valves located before and after the cell and/or by varying the temperature of the liquid sample. Maximum oven temperature achievable is approximately 1100 ^{o}C, which corresponds to just below the melting point of the quartz glass tube contained within the oven.

The region where the sample-light interaction occurs is known as the cell, and is shown in figure 2.4. This cell, of approximately 60 cm length, has three gold plated mirrors which are set up as a White cell[8] so that the beam can be reflected up to 32 times, achieving a maximum possible path length of approximately 20 m. Since most of the experiments were of transient or unstable molecules, a flow-through setup could be attached to the cell. This setup allowed us to perform pyrolysis reactions and quickly pump the short-lived products through the cell where spectra could be recorded. The reactants are pumped out of the cell quickly enough so that contamination from degradation products is minimized.

2.1.3 Pure rotation studies – comparison of techniques

Fundamentals of micro/millimeter wave and lamb-dip spectroscopy presented in this section are largely taken from and covered in more detail in Hollas[9]

Standard microwave (1-100 GHz) and millimeter-wave (100-500 GHz) frequency scanning spectrometers operate in a fundamentally similar way and are more electronically based (as opposed to optically based) instruments compared to FTIR. Typical sources for these types of instruments once included klystrons and now the more modern backward wave oscillators or solid state sweep oscillators (these use harmonic multipliers to get the higher frequencies) which are both highly monochromatic and easily tunable. The bandwidth of the spectrometer is primarily limited by the dimensions of the waveguides used (effectively copper or brass tubing coated internally with silver to

prevent loss of power). Resonant cavities, which effectively restrict the path propagation in all three spatial directions, can be used to increase the radiation power and effective tunability range by setting up standing waves. The wavelength of the radiation in the resonator will be dependant on the length of the cavity, and thus a more continuous range of tunability can be achieved by variation of this distance. Development of the backward wave oscillator has allowed frequencies in the THz region to be accessed, and although output power is sacrificed at higher frequencies, this is balanced by the absorption increasing as the square of the frequency.

Fourier transform microwave (FTMW) techniques are currently also continuing to develop. The first FTMW techniques were introduced over 30 years ago by Balle and Flygare[10] which was able to produce a spectrum with resolution of 3.9 kHz / point. These techniques record the emission of excited molecules over the time domain, which is related to the frequency domain spectra via a Fourier transform operation. For an extensive review of modern FTMW theory and experimentation see Grabow[11]. Relatively recent development in high speed electronics have allowed chirped pulse base instruments to simultaneously record over a bandwidth greater than 10 GHz, which has lead to a resurgence in FTMW (See Pate[12]).

Since the micro/millimeter-wave sources are generally highly monochromatic, the line-width of transitions is generally limited by pressure and Doppler broadening (line-widths typically of the order of 10 kHz). A method of overcoming the Doppler broadening is known as Lamb dip spectroscopy. Lamb dip spectroscopy overcomes the Doppler

broadening by comparison of the absorption of a light-beam and its reflection in a cavity. If the energy of the light beam is offset slightly from the centre frequency, it will be absorbed by molecules only moving with some velocity v_a. Upon reflection of this beam, absorption will only occur if the velocity of the molecule is $-v_a$. As the molecules absorb light, they are excited and temporarily unable to absorb more light until they relax. When the situation $v_a = -v_a$ occurs, the net absorption will be lower since the initial pass of the light reduces the number of molecules able to absorb light. $v_a = -v_a$ is only satisfied for $v_a = 0$, and thus the frequency where the net amount of absorption is lowest corresponds to the frequency at which stationary molecules absorb. Although this method can theoretically reduce the effect of Doppler broadening, it requires that *a)* the monochromaticity is low enough that the line width is limited by Doppler broadening and *b)* that the source is powerful enough that a high percentage of molecules are excited in the first pass.

FTIR is a relative late-comer for pure rotational spectroscopy since *a)* thermal sources have such low output in the 1-100 cm^{-1} region and *b)* since the resolution of FTIR instruments could not compare to that of the more widely used microwave spectrometers. By using the synchrotron as a source, many of these obstacles can be overcome. Firstly, the technique can record a much wider continuous bandwidth compared to micro/millimeter-wave sources which extends deep into the FIR region. As shown in figure 2.1, the brilliance of the synchrotron in the millimeter and FIR regions is far superior to that of standard thermal sources, which allows FTIR to be become useable for

pure rotational studies. The two techniques can be considered complementary, since they cover different energy scales.

A new development, known as coherent synchrotron radiation (CSR), is also currently under development at the AS FIR beamline. This is achieved by "bunching up" the electron packets in the storage ring, causing them to emit coherently in a relatively narrow bandwidth. This technique has been shown to increase the signal in the region between 10-20 cm^{-1} by a factor of up to 100 compared to the normal synchrotron emission. This will allow pure rotational FTIR studies to be performed in this region with greater sensitivity in the near future. The continuing development of the CSR technique further extends the usefulness of the synchrotron source for pure rotational spectroscopy, giving a major signal enhancement in the THz region as shown in figure 2.1.

2.1.4 Ro-vibrational studies – comparison with other techniques

The proceeding section is based largely on that presented in McNaughton[13] and McKellar[14] unless otherwise indicated.

Thermal IR sources have sufficient emission in the mid/near-infrared, visible and UV regions of the electromagnetic spectrum and FTIR has been a highly utilized technique for characterization of ro-vibrational modes contained in these regions. The lack of quality sources in the FIR has however meant that a large number of lowest energy ro-vibrational modes have not been observed, even if the corresponding higher energy

modes have been extensively studied. The relatively recent development of FIR synchrotron sources has allowed these regions to be explored. The FIR region is particularly important since the lowest energy modes are the most likely to be thermally populated in atmospheric or interstellar conditions.

Complementary laser based techniques are other commonly used methods for obtaining high-resolution ro-vibrational spectra. The major difference is that a tunable laser is used as a source, and the available laser wavelengths are tuned over the desired range (not a FT technique). Laser radiation is highly monochromatic and coherent and can be orders of magnitude more intense than synchrotron light, making it ideal for spectroscopic studies. The range of tunability of these lasers is highly dependant on the mechanism of the laser. Although highly monochromatic and tunable lasers with a continuous and reasonably wide scanning bandwidth have been developed for most of the mid and near IR, the same cannot be said for the FIR.

Tunable diode lasers are commonly used in this spectroscopy since they cover most of the mid and near IR region up to 3000 cm^{-1}. Microwave or millimeter-wave sideband lasers cover the region between 1041 – 943 cm^{-1} with a maximum achieved resolution of 0.0001 cm^{-1}. Similar systems, in which a CO_2 laser is used as a pump, provide output in the 200 – 10 cm^{-1} region which is achieved by using a large number of lasing molecules each of which providing ~ ± 5 cm^{-1} range. It can be seen that although some of the FIR region is covered, there are large gaps present between these systems. Secondly, the regions expressed generally contain gaps within the scanning bandwidth. Quantum

cascade lasers (see Curl et. al.[15]) offer a possible solution to some of these problems, with lasers of this type ranging from the mid-IR to the THz region. While these lasers have been in existence for over 15 years, they have yet to find wide-spread acceptance for high-resolution studies, particularly in the FIR and THz regions, since they produce so much resolution limiting noise (see Hancock[16]). It is also of note that FTIR can collect data at a much faster rate compared to current laser based techniques.

Free electron lasers (FEL), which fundamentally operate on similar principles as a synchrotron undulator, emit highly coherent light with brilliance more comparable to that of infrared lasers. The frequency of emission is highly tunable by variation of the magnetic field strengths of the magnets associated with the FEL, and a list of tunable infrared FELs currently in operation is shown in table 2.1. It can be seen that the FIR and THz region is well covered by these sources. To date, the resolution achieved using the FEL as a source has been modest compared to what is achievable by synchrotron FTIR techniques.

Table 2.1: List of tunable infrared FEL facilities with possible output wavelength longer than 10 micron[17].

Location	Name	Range
iFEL (Japan)	1	5 – 22 μm
	4	20 – 60 μm
	5	50 – 100 μm
FOM (Netherlands)	FELIX1	3.1 – 35 μm
	FELIX2	25 - 250 μm
Stanford (USA)	SCA-FEL	3 – 10 μm
	FIREFLY	15 – 65 μm
LURE (France)	CLIO	3 – 150 μm
Science Univ. Tokyo (Japan)	FEL-SUT	5 – 16 μm
FZ Rossendorf (Germany)	FELBE	4 – 22 μm
		18 – 250 μm
UCSB (USA)	FIR-FEL	63 – 340 μm
	MM-FEL	340 μm – 2.5 mm
	30 μ-FEL	30 – 63 μm
IHEP (China)	Beijing FEL	5 – 25 μm
CEA (France)	ELSA	18 – 24 μm
ISIR (Japan)		21 – 126 μm
LASTI (Japan)	LEENA	65 – 75 μm
KAERI (Korea)		80 – 170 μm
Budker Inst. (Russia)		110 – 240 μm
Univ. of Twente (Netherlands)	TEU-FEL	200 – 500 μm

2.2 Basics of Analysis

2.2.1 Loomis-Wood diagrams

Since an equation for the allowable energies of asymmetric rotors cannot be explicitly written, we will use the symmetric rotor Hamiltonian for our derivations (all that is presented here is applicable for asymmetric rotor molecules as well). The symmetric rigid rotor Hamiltonian, without Coriolis interactions included is as follows:

$$E(v_0, J, K) = v_0 + BJ(J+1) + (A-B)K^2$$

Most transitions occur between states with a difference in J of one unit, and either K does not change or it changes by 1 unit. The difference in energy of these levels is the energy of the transition. If we assume for simplicity that the rotational constants of the ground state are the same as that of the upper state, for the 2 situations presented this corresponds to an energy difference of:

$$E(v_0, J+1, K) - E(0, J, K) = v_0 + 2B(J+1)$$

$$E(v_0, J+1, K+1) - E(0, J, K) = v_0 + 2B(J+1) + (A-C)(2K+1)$$

Under this approximate Hamiltonian, the energy of transitions is regularly spaced with the energy of separation being $2B$. For the case where K changes, transitions of a given

46

sub-band (collection of transitions with a common value of K) are separated by an amount equal to $2(A - C)$. When attempting to find order in complex spectra, these simple yet fundamental observations are particularly useful. Although some of the order breaks down for the case of asymmetric rotor molecules, the pattern recognition process follows a very similar logic.

Loomis-Wood diagrams make use of this regularity, and assist in the pattern recognition process. By cutting the spectra at intervals of $2B$ and displaying them vertically, patterns are more easily recognized and initial assignments of quantum numbers to transitions can be made. Figure 2.5 shows the relationship between spectra and Loomis-wood diagram. During this project the program Macloomis[18] was used to produce and manipulate the Loomis-Wood diagrams for all analyses.
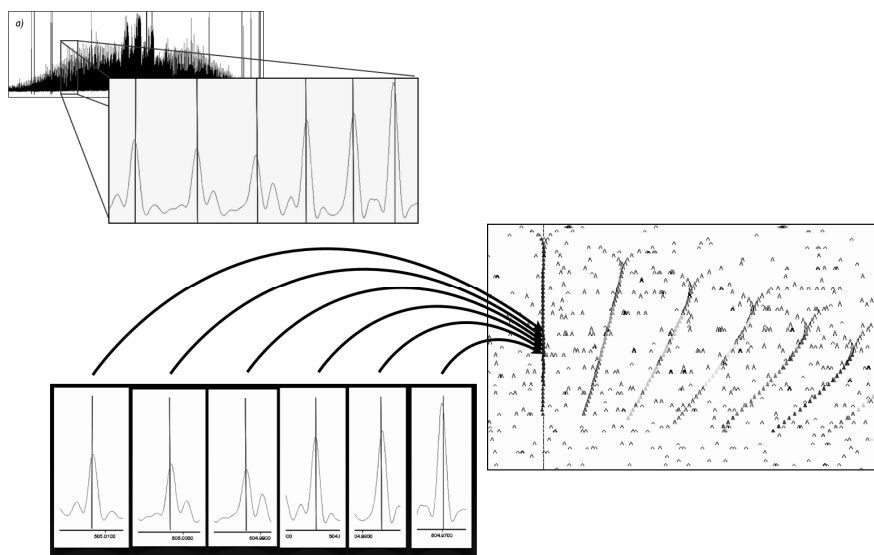
Figure 2.5: Illustration of Loomis-Wood diagrams.

It can be seen from the figure, that displaying the spectrum in this manner greatly assists in pattern recognition, aiding both assignment of quantum numbers to transitions and the separation of useful data from noise. Figure 2.5 also shows the K dependant separation, with series of like K separated by an energy of approximately $2(A - C)$.

2.2.2 Combination differences

Visual inspection of the Loomis-Wood diagram only allows for an initial tentative assignment, which can be confirmed using ground state combination differences (GSCD). The concept of confirmation by GSCD is most easily explained with reference to figure 2.6.
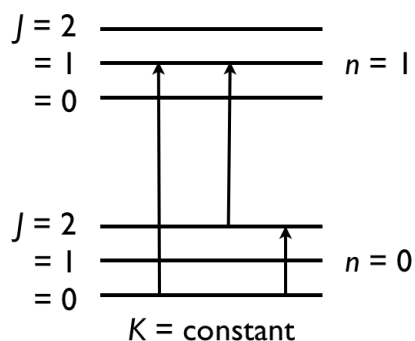
Figure 2.6: Diagram of R-type (left), P-type (centre) and GSCD (right) transitions.

If the molecular parameters are known for the lower state, a set of GSCD can be very accurately calculated. If the energy of a transition which is decreasing in J (P-type) is subtracted from the energy of a transition where J increases (R-type), where both transitions are to the same state, it will compare with high accuracy to the calculated

GSCD. By this method, assignments of quantum numbers can be confirmed with high certainty, since the GSCD can only depend on the energies of the lower state. This technique is only useful however if the lower state parameters, which can be determined by complementary techniques, are known. Since these GSCDs are derived through real experimental data, they can be treated as pseudo pure-rotational transitions and included in an analysis.

It is important to note that only the ground state quantum numbers can be confirmed using this method, and the upper state quantum numbers are implied from the selection rules. As is revealed in the publications presented in this thesis, there are situations where the transition dipole moment of a mode may be more complex than first assumed, and this can change the selection rules leading to initial miss-assignment.

2.2.3 Energy levels plots

Calculation of the ro-vibrational energy levels (as opposed to the energy of transitions) can provide an insight into the likely sources of perturbations.

The observable effects of perturbations are dependant on how close symmetry allowed interacting states are in energy. Simulation of energy levels is particularly important for weak, local interactions where only specific values of J and K are affected. Since upper state parameters do not generally vary greatly from ground state parameters, the plots can

be calculated approximately at an early stage of an analysis, and give great insight into

the various perturbations which might occur.
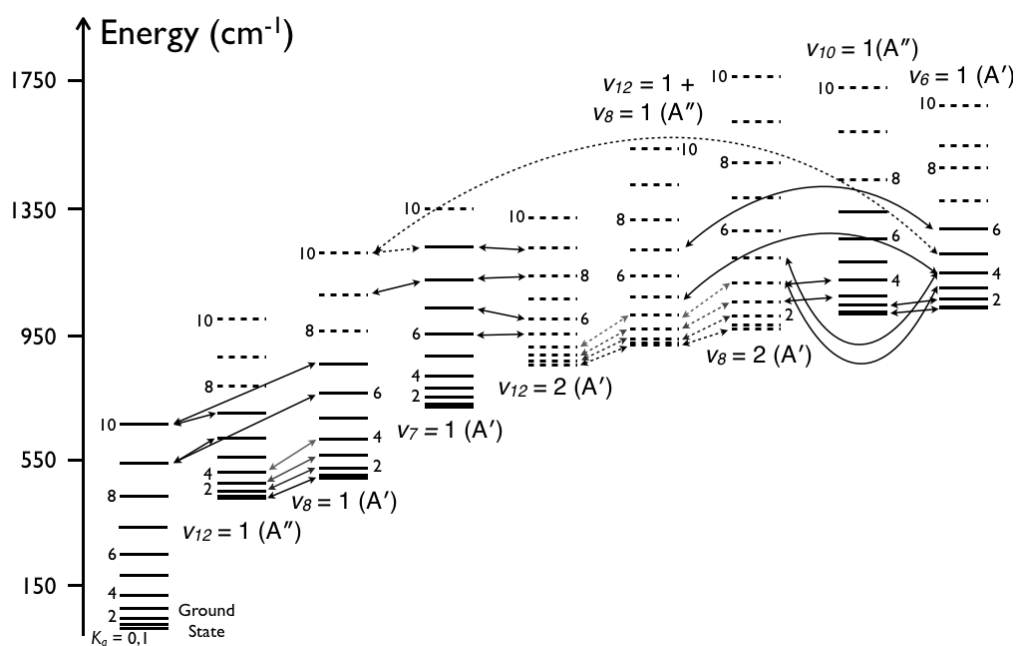
Figure 2.7: Example of an energy levels plot which shows symmetry allowed interaction

occurring between levels of similar energy.

2.2.4 Least-squares fitting

Once the spectra have been assigned accurately, the next stage is fitting. The Hamiltonian

described in section 1.1 can be used to calculate the energies of transitions based on input

molecular parameters and effectively output an assigned spectrum. This process can be

made to work in reverse and an assigned spectrum, based on experimental observation,

can be used to determine the molecular parameters through the process of least-squares fitting. Effectively the fitting software attempts to find minima in the difference between the energies of observed and calculated spectra by iteration of the parameters in the molecular Hamiltonian.

The program used for this during the project was Pickett's SPFIT[19] which uses either the *A*- or *S*-reduction of Watsons's asymmetric rotor Hamiltonian[20] (see section 1.1.3). The efficiency of the fitting program is dependant on the complexity of the Hamiltonian matrix which is to be repeatedly diagonalized, and large numbers of off-diagonal elements can slow calculations. With modern computing power, any slowdown is only noticeable for very complex systems containing multiple coupled modes. The computing power of a standard laptop was only challenged during the final ketenimine analysis (see section 3.3) which involved a co-fitting routine of nine states, all of which were either directly or indirectly coupled to each other.

2.2.5 Residual error plots

Residual error plots, as shown in figure 2.8, effectively map out the error in a fitting routine as a function of the quantum numbers.

This type of plot is particularly useful when fitting complex spectra which contain perturbations. By presenting the fits in this graphical form, it becomes clearer where the fit is performing poorly, and along with energy level diagrams, can be used to diagnose

perturbations and mis-assignments. The magnitude, shape and location of high residual error give insight into the type of interaction, which levels are interacting, and whether they are J-dependant, K-dependant or both.
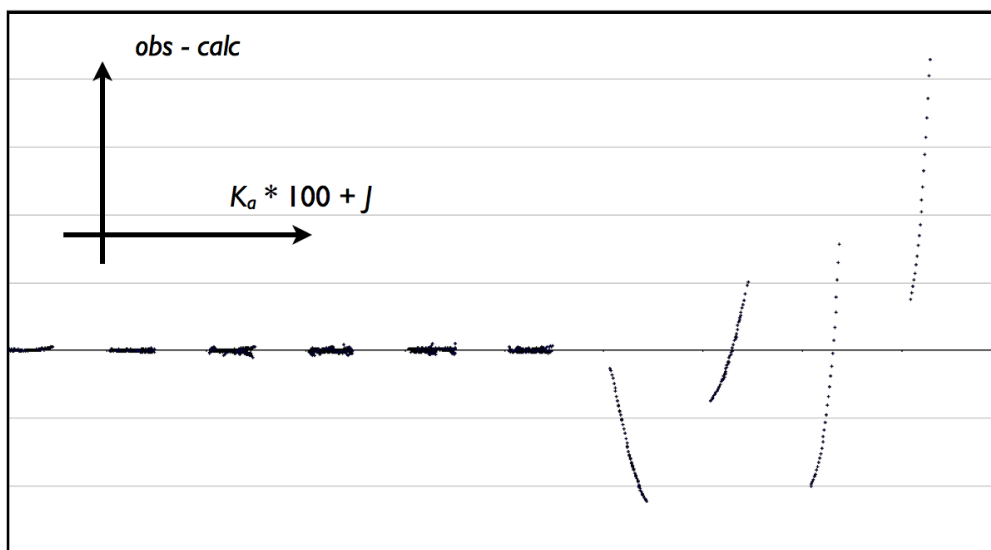
Figure 2.8: Example of a residual error plot taken from the ketenimine v_7 study. The horizontal scale is dependant on the quantity $K_a * 100 + J$ which is chosen since series of common K_a group together while still showing the J dependence of error. This example shows that while series between $K_a = 0$ and 5 are well described without the introduction of perturbation mechanics, higher K_a series cannot be due to local perturbations.

2.2.6 Computational studies

Computational studies serve two major purposes for this project. Firstly, they assist in both the understanding of an approximate form that the spectra should take, as well as the

process of actually fitting the transitions to the Hamiltonian once a spectrum has been assigned. The most useful parameters which can be determined through calculation are the Coriolis coupling parameters, ζ, which play a vital role in the complexity of the ro-vibrational structure. Since this parameter is so pivotal, having at least an approximate idea of what value it should take can assist in the fitting procedure, and it was usually kept fixed at a calculated value early on in an analysis.

The second use of computational studies is for comparison upon a successful assignment and fitting. The calculations build a theoretical groundwork which generally should compare well to any experimental values obtained. Although the accuracy of determined parameters can be quite variable, computational studies can be used to pick up mistakes in analyses, where the comparison between theory and experiment is worse than expected.

Calculations were carried out using the software packages Gaussian09[21] and GAMESS[22]. These programs were used in conjunction with the NCI and Monash Sun-grid supercomputer facilities, which allow the complexity of the calculations to be vastly greater than what could be achieved using a standard desktop computer. Coriolis coupling constants were extracted from the GAMESS outputs by the harmonic force field analysis program VIBCA[23] (these were explicitly stated in the Gaussian09 output). Other parameters which were determined included IR activity and mode energies, which were particularly useful when attempting to record spectra.

2.3 Molecules of interest

2.3.1 Selection criteria
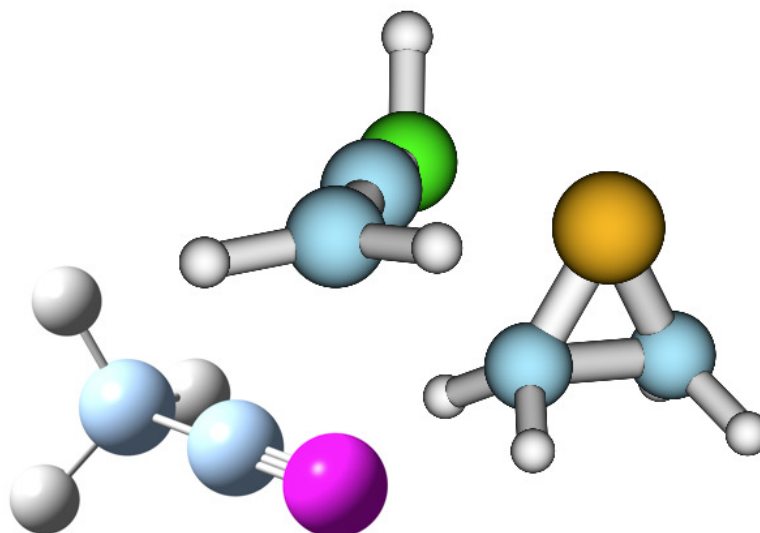
Figure 2.9: Target molecules ketenimine (top), 1-phosphapropyne (left) and thiirane (right) molecules, with structure determined by density functional theory optimization routine. CH_3CP rendered using Molden[24].

The molecules to be studied were selected based on the following criteria

- Does the molecule have low energy modes which are the most likely to be thermally populated in interstellar systems? Utilizing the high FIR flux to observe

modes which were previously uncharacterized at high-resolution was one of the major goals of the project.

- Does the molecule have some astrophysical significance? This either means that the molecule has already been detected in the interstellar medium or a case can be made for possible future detection. Determination of molecular parameters for use in interstellar detection was another major goal of the project.

- Does the molecule exhibit interesting and/or novel coupling dynamics? The investigation of intensity stealing and Coriolis coupling dynamics in molecules in general became a major goal of the project.

2.3.2 Ketenimine

Ketenimine (CH_2CNH) is a molecule of astrophysical importance and has been located in the star forming region Sagittarius B2(N)[25]. This molecule was predicted to be a part of the interstellar medium due to the abundance of the tautomer acetonitrile (CH_3CN). Ketenimine has been postulated as the product of low-temperature reactions in ices relevant to the chemistry of Titan, comets and the interstellar medium[26], and has been shown to be effectively stable under the conditions in these regions[26,27]. Very recent observations of Pluto's atmosphere has also determined that it likely contains small nitrogen containing organic compounds[28], and reactions involving ketenimine may be relevant in explaining this low temperature chemistry. In the laboratory however, ketenimine readily tautomerises to the more stable acetonitrile configuration and spectra generally need to be recorded within a second of generation.

This asymmetric top molecule was the first to be analyzed in this project, and due to highly coupled ro-vibrational spectra, was the most challenging. The analysis of ketenimine ranged from the FIR pure rotational spectra starting at approximately $10 \, \text{cm}^{-1}$ to the ν_{10} mode which is located at just over $1000 \, \text{cm}^{-1}$. Three separate analyses were performed on this molecule[29,30], which were separated by natural breaks or weakness in the Coriolis interaction. The initial aim was to determine the structural parameters for the low-energy modes since these were most likely to be populated in interstellar systems, however due to the interesting coupling mechanics exhibited by the molecule, higher energy modes were also recorded and analyzed.

The studies of ketenimine have covered a full range of common, uncommon, and previously uncharacterized manifestations of Coriolis coupling, including;

- Strong coupling.

- Localized coupling.

- Coupling of the ground state.

- Coupling with multiple theoretically described dark-state systems, which are themselves strongly coupled.

- Coupling facilitated by bridging mechanisms.

- Intensity stealing mechanisms which are strong enough that they can provide effectively IR inactive modes with observable intensity.

Ketenimine, in a nutshell, is the "perfect storm" with coupling so intense that novel intensity stealing dynamics could be observed and characterized for the first time for inclusion in the literature. The first observation of weak modes which are only observable because of this intensity stealing serves as an example of the quality of the synchrotron source in the FIR.

2.3.3 1-phosphapropyne

1-phosphapropyne (CH_3CP) belongs to a class of compounds characterized by the C≡P triple bond, that have only recently had their chemistry thoroughly investigated[31]. All but the simplest of these (HCP) are unstable at room temperature, and require constant cooling at dry ice temperature to avoid degradation. 1-phosphapropyne has not been located in the interstellar medium, however molecules with the characteristic CP bond such as CP[32], HCP[33] and CCP[34] have been observed. The abundance of the iso-electric *N* analogue acetonitrile (CH_3CN) may also be a clue as to the possible formation of 1-phosphapropyne. The instability of the molecule at high temperature implies that the molecule is most likely to be located in colder regions of the interstellar medium.

The lowest energy v_8 mode of 1-phosphapropyne at 308 cm^{-1} was the primary target of the study[35], however the v_7 mode at 693 cm^{-1} was also analyzed, since it had not been previously observed in the gas phase. The enhanced FIR flux of the synchrotron source would allow us to observe the ro-vibrational structure of v_8 mode and its associated hot-bands.

The 1-phosphapropyne spectrum is also affected by strong Coriolis coupling mechanics which act to split the ro-vibrational energies of degenerate modes. Another form of coupling specific to symmetric rotors, l-coupling, was also observed and played a major role in the analysis. The analysis of the v_8 hot-band serves as an example of a complex transition for which both the upper and lower states are degenerate and highly coupled by both mechanisms. There are few examples of such a transition in the literature for molecules of this symmetry[36].

2.3.4 Thiirane

Thiirane (c-C_2H_4S) is a known spontaneous product of the reaction between ethylene and activated sulfur atoms[37], as is the case for the O analogue oxirane[38,39]. Oxirane has been located in the interstellar medium[38,40], and due to its similar thermodynamic properties, thiirane can be postulated as a probable component as well. Activated sulfur atoms are known to be produced by photolysis of known interstellar molecules[41], and are implicated in the chemistry of many known sulfur containing molecules[42].

The high-resolution spectroscopy of thiirane has been largely neglected, and the lowest energy modes around 650 cm^{-1} have not previously been observed at high-resolution. The modes to be analyzed are strongly Coriolis coupled, and a variation of the intensity stealing mechanic which was observed in the ketenimine analyses[29] was also observed, somewhat unexpectedly, in this system. As is the case with the previous analyses, the

increased flux in the FIR allows for the observation of the modes enhanced by intensity stealing.

2.4.5 Chlorodifluoromethane

High-resolution spectroscopy is also a useful technique for monitoring the concentrations of known greenhouse gases in the earth's atmosphere. A contribution was made during this project to the analysis of the v_5 mode of the ^{37}Cl isomer of chlorodifluoromethane ($CH^{37}ClF_2$), and this is presented as new work in what was primarily a review article[43].

References

[1] G. Geloni, V. Kocharyan, E. Saldin, E. Schneidmiller, and M. Yurkov, Nucl. Instrum. Meth. A, **605** (3), 409- 429 (2009).

[2] D. Creagh, M. Tobin, A. Broadbent, and J. McKinlay, AIP Conf. Proc. **879** (1), 615- 618 (2007).

[3] C. Medcraft, D. Appadoo, A. Wong, E. G. Robertson, and D. McNaughton, (Article not yet submitted).

[4] *Bruker IFS 125HR User Manual*, 1st ed. (Bruker Optics, 2006).

[5] P. Fellgett, J. Phys. Radium **19** (3), 237 (1958).

[6] W. Herres and J. Gronholz, in *Understanding FT-IR Data Processing*.

[7] P. Jacquinot, J. Opt. Soc. Am. **44** (10), 761 (1954).

[8] J. U. White, J. Opt. Soc. Am. **32** (5), 285 (1942).

[9] J. M. Hollas, *High Resolution Spectroscopy*. (Wiley: Chichester, 1998).

[10] T. J. Balle and W. H. Flygare, Rev. Sci. Instrum. **52** (1), 33 (1981).

[11] J. Grabow, in *Handbook of High-Resolution Spectroscopy*, edited by M. Quack and F. Merkt (Wiley, 2011).

[12] B. Pate, (see http://faculty.virginia.edu/bpate-lab/Frequency%20Domain/BroadBand/BB%20FTMW.html).

[13] D. McNaughton, in *Handbook of Vibrational Spectroscopy* (John Wiley & Sons Ltd., 2002), Vol. 1.

[14] A. R. W. McKellar, J. Mol. Spec. **262** (1), 1.

[15] R. F. Curl, F. Capasso, C. Gmachl, A. A. Kosterev, B. McManus, R. Lewicki, M. Pusharsky, G. Wysocki, and F. K. Tittel, Chem. Phys. Lett. **487** (1–3), 1.

[16] G. Hancock, G. Ritchie, J.-P. v. Helden, R. Walker, and D. Weidmann, Op. Eng. **49** (11), 111121.

[17] G. Ramian, (see http://sbfel3.ucsb.edu/www/fel_table.html).

[18] D. McNaughton, D. McGilvery, and F. Shanks, J. Mol. Spec. **149** (2), 458 (1991).

[19] H. M. Pickett, J. Mol. Spec. **148** (2), 371 (1991).

[20] J. K. G. Watson, in *Vibrational Spectra an Structure*, edited by J. R. Durig (Elsevier scientific publishing company, 1977), Vol. 6.

[21] M. J. Frisch, G. W. Trucks, H. B. Schlegel, G. E. Scuseria, M. A. Robb, J. R. Cheeseman, G. Scalmani, V. Barone, B. Mennucci, G. A. Petersson, H. Nakatsuji, M. Caricato, X. Li, H. P. Hratchian, A. F. Izmaylov, J. Z. Bloino, G.;, J. L. Sonnenberg, M. Hada, M. Ehara, K. Toyota, R. Fukuda, J. Hasegawa, M. Ishida, T. Nakajima, Y. Honda, O. Kitao, H. Nakai, T. Vreven, J. Montgomery, J. A.;, J. E. Peralta, F. Ogliaro, M. Bearpark, J. J. Heyd, E. Brothers, K. N. Kudin, V. N. Staroverov, R. Kobayashi, J. Normand, K. Raghavachari, A. Rendell, J. C. Burant, S. S. Iyengar, J. Tomasi, M. Cossi, N. Rega, N. J. Millam, M. Klene, J. E. Knox, J. B. Cross, V. Bakken, C. Adamo, J. Jaramillo, R. Gomperts, R. E. Stratmann, O. Yazyev, A. J. Austin, R. Cammi, C. Pomelli, J. W. Ochterski, R. L. Martin, K. Morokuma, V. G. Zakrzewski, G. A. Voth, P. Salvador, J. J. Dannenberg, S. Dapprich, A. D. Daniels, Ö. Farkas, J. B. Foresman, J. V. Ortiz, J. Cioslowski, and D. J. Fox, Gaussian, Inc., Wallingford CT, 2009.

22   M. W. Schmidt, K. K. Baldridge, J. A. Boatz, S. T. Elbert, M. S. Gordon, J. H. Jensen, S. Koseki, N. Matsunaga, K. A. Nguyen, S. Su, T. L. Windus, M. Dupuis, and J. A. Montgomery Jr., J. Comput. Chem. **14** (11), 1347 (1993).

23   Information for VIBCA and FCONV can be found at: http://info.ifpan.edu.pl/~kisiel/vibr/vibr.htm#vibca.

24   G. Schaftenaar and J. H. Noordik, J. Comput. Aided Mol. Design **14**, 123 (2000).

25   F. J. Lovas, J. M. Hollis, A. J. Remijan, and P. R. Jewell, ApJ. **645** (2), L137 (2006).

26   R. L. Hudson and M. H. Moore, Icarus **172** (2), 466 (2004).

27   A. Doughty, G. B. Bacskay, and J. C. Mackie, J. Phys. Chem. **98** (51), 13546 (1994).

28   S. A. Stern, N. J. Cunningham, M. J. Hain, J. R. Spencer, and A. Shinn, Astron. J. **143** (1), 22.

29   M. K. Bane, C. D. Thompson, E. G. Robertson, D. R. T. Appadoo, and D. McNaughton, Phys. Chem. Chem. Phys. **13**, 6793 (2011); M. K. Bane, E. G. Robertson, C. D. Thompson, D. R. T. Appadoo, and D. McNaughton, J. Chem. Phys. **135** (22), 224306 (2011).

30   M. K. Bane, E. G. Robertson, C. D. Thompson, C. Medcraft, D. R. T. Appadoo, and D. McNaughton, J. Chem. Phys. **134** (23), 234306 (2011).

31   J.-C. Guillemin, T. Janati, and J.-M. Denis, J. Org. Chem. **66** (23), 7864 (2001); C. Jones and A. Richards, J. Org. Chem. **645**, 256 (2002); C. Jones and M. Waugh, J. Org. Chem. **692**, 5086 (2007); C. Jones, C. Schulten, and A. Stasch, Dalton Trans. (31), 3733 (2006); C. Jones, C. Schulten, and A. Stasch, Dalton Trans. (19), 1929 (2007); C. Jones, C. Schulten, and A. Stasch, Inorg. Chem. **47** (4), 1273 (2008); S. L. Choong, C. Jones, and A. Stasch, Dalton Trans. **39** (25), 5774 (2010).

32   M. Guelin, J. Cernicharo, G. Paubert, and B. E. Turner, A&A **230**, L9 (1990).

33   A. N. Marcelino, C. José and G. l. Michel, ApJ. Lett. **662** (2), L91 (2007).

34   D. T. Halfen, D. J. Clouthier, and L. M. Ziurys, ApJ. Lett. **677** (2), L101 (2008).

35   M. K. Bane, C. Jones, S. L. Choong, C. D. Thompson, P. D. Godfrey, D. R. T. Appadoo, and D. McNaughton, J. Mol. Spec. **275** (276), 9 (2012).

36   G. Graner, J. Mol. Spec. **161** (1), 58 (1993).

37   F. Leonori, R. Petrucci, N. Balucani, P. Casavecchia, M. Rosi, D. Skouteris, C. Berteloite, S. b. D. Le Picard, A. Canosa, and I. R. Sims, J. Phys. Chem. A **113** (52), 15328 (2009).

38   J. E. Dickens, W. M. Irvine, M. Ohishi, M. Ikeda, S. Ishikawa, A. Nummelin, and A. Hjalmarson, ApJ **489** (2), 753 (1997).

39   C. Patrice, B. Jean-Michel, N. Rafael, and R. Franacois, ApJ **598** (1), 700 (2003).

40   A. Nummelin, J. E. Dickens, P. Bergman, A. Hjalmarson, W. M. Irvine, M. Ikeda, and M. Ohishi, A&A **337** (1), 275 (1998); M. Ikeda, M. Ohishi, A. Nummelin, J. E. Dickens, P. A. H. Bergman, and W. M. Irvine, ApJ **560**, 792 (2001); M. A. Requena-Torres, J. Martín-Pintado, S. Martín, and M. R. Morris, ApJ **672**, 352 (2008).

41   J. Steadman and T. Baer, The Journal of Chemical Physics **89** (9), 5507 (1988); J. R. Appling, M. R. Harbol, R. A. Edgington, and A. C. Goren, The Journal of Chemical Physics **97** (6), 4041 (1992); S. T. Pratt, Phys. Rev. A **38** (3), 1270 (1988).

[42] M. Oppenheimer and A. Dalgarno, ApJ, **187**, 231 (1974).

[43] D. McNaughton, E. G. Robertson, C. D. Thompson, T. Chimdi, M. K. Bane, and D. Appadoo, Anal. Chem. **82** (19), 7958.

Chapter 3

Publications

Declaration for Thesis Chapter 3.1

Declaration by candidate

In the case of Chapter 3.1, the nature and extent of my contribution to the work was the following:

Nature of contribution	Extent of contribution (%)
Initiation, key ideas, development, writing up	80

The following co-authors contributed to the work. Co-authors who are students at Monash University must also indicate the extent of their contribution in percentage terms:

Name	Nature of contribution	Extent of contribution (%) for student co-authors only
C. D. Thompson	Initiation, key ideas	
E. G. Robertson	Initiation, key ideas	
D. R. T. Appadoo	Experiment assistance	
D. McNaughton	Initiation, key ideas	

Candidate's Signature	Date

Declaration by co-authors

The undersigned hereby certify that:

(1) the above declaration correctly reflects the nature and extent of the candidate's contribution to this work, and the nature of the contribution of each of the co-authors.
(2) they meet the criteria for authorship in that they have participated in the conception, execution, or interpretation, of at least that part of the publication in their field of expertise;
(3) they take public responsibility for their part of the publication, except for the responsible author who accepts overall responsibility for the publication;
(4) there are no other authors of the publication according to these criteria;
(5) potential conflicts of interest have been disclosed to (a) granting bodies, (b) the editor or publisher of journals or other publications, and (c) the head of the responsible academic unit; and
(6) the original data are stored at the following location(s) and will be held for at least five years from the date indicated below:

Location(s)	Monash University, School of Chemistry

Signature 1		Date
Signature 2		20·8·12
Signature 3		
Signature 4		

PCCP

Physical Chemistry Chemical Physics
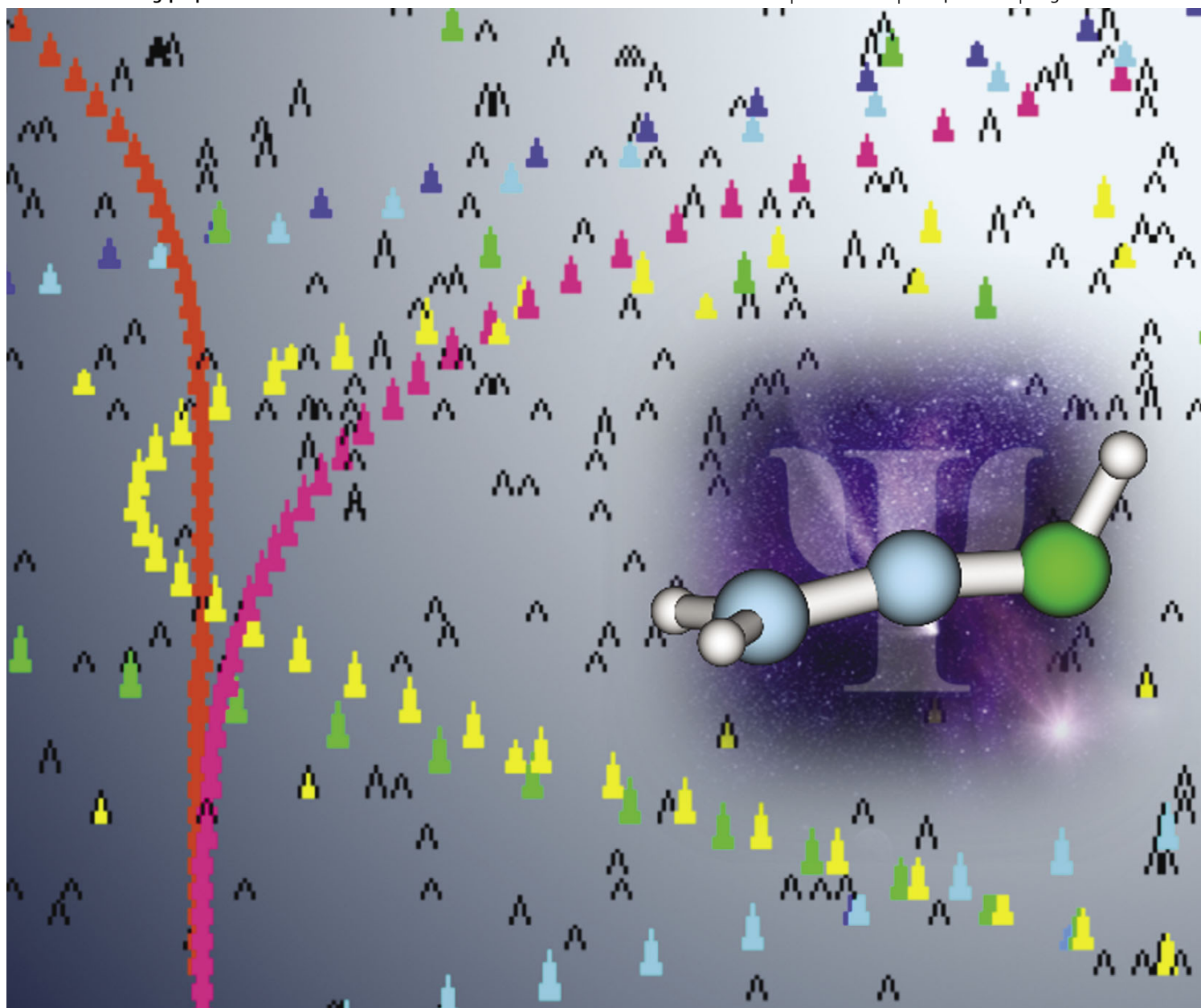
COVER ARTICLE
McNaughton *et al.*
High-resolution FTIR spectroscopy
of the ν_8 and Coriolis perturbation
allowed ν_{12} bands of ketenimine

HOT ARTICLE
Endres *et al.*
An *in situ* STM/AFM and impedance spectroscopy study of the extremely
pure 1-butyl-1-methylpyrrolidinium tris(pentafluoroethyl)trifluorophosphate/
Au(111) interface

High-resolution FTIR spectroscopy of the ν_8 and Coriolis perturbation allowed ν_{12} bands of ketenimine†‡

Michael K. Bane,[a] **Christopher D. Thompson,**[a] **Evan G. Robertson,**[b]
Dominique R. T. Appadoo[c] **and Don McNaughton***[a]

High resolution FTIR spectra have been recorded in the region 250–770 cm^{-1} using synchrotron radiation and over 2000 transitions to the ν_8 and ν_{12} states of the short lived species ketenimine have been assigned. Ground state combination differences combined with published microwave transitions were used to refine the constants for the ground vibrational state. Rotational and centrifugal distortion parameters for the $v_8 = 1$ and $v_{12} = 1$ levels were determined by co-fitting transitions, and treating a strong *a*-axis Coriolis interaction. Selection rules for the observed ν_{12} transitions indicate that they arise solely from "perturbation allowed" intensity resulting from this Coriolis interaction.

Introduction

Ketenimine ($H_2C{=}C{=}NH$, Fig. 1), a short lived molecule of *ca.* 1 s lifetime, was first generated and studied in the gas phase by microwave spectroscopy[1,2] and subsequently by photo-electron spectroscopy.[3] Its gas phase infrared spectrum was later recorded and analyzed at low resolution[4] but due to the complexity of its high-resolution spectrum no further analysis was undertaken. Due to it being a structural isomer of acetonitrile ($H_3CC{\equiv}N$), a known interstellar molecule, ketenimine was predicted to be a likely chemical component of the interstellar medium and in 2006 was located by Lovas *et al.*[5] in the star forming region Sagittarius B2(N) by observing microwave emissions predicted from a previous microwave study.[2]

Ketenimine has 12 vibrational modes belonging to A′ and A″ symmetry. Its initial, tentative identification by Jacox and Milligan[6] was later confirmed by Jacox[7] using low resolution
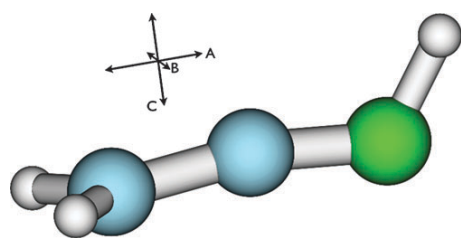
Fig. 1 Ketenimine molecule with internal axes labeled and a B3LYP/cc-pVTZ optimized geometry.

[a] School of Chemistry, Monash University, Wellington Rd, Clayton, Victoria 3800, Australia. E-mail: Donald.McNaughton@monash.edu
[b] Department of Chemistry, La Trobe University, Bundoora, Victoria 3086, Australia
[c] Australian Synchrotron, 800 Blackburn Rd, Clayton, Victoria 3168, Australia
† This article was submitted as part of an issue to coincide with Faraday Discussion 150: Frontiers in Spectroscopy.
‡ Electronic supplementary information (ESI) available: Least-squares fit file output leading to the constants in Table 2. See DOI: 10.1039/c0cp01816c

matrix isolation vibrational and electronic spectroscopic techniques. The gas phase vibrational spectrum and assignment of modes are presented by August,[4] and these assignments are reproduced in Table 1. The first rotational constants from a microwave study performed by Rodler *et al.*[1] were subsequently revised to account for a mis-assignment in a later rotation–inversion study by Rodler *et al.*[2] The rotational spectrum contained both *a*-type and *c*-type transitions, with the analysis resulting in the ground state (G. S.) structural parameters shown in Table 2. A small inversion splitting was observed in the microwave study of Rodler *et al.*,[2] however inversion splitting was not resolved in this work and hence the symmetry group is assumed to be C_s.

Molecules of a similar structure to ketenimine have been shown to exhibit a high degree of Coriolis coupling, and consequently a complex ro-vibrational structure, particularly in their lowest energy modes. Some of these molecules include the iso-electronic asymmetric rotors ketene[8] ($H_2C{=}C{=}O$) and thioketene[9] ($H_2C{=}C{=}S$) and extend to the asymmetric rotors methyleneimine[10] ($H_2C{=}NH$), formaldehyde[11] ($H_2C{=}O$) and thioformaldehyde[12] ($H_2C{=}S$). This trend is expected to continue in ketenimine and subsequently all coupled modes must be co-fitted with the perturbations properly accounted for.

In this work we present the assignment and analysis of the Coriolis coupled lowest energy modes of ketenimine, ν_8 and ν_{12}. In order to derive an improved set of ground state rotational constants we have first refitted the microwave data together with ground state combination differences from our analysis.

Experimental

Ketenimine, a transient species, was generated by flow pyrolysis of 3-hydroxypropionitrile as described by Rodler *et al.*[1] The oven temperature was maintained at $\sim$1100 °C to ensure that the precursor was completely decomposed. The sample was pumped through a multi-pass White cell at a rate high enough to ensure that the amount of the more stable

Table 1 Summary of the observed vibrational modes of ketenimine

Wavenumber[a]	Wavenumber[b]	IR intensity[c]	Assignment[a]
3321.8	3347.9	0.425	ν_1 (A′) NH str.
3155			$\nu_3 + \nu_5$
—	3129.5	0.018	ν_9 (A″) CH_2 a. str.
—	3047.9	0.198	ν_2 (A′) CH s. str.
2128.4			$\nu_5 + \nu_6$
2037	2045.4	9.382	ν_3 (A′) C=C=N str.
1959			$2\nu_6$
1355	1385.7	0.121	ν_4 (A′) CH_2 def.
1127	1124.9	0.455	ν_5 (A′) C=C=N str.
1004	993.3	5.055	ν_6 (A′) CNH bend
—	967.0	0.003	ν_{10} (A″) CH_2 rock
872	868.5	1.258	ν_{11} (A″) torsion
—	692.0	2.170	ν_7 (A′) CH_2 wag
466.454373[d]	470.1	0.512	ν_8 (A′) C=C=N in-plane bend
409.035997[d]	406.6	0.008	ν_{12} (A″) C=C=N out of plane bend

[a] From previous work.[4] [b] Mode energies determined by B3LYP/cc-pVTZ GAMESS calculation and VIBCA. [c] IR intensity in units of D^2 Å^{-2} amu^{-1} determined by B3LYP/cc-pVTZ GAMESS calculation. [d] From this work.

Table 2 Fitted band parameters to Watson's S-reduced I^r Hamiltonian for the G. S., $v_8 = 1$ and $v_{12} = 1$ modes of ketenimine. Presented in frequency units for consistency with previous work (wavenumber values of band-centers given in Table 1)

Constant	G. S.[a]	G. S.[b]	G. S.[c]	ν_{12}	ν_8
Band centre/GHz	—	—	—	12 262.5907 (18)[d]	13 983.95031 (66)
A/MHz	201 445.47 (4)	201 445.322 (45)	204 523.235	195 716 (23)	203 636 (22)
B/MHz	9663.144 (2)	9663.1408 (13)	9744.0295	9698.198 (67)	9670.8614 (99)
C/MHz	9470.126 (1)	9470.1213 (13)	9555.0030	9482.266 (70)	9492.709 (10)
D_J/kHz	3.032 (6)	2.9806 (15)	2.8260	3.1061 (16)	3.00455 (66)
D_{JK}/kHz	233.1 (3)	231.93 (19)	235.76	−18.15 (43)	448.84 (19)
D_K/kHz	10 128 (19)	10 031 (48)	9866	1730 (71)	23 480 (69)
d_1/kHz	−0.071 (4)	−0.0662 (20)	−0.0586	−0.0662[e]	−0.04895 (77)
d_2/kHz	−0.004 (2)	—	−0.002		
H_{JK}/kHz	—	0.00091 (11)		0.00091[e]	0.000553 (38)
H_{KJ}/kHz	−0.19 (2)	−0.2841 (95)		−0.2841[e]	−0.2799 (53)
G^a/MHz					307 575 (64)
$\eta_k{}^a$/MHz					−88.00 (50)
F^a/MHz					3.3644 (26)
J(max)	24	54		49	54
K_a(max)	4	7		7	7
Number trans.	29	680[f]		666	1359
σ_{dev}		0.386		1.544	

[a] From previous work.[2] [b] G. S. fitted from published microwave lines and combination differences from the ν_8 band. [c] Parameters determined by B3LYP/cc-pVTZ GAMESS calculation and VIBCA. [d] Figures in brackets are one standard deviation according to the least squares fit in units of the least significant figure quoted. [e] Parameter constrained to G. S. value. [f] Comprised of 29 microwave lines and 651 IR combination differences.

acetonitrile conformation was minimized. The tautomerization of ketenimine to acetonitrile was studied by theoretical methods by Doughty *et al.*[13] From the microwave studies it was expected that the half-life of ketenimine in the cell would be *ca.* 1 s.

The experiment was performed at the Australian synchrotron, using the infrared synchrotron edge radiation continuum source and a Bruker IFS 125HR spectrometer capable of achieving an unapodised resolution of 0.00096 cm^{-1}. The high Far-IR flux of the synchrotron source ensured sufficient sensitivity for assignment of the weak ν_{12} band. The ν_8 band was measured using a KBr beam-splitter and silicon–boron bolometer and the ν_{12} band with a 6-micron Mylar beam-splitter and silicon bolometer. The pressure within the cell was maintained at approx. 0.3 mbar for the ν_8 band and doubled for the ν_{12} band, with an optical path-length of 24 m and a temperature assumed to be 300 K. Spectra were apodized using the 4P function. Overall 57 and 23 high-resolution

spectra of 0.00096 cm^{-1} and 0.002 cm^{-1} resolution were averaged and post zero-filled by a factor of 8 to obtain the final ν_8 and ν_{12} spectra respectively. Due to the high sample throughput required to reduce the residence time of the pyrolysis products in the cell the resolution of the ν_{12} spectrum was reduced to increase the number of completed scans before the sample was depleted. The spectra were calibrated by comparison with water line positions from the HITRAN database.[14]

Computational details

It was considered important to obtain calculated values of the centrifugal distortion and Coriolis coupling constants as a guide for fitting and for comparison with a successful fit. Density functional theoretical calculations were carried out using GAMESS[15] at the B3LYP level with a cc-pVTZ basis set. The program FCONV[16] was then used to convert the

6794 | *Phys. Chem. Chem. Phys.*, 2011, **13**, 6793–6798

This journal is © the Owner Societies 2011

GAMESS output for use with another program VIBCA.[16] VIBCA is a harmonic force field analysis program which produces "ζ-matrices" describing the a-axis, b-axis and c-axis Coriolis interactions between all vibrational modes as one of its outputs. The ground state rotational and some centrifugal constants, as well as the scaled band centres (scaling factor of 0.965) of all 12 modes are predicted by VIBCA. The GAMESS output alone predicted IR intensities.

Results

The spectral region between 770–250 cm^{-1} was recorded in two separate spectral scans which are shown in Fig. 2. The IR intensity ratio of ν_8/ν_{12} was calculated from the DFT predictions as approximately 64 : 1, with ν_{12} having very low IR intensity of 0.008 D^2 Å^{-2} amu^{-1}.

ν_8, the lowest in-plane bending mode, has A$'$ symmetry corresponding to an a-type mode with selection rules eo $\leftrightarrow$ ee and oe $\leftrightarrow$ oo ($\Delta K_a = 0, \pm 2 \ldots, \Delta K_c = \pm 1, \pm 3 \ldots$). The ν_8 spectrum was peak-picked and presented in the Loomis–Wood format using MacLoomis,[17] which groups regularly spaced lines, such as those differing in J but sharing the constant K_a, into approximately vertical series of the constant K_a. Presenting the spectra in this way allowed the series between $K_a = 0$ and 7 to be assigned, with J(max) = 54. Overall 1359 rovibrational transitions were assigned from this mode, and given uncertainty 0.0002 cm^{-1} (10% of the FWHM of the peak) in the fitting procedure. These assignments were confirmed by comparison with ground state combination differences generated from the known ground state constants. However the difference between calculated and experimental values became increasingly inaccurate at higher J and K_a, and therefore further treatment of the ground state was needed.

The ground state combination differences for the ν_8 mode were added to the 29 microwave lines from Rodler *et al.*[1] and fitted to Watson's S-reduced rotor Hamiltonian in the I^r representation using Pickett's SPFIT[18] to give a higher range of K_a for the ground state fit, with results shown in Table 2. By including the combination differences, we were able to determine another sextic centrifugal distortion term, H_{JK}, with acceptable certainty and improve the standard deviations of H_{KJ} by around an order of magnitude. Also it was found that the d_2 term was not required to fit these transitions, and it was removed since it could not be fitted with an acceptable certainty. It was found that by improving the ground state parameters, the standard deviation of the excited state fits was substantially reduced.

The out of plane bending mode, ν_{12}, has A$''$ symmetry corresponding to a b-type band with selection rules eo $\leftrightarrow$ oe and ee $\leftrightarrow$ oo ($\Delta K_a = \pm 1, \pm 3 \ldots, \Delta K_c = \pm 1, \pm 3 \ldots$). This band was also peak-picked, and displayed in Loomis–Wood format to aid assignment. It was found by comparison to known transitions[19] that a large proportion of the transitions recorded in the spectrum were due to the presence of small amounts of acetonitrile with the ν_8 mode of acetonitrile centered at 365 cm^{-1}. The remaining transitions were confirmed to be ketenimine using ground state combination differences. SPFIT[18] was then used to perform a least-squares fit to Watson's S-reduced rotor Hamiltonian in the I^r
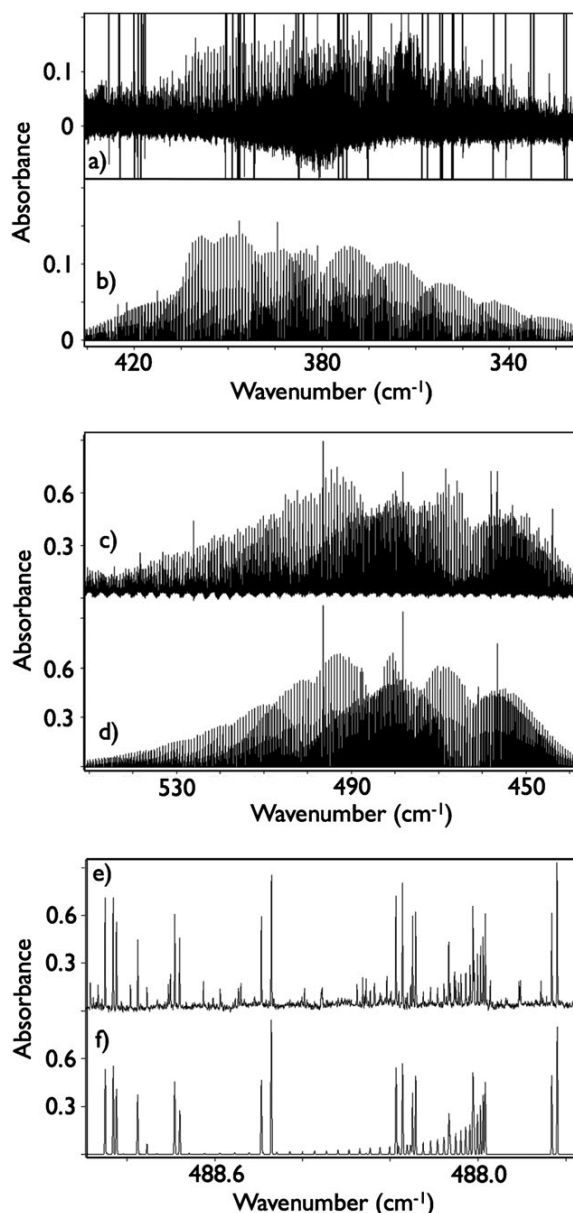
Fig. 2 Survey spectra of (a) ν_{12} experimental spectrum, (b) ν_{12} simulation, (c) ν_8 experimental, (d) ν_8 simulation. (e) (exp) and (f) (sim) show an example of the agreement between experiment and simulation. (a) contains intense q-branch sub-bands belonging to the ν_8 mode of acetonitrile at approx. 365 cm^{-1} which do not appear in the simulation. (e) contains a hot-band structure which does not appear in the simulation. A region of high noise centered approx. 380 cm^{-1} is attributed to the beam-splitter, and could not be removed. Additional lines due to residual water.

representation. When the b-type transitions were input into SPFIT assuming b-type selection rules an acceptable fit could not be achieved. However, it was found that these lines did fit well if it was assumed that K_a did not change over the transition. From this we explored the possibility that these lines were enhanced *via* a Coriolis intensity stealing mechanism. The selection rules for an a-type transition moment being

shared *via* an *a*-axis Coriolis interaction are ee $\leftrightarrow$ ee and oo $\leftrightarrow$ oo ($\Delta K_a = 0, \pm 2 \ldots, \Delta K_c = 0, \pm 2 \ldots$), which is consistent with ΔK_a being fixed. After modification of the upper state quanta to reflect the new selection rules, 666 transitions were assigned, with K_a between 2 and 7 and $J(\text{max}) = 49$. These lines were then co-fit with the ν_8 transitions of ketenimine to give the parameters shown in Table 2. The *d* and *H* terms in the ν_{12} mode were constrained to their ground state values, whilst the *D* parameters were allowed to vary. The ground state and excited state fits are available as ESI.‡

Discussion

Simulation of the ν_{12} spectrum with these fitted parameters allowed us to confirm the nature of the observed ν_{12} transitions. Simulated spectra were achieved by inputting the fitted parameters into Pickett's prediction software SPCAT.[18] The resulting calculated transitions were then convolved with a Gaussian line shape, with appropriate FWHM (0.00096 cm^{-1} and 0.002 cm^{-1}) to produce simulated spectra. Firstly, the simulations showed where the natural *b*-type transitions should appear. However, the *b*-type lines were too weak to be observed given the signal-to-noise that was attainable at high resolution. Secondly, the intensities of the observed peaks were independent of the transition dipole moment of the ν_{12} mode, and were still apparent, even if the transition dipole was set to zero. Also it was found that $K_a = 4$ was the most intense sub-band in both the simulation and experimental spectra, which is not consistent with a simple Boltzmann distribution of intensities.

The line strengths, *S*, of two interacting states *X* and *Y* can be summarized by eqn (1) obtained from Mills,[20]

$$S_{X'} = a_k^2 M_X^2 + b_k^2 M_Y^2 + \sigma_\zeta a_k b_k M_X M_Y$$
$$S_{Y'} = a_k^2 M_Y^2 + b_k^2 M_X^2 + \sigma_\zeta a_k b_k M_X M_y \qquad (1)$$

with

$$a_k = [(\Delta_k + \delta)/2\Delta_k]^{1/2}$$

$$b_k = [(\Delta_k - \delta)/2\Delta_k]^{1/2}$$

$$\Delta_k^2 = \delta^2 + 16 A_e^2 k^2 \zeta_{X,Y}^2 \Omega_{X,Y}$$

$$\Omega_{X,Y} = (\omega_X + \omega_Y)(\omega_X \omega_Y)^{-1/2}$$

$$\delta = \omega_X - \omega_Y$$

where *M* is the unperturbed transition dipole moment, *k* is the *z*-projection of angular momentum quantum number, ζ is the Coriolis coupling parameter and ω is the frequency of the interacting mode. The two limiting cases of this Coriolis interaction give insights into the way intensity is distributed between the coupled pair of states. If the product $k^2 \zeta_{X,Y}^2 = 0$, the line strengths reduce to $S_{X'} = M_X^2$ and $S_{Y'} = M_Y^2$, which describes two independent wave-functions as required. As $k^2 \zeta_{X,Y}^2 \gg 0$, $a_k^2 = b_k^2 \cong \frac{1}{2}$ and the line intensities of both perturbed states become equal. This implies that as the product $k^2 \zeta_{X,Y}^2$ increases, intensity is drawn from the least to the most intense mode in the doublet, until they both have equal line strengths. The dependence of a_k^2 and b_k^2 on *k* for ketenimine is shown in Fig. 3.

The ν_{12} spectrum we have obtained is effectively a result of the product $b_k^2 M_8^2$ from eqn (1) being much greater than the product $a_k^2 M_{12}^2$ due to the significantly larger transition dipole moment of the ν_8 mode, the large Coriolis coupling constant, the large value of the *A* rotational constant and the reasonably small energy difference between the coupled modes. Secondly, the intensity distribution which led us to only being able to observe transitions originating from between $K_a = 2$ and 7 of ν_{12} can be explained by the *k* dependence of Coriolis intensity stealing. In fact, the $K_a = 0$ transitions have zero intensity *via* this mechanism. For $K_a > 0$, the non-Boltzmann distribution of intensities is the result of two competing mechanisms, the standard Boltzmann distribution of population in the ground state and the unusual *k* dependence of the dipole moment. This acts to distribute a larger portion of intensity to states with higher *k* than what would be observed with a standard *k*-independent dipole moment. Fig. 3 shows the *k* dependence of the contributions from the "stolen" and "natural" dipole moments, which supports these conclusions. Any value along line (b) in Fig. 3 is lower than the value of line (a) at $k = 1$, implying that any "natural" *b*-type transitions are truly too weak to be detected, since we were unable to detect the $k = 1$ series of the perturbation allowed transitions.

The final fit to the S-reduced Hamiltonian incorporated 2025 transitions and delivered a fit with $\sigma_{\text{dev}} = 1.544$ and the resultant constants are given in Table 2. The larger dataset for the ν_8 mode allowed higher order centrifugal distortion terms to be fitted, whilst for ν_{12} with a smaller dataset, they were held constant. The D_{JK} and D_K constants for ν_8 and ν_{12} differ markedly from the corresponding ground state parameters, and the deviations are of similar magnitude but opposite sign
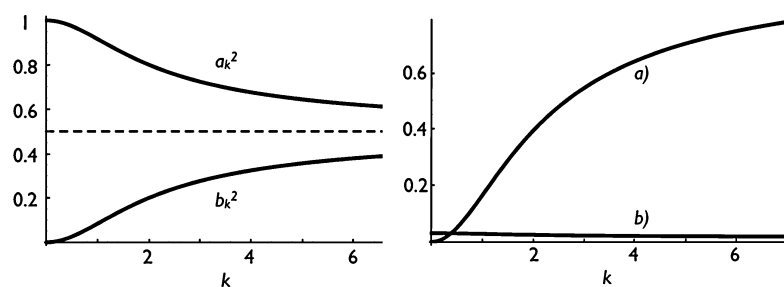
Fig. 3 Variation of a_k^2 and b_k^2 with quantum number *k* (left) and relative contributions to the dipole moment of ν_{12} (right) for ketenimine. Contributions defined as (a) the contribution from the "stolen" dipole moment, $b_k^2 M_8^2/M_\infty$, and (b) from the "natural" dipole moment, $a_k^2 M_{12}^2/M_\infty$, where $M_\infty = \frac{1}{2}(M_8 + M_{12})$ is a normalizing factor. Plots calculated by inputting values from Tables 1 and 2 into eqn (1).

6796 | *Phys. Chem. Chem. Phys.*, 2011, **13**, 6793–6798

This journal is © the Owner Societies 2011
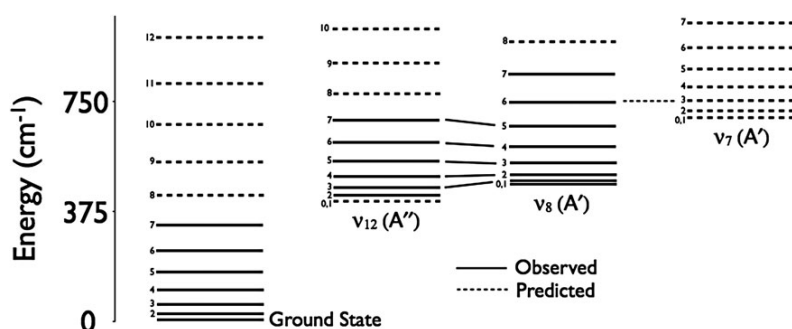
Fig. 4 Calculated energies of the K_a sub-band origins of the lowest energy modes of ketenimine. G. S., $v_8 = 1$ and $v_{12} = 1$ energies calculated from parameters in Table 2. $v_7 = 1$ calculated from theoretical predictions of this band. Some allowed Coriolis interactions between states are indicated.

so that the average value from the two upper states is close to that of the ground state. This is commonly observed when strong resonance interactions are present, particularly when transitions have a restricted range of assigned quantum numbers. In the present case, K_a is limited to 7, so the K_a-dependant terms are highly correlated. Alternative fits allowing all or some of the higher order centrifugal distortion constants to vary gave slightly improved σ_{dev} but values of the centrifugal distortion constants markedly different to those of the ground state. The constants in Table 2 were used in the simulated spectra in Fig. 2 and reproduce the experimental spectra well. A reasonable portion of the error in the excited state fits can be attributed to the possibility of another weak b-type Coriolis interaction with $v_7 = 1$ which has not been treated in this work. A small deviation of approx. 0.0004 cm^{-1} in the residual error at $K_a = 6$, VIBCA calculations ($\zeta^b_{7,8} = 0.0044$) and energy level predictions support this prediction. This potential interaction and some of the allowed first order Coriolis interactions between the energy levels of v_8 and v_{12} are shown in Fig. 4. The a-axis Coriolis interaction parameter, $\zeta^a_{8,12}$, can be calculated from the G^a fitted parameter as 0.7634. This compares favorably with the value calculated by GAMESS and VIBCA of $\zeta^a_{8,12} = 0.7977$. This was obtained using the relationship $G^a_{8,12} \approx 2A\zeta^a_{8,12}$. Additionally, the inclusion of higher order Coriolis interaction parameters $\eta_k{}^a$ and F^a was found to be crucial in lowering the standard deviation of the fit to an acceptable level.

The wavenumber values of the two lowest modes have been included in Table 1 where it can be seen that they agree to be within better than 4 cm^{-1} with the *ab initio* predictions. It can be seen that there are larger discrepancies for the higher modes where the band centres taken from August[4] have been estimated from band profiles only and where the other pyrolysis products, formaldehyde, HCN and CO, confuse the spectrum. We would expect these differences to be minimized on full analysis of these bands.

Conclusion

Ro-vibrational transitions within the Coriolis coupled doublet v_8 and v_{12} have been assigned, and rotational, centrifugal distortion and Coriolis interaction parameters determined by fitting a-type transitions in the v_8 mode and "perturbation allowed" transitions in the v_{12} mode. The rare combination of the transition dipole moment of v_8 being 64 times greater than that of the v_{12} band, the large Coriolis coupling constant, the large A rotational constant and the close proximity of the two interacting modes make ketenimine an ideal candidate for recording, and subsequently analyzing "perturbation allowed" transitions. By analyzing these transitions, we have gained an insight into a state which otherwise would be undetectable due to its very small unperturbed transition dipole moment. The spectral resolution of the study is such that no torsional splittings were observed and therefore the torsional potential function is not changed upon excitation of the two studied here.

References

1 M. Rodler, R. D. Brown, P. D. Godfrey and L. M. Tack, *Chem. Phys. Lett.*, 1984, **110**, 447–451.
2 M. Rodler, R. D. Brown, P. D. Godfrey and B. Kleibömer, *J. Mol. Spectrosc.*, 1986, **118**, 267–276.
3 H. W. Kroto, G. Y. Matti, R. J. Suffolk, J. D. Watts, M. Rittby and R. J. Bartlett, *J. Am. Chem. Soc.*, 1990, **112**, 3779–3784.
4 J. August, *PhD thesis*, Sussex University, 1986.
5 F. J. Lovas, J. M. Hollis, A. J. Remijan and P. R. Jewell, *Astrophys. J.*, 2006, **645**, L137–L140.
6 E. Jacox and D. E. Milligan, *J. Am. Chem. Soc.*, 1963, **85**, 278–282.
7 M. E. Jacox, *Chem. Phys.*, 1979, **43**, 157–172.
8 L. Nemes, D. Luckhaus, M. Quack and J. W. C. Johns, *J. Mol. Struct.*, 2000, **517–518**, 217–226.
9 D. McNaughton, E. G. Robertson and L. D. Hatherley, *J. Mol. Spectrosc.*, 1996, **175**, 377–385.
10 G. Duxbury and M. L. Le Lerre, *J. Mol. Spectrosc.*, 1982, **92**, 326–348.
11 H. H. Blau and H. H. Nielsen, *J. Mol. Spectrosc.*, 1957, **1**, 124–132.
12 P. H. Turner, L. Halonen and I. M. Mills, *J. Mol. Spectrosc.*, 1981, **88**, 402–419.
13 A. Doughty, G. B. Bacskay and J. C. Mackie, *J. Phys. Chem.*, 1994, **98**, 13546–13555.
14 L. S. Rothman, I. E. Gordon, A. Barbe, D. C. Benner, P. F. Bernath, M. Birk, V. Boudon, L. R. Brown, A. Campargue, J. P. Champion, K. Chance, L. H. Coudert, V. Dana, V. M. Devi,

This journal is © the Owner Societies 2011

Phys. Chem. Chem. Phys., 2011, **13**, 6793–6798 | 6797

S. Fally, J. M. Flaud, R. R. Gamache, A. Goldman, D. Jacquemart, I. Kleiner, N. Lacome, W. J. Lafferty, J. Y. Mandin, S. T. Massie, S. N. Mikhailenko, C. E. Miller, N. Moazzen-Ahmadi, O. V. Naumenko, A. V. Nikitin, J. Orphal, V. I. Perevalov, A. Perrin, A. Predoi-Cross, C. P. Rinsland, M. Rotger, M. Simecková, M. A. H. Smith, K. Sung, S. A. Tashkun, J. Tennyson, R. A. Toth, A. C. Vandaele and J. V. Auwera, *J. Quant. Spectrosc. Radiat. Transfer*, 2009, **110**, 533–572.

15 M. W. Schmidt, K. K. Baldridge, J. A. Boatz, S. T. Elbert, M. S. Gordon, J. H. Jensen, S. Koseki, N. Matsunaga, K. A. Nguyen, S. Su, T. L. Windus, M. Dupuis and J. A. Montgomery Jr., *J. Comput. Chem*., 1993, **14**, 1347–1363.

16 Information for VIBCA and FCONV can be found at: http://info.ifpan.edu.pl/∼kisiel/vibr/vibr.htm#vibca.

17 D. McNaughton, D. McGilvery and F. Shanks, *J. Mol. Spectrosc.*, 1991, **149**, 458–473.

18 H. M. Pickett, *J. Mol. Spectrosc.*, 1991, **148**, 371–377.

19 M. Koivusaari, V. M. Horneman and R. Anttila, *J. Mol. Spectrosc.*, 1992, **152**, 377–388.

20 I. M. Mills, *Pure Appl. Chem.*, 1965, **11**, 325–344.

Declaration for Thesis Chapter 3.2

Declaration by candidate

In the case of Chapter 3.2, the nature and extent of my contribution to the work was the following:

Nature of contribution	Extent of contribution (%)
Initiation, key ideas, development, writing up	80

The following co-authors contributed to the work. Co-authors who are students at Monash University must also indicate the extent of their contribution in percentage terms:

Name	Nature of contribution	Extent of contribution (%) for student co-authors only
E. G. Robertson	Initiation, key ideas	
C. D. Thompson	Initiation, key ideas	
C. Medcraft	Experiment assistance	5
D. R. T. Appadoo	Experiment assistance	
D. McNaughton	Initiation, key ideas	

Candidate's Signature	Date

Declaration by co-authors

The undersigned hereby certify that:

(1) the above declaration correctly reflects the nature and extent of the candidate's contribution to this work, and the nature of the contribution of each of the co-authors.
(2) they meet the criteria for authorship in that they have participated in the conception, execution, or interpretation, of at least that part of the publication in their field of expertise;
(3) they take public responsibility for their part of the publication, except for the responsible author who accepts overall responsibility for the publication;
(4) there are no other authors of the publication according to these criteria;
(5) potential conflicts of interest have been disclosed to (a) granting bodies, (b) the editor or publisher of journals or other publications, and (c) the head of the responsible academic unit; and
(6) the original data are stored at the following location(s) and will be held for at least five years from the date indicated below:

Location(s)	Monash University, School of Chemistry

Signature 1		Date 20·8·12
Signature 2		
Signature 3		
Signature 4		
Signature 5		

High-resolution Fourier-transform infrared spectroscopy of the Coriolis coupled ground state and ν_7 mode of ketenimine

Michael K. Bane,[1] Evan G. Robertson,[2] Christopher D. Thompson,[1] Chris Medcraft,[1] Dominique R. T. Appadoo,[3] and Don McNaughton[1,a)]

[1]*School of Chemistry, Monash University, Wellington Rd., Clayton, Victoria 3800, Australia*
[2]*Department of Chemistry, La Trobe University, Bundoora, Victoria 3086, Australia*
[3]*Australian Synchrotron, 800 Blackburn Rd, Clayton, Victoria 3168, Australia*

High resolution FTIR spectra of the short lived species ketenimine have been recorded in the regions 390–1300 cm^{-1} and 20–110 cm^{-1} using synchrotron radiation. Two thousand six hundred sixty transitions of the ν_7 band centered at 693 cm^{-1} and 126 far-IR rotational transitions have been assigned. Rotational and centrifugal distortion parameters for the ν_7 mode were determined and local Fermi and b-axis Coriolis interactions with $2\nu_{12}$ are treated. A further refinement of the ground state, ν_{12} and ν_8 parameters was also achieved, including the treatment of previously unrecognized ac-axis and ab-axis second order perturbations to the ground state. © *2011 American Institute of Physics.* [doi:10.1063/1.3597775]

I. INTRODUCTION

The short lived molecule ketenimine (CH$_2$CNH, Fig. 1) was tentatively identified in a cold matrix by Jacox and Milligan[1] and its identity confirmed using low resolution matrix isolation vibrational and electronic spectroscopic techniques by Jacox.[2] In the gas phase, it was characterized first by microwave spectroscopy[3,4] and subsequently by photoelectron spectroscopy.[5] Since ketenimine is a structural isomer of acetonitrile, a known interstellar molecule, it was predicted to be a probable chemical component of the interstellar medium. In 2006, ketenimine was located by Lovas *et al.*[6] in the star forming region Sagittarius B2(N) by observing microwave emissions predicted from rotational constants determined by the previous microwave study.[4]

The microwave assignment of Rodler *et al.*,[3] was subsequently revised in a later rotation-inversion study by Rodler *et al.*,[4] and those rotational constants have recently been improved by incorporating combination differences from the ν_8 mode into the ground state (G.S.) least-squares fit.[7] A small inversion splitting was observed in the microwave study of Rodler *et al.*,[4] however, in this work we assume the symmetry of the molecule to be C_s since inversion splitting was not resolved, and therefore the normal modes have A$'$ and A$''$ symmetry.

The low frequency modes of ketenimine and molecules of similar structure, such as ketene,[8] thioketene,[9] methyleneimine,[10] formaldehyde,[11,12] and thioformaldehyde,[13] have been shown to exhibit a high degree of Coriolis coupling and consequently complex ro-vibrational structure. The strongly Coriolis coupled ν_{12} and ν_8 modes of ketenimine were analyzed in our previous high-resolution FTIR study,[7] which uncovered an a-axis Coriolis interaction of sufficient strength that the rotational constants of the

very weak ν_{12} mode were determined purely by analyzing transitions with intensities enhanced via Coriolis intensity stealing. A table of all fundamental modes is available in Ref. 7. Perturbations were also located during the analysis of the ν_6 mode of ketenimine in a very recent high resolution (0.005 cm^{-1}) FTIR study by Ito *et al.*,[14] however, due to the complexity of the ro-vibrational structure a satisfactory set of molecular constants for ν_6 could not be derived.

In this work, we present the assignment and analysis of the G.S. and ν_7 mode of ketenimine. Both are perturbed by resonances with the previously studied ν_{12} and ν_8 system of strongly Coriolis coupled modes, and/or their overtones and combination bands (which are also strongly coupled). In order to derive an improved set of ground state, $\nu_{12} = 1$ and $\nu_8 = 1$ rotational constants to adequately fit the new data, we have refitted the microwave data together with the observed pure rotational transitions in the far-IR and ground state combination differences (GSCD) from both this study and the previous high-resolution IR study.[7]

II. EXPERIMENTAL

The transient species ketenimine was generated by flow pyrolysis of 3-hydroxypropionitrile as described previously.[7] Under the experimental conditions formaldehyde, hydrogen cyanide, carbon monoxide, and acetonitrile are also present in varying concentrations depending on the precise experimental conditions. Acetonitrile is present from the rapid tautomerization of ketenimine, a reaction studied theoretically by Doughty *et al.*[15] whilst the other species are the side products of the pyrolysis. From the microwave studies the half-life of ketenimine in the cell was <1 s and our flow experiments are consistent with a similar half life. The optimum experimental conditions were found to be an oven temperature of ∼1100 °C, to ensure the precursor was completely decomposed, whilst pumping the products through the multi-pass

---

a)Author to whom correspondence should be addressed. Electronic mail: donald.mcnaughton@monash.edu.

134, 234306-1
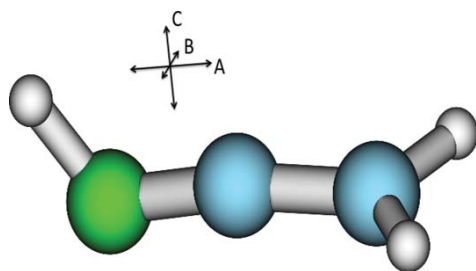
FIG. 1. Ketenimine molecule with axes labeled. Geometry optimized via B3LYP/cc-pVTZ calculations. Note: in the I^r representation $z = a$, $x = b$, and $y = c$.

White cell at a rate high enough to ensure that the amount of the more stable acetonitrile conformation was minimized.

The experiments were performed at the Australian synchrotron, using the infrared synchrotron edge radiation continuum source and a Bruker IFS 125HR spectrometer capable of achieving a nominal resolution of 0.001 cm^{-1}. The spectrum was recorded in two separate spectral regions, between 770 and 390 cm^{-1} (region 1) which utilized the synchrotron source and between 1300 and 700 cm^{-1} (region 2) using an internal source. Both regions were recorded using a KBr beam-splitter. A silicon-boron bolometer equipped with a cold filter cutoff at 770 cm^{-1} was used for region 1 and a mercury cadmium telluride detector for region 2. For region 1 an aperture of 3.15 mm was used, which is wide enough for the already highly collimated synchrotron beam to pass through unimpeded, whereas for region 2, a 1.5 mm aperture was used. Both regions were scanned at a speed of 40 kHz. The pressure within the cell was maintained at ~0.3 mbar, with optical path-lengths between 8 and 18 m and the temperature in the cell was assumed to be 300 K for simulations. Overall 58 and 19 spectra were recorded in regions 1 and 2, respectively, separately averaged then apodized using a 4P function and post-zero filled by a factor of 8. Region 1 was recorded at the highest spectral resolution of the instrument, thus, requiring ~12 h of continuous flow pyrolysis to obtain the data. Region 2 was recorded at a spectral resolution of 0.002 cm^{-1} and required significantly less recording time.

The pure rotational structure was also recorded using the synchrotron source in the far-IR region between 20 and 110 cm^{-1} (region 3). The experimental conditions were identical to the recording of regions 1 and 2, however, the spectrometer was equipped with a 75 μm mylar beam-splitter and silicon bolometer. An aperture of 12.5 mm was used and spectra were scanned at a speed of 40 kHz. Overall 83 scans were recorded at the instrument's highest spectral resolution and averaged. This was then apodized using a 4P function and post-zero filled by a factor 8 to produce the final far-IR spectrum. All spectra were calibrated by comparison with water line positions from the HITRAN database.[16]

Density functional calculations were performed using GAMESS (Ref. [17]) at the B3LYP/cc-pVTZ level of theory and were input into the harmonic force-field analysis program VIBCA (Ref. [18]) as described in the previous study.[7] The primary objective of the calculations was to determine the values for the derivatives of the component of the recipro-

cal moment of inertia tensor, α_i, which are a measure of the strength of Coriolis interactions between the G.S. and mode i. These calculations were also used to predict the G.S. rotational and quartic (D and d) centrifugal distortion parameters. GAUSSIAN (Ref. [19]) DFT calculations at the same level of theory provided a prediction of the sextic (H) centrifugal distortion parameters.

Spectral simulation data are achieved by inputting the parameters obtained from the fits into Pickett's prediction software SPCAT.[20] The resulting calculated transitions were then convolved with a Gaussian line shape, with appropriate FWHM (~0.002 cm^{-1}) to produce a simulated spectrum.

III. RESULTS/DISCUSSION

The section of region 1 containing the ν_7 mode of ketenimine is shown in Fig. 2(a) (~83% of the assigned transitions were picked from this region). The spectrum is contaminated with the ν_2 mode of HCN,[21] an undesired by-product of the pyrolysis, centered about 712 cm^{-1}. Since HCN is a linear rotor with simple ro-vibrational structure, transitions attributed to this molecule introduced little complication to the analysis.

ν_7, a CH$_2$ wag with A′ symmetry has predominantly c-type character with selection rules $oe \leftrightarrow ee$ and $eo \leftrightarrow oo$
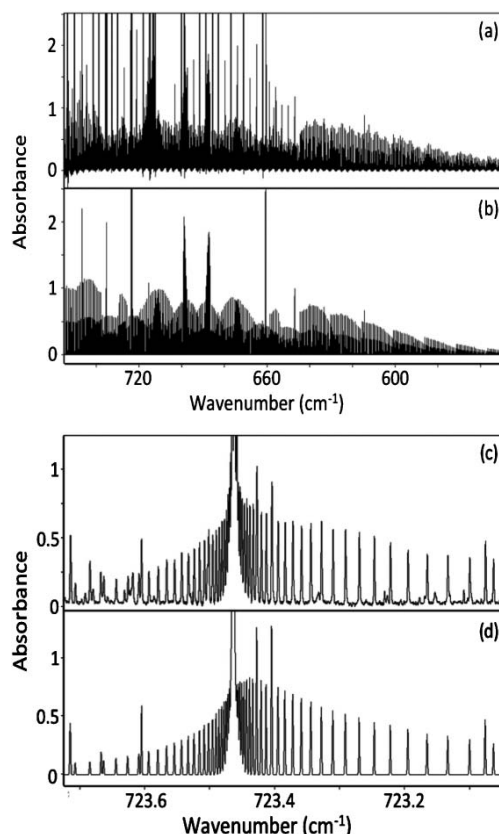
FIG. 2. (a) Experimental, survey spectrum of ν_7 (region 1) and (b) corresponding simulation. The expanded experimental (c) and simulated (d) sections illustrate the agreement between the two. (a) Intense transitions attributed to the ν_2 mode of HCN centered about 712 cm^{-1} which do not appear in the simulation. (c) Weak hot-band structure which does not appear in the simulation. Further additional lines are due to residual water.

($\Delta K_a = \pm 1, \pm 3,\dots, \Delta K_c = 0, \pm 2\dots$). The ν_7 spectra were peak-picked and presented in the Loomis-Wood format using MacLoomis,[22] which groups regularly spaced lines, such as those differing in J but sharing constant K_a, into approximately vertical series of constant K_a. Presenting the spectra in this way allowed series up to K_a (max) = 9 to be assigned quantum numbers, with J(max) = 52. Overall, 2660 ro-vibrational P, Q, and R branch transitions were assigned to this mode, and given an uncertainty of 0.0002 cm^{-1} (10% of the FWHM of the peak) in the fitting procedure. These assignments were confirmed by comparison of the experimentally determined ground state combination differences with those generated from the known ground state constants. The assigned transitions were least-squares fitted to Watson's S-reduced rotor Hamiltonian in the I^r representation using Pickett's SPFIT.[20] The S-reduced Hamiltonian was used for consistency and comparison with the previous work. From the resultant high residual errors in this fit, it was apparent that the system contains perturbations.

A. Fit and treatment of perturbations to the G.S.

Prior to a successful fitting of the ν_7 mode , the G.S. parameters needed to be improved because the previous study incorporated GSCD up to K_a (GS) = 7 only, and the resultant constants were inaccurate for the range of K_a (GS) recorded in this study. The ν_7 mode contains GSCD up to K_a (GS) = 10, and a least squares fit to these, the observed transitions from the microwave study[4] and the GSCD from the ν_{12} and ν_8 modes from the previous IR study[7] was performed. It was found that only combination differences involving states with K_a (GS) ≤ 8 could be accurately fitted with low residual error and it was apparent that the K_a (GS) = 9 and 10 states are perturbed. Consequently, it was necessary to fit the ground state together with the coupled low frequency modes to obtain a satisfactory fit. Although it is rare for the G.S. to be perturbed, the iso-electronic molecule thioketene has also been shown to exhibit this same property in a previous study by McNaughton *et al.*[9]

The DFT calculations determined that the most significant interactions between the G.S. and excited states were *ac*-axis and *ab*-axis second order Coriolis interactions with the lowest energy modes ν_{12} (409 cm^{-1}) and ν_8 (466 cm^{-1}), respectively. Parameters describing these interactions were introduced to the fit, and the microwave transitions,[3] the GSCD from the ν_{12}, ν_8, and ν_7 modes and the IR ro-vibrational transitions of ν_{12} and ν_8 were co-fitted (see below for weightings).

The resulting co-fit obtained improved G.S. parameters, which were used to simulate the μ_a and μ_c components of the pure rotational spectrum in an attempt to locate and assign transitions that occur in far-IR spectrum above 20 cm^{-1}. The dipole moments used in the simulation were $\mu_a = 0.434$ D and $\mu_c = 1.371$ D as determined by the microwave study.[3] The experimental far-IR spectrum contained a large number of lines from other products of the pyrolysis, as well as regions of high noise. The simulation did, however, locate with high

TABLE I. Band parameters fitted to Watson's S-reduced I^r Hamiltonian for the G.S., ν_8, and ν_{12} system of coupled modes of ketenimine. Presented in the frequency units for consistency with previous work.

Constant	G.S.[a]	G.S.[b]	G.S.[c]	ν_{12}	ν_8
Band center (cm^{-1})				409.036624 (63)[d]	466.454164 (23)
A (MHz)	204523.235	201445.422 (30)	201445.279 (28)	195260. (160)	204290. (160)
B (MHz)	9744.0295	9663.14123 (93)	9663.1593 (10)	9697.170 (79)	9671.280 (12)
C (MHz)	9555.0030	9470.12039 (79)	9470.1547 (10)	9483.557 (85)	9492.265 (12)
D_J (kHz)	2.8260	2.98288 (70)	2.98672 (66)	3.0558 (17)	3.02893 (88)
D_{JK} (kHz)	235.76	232.178 (77)	130.52 (60)	56.3 (18)	508.8 (16)
D_K (kHz)	9866.	10126.3 (20)	10218.0 (11)	3290. (290)	21750. (290)
d_1 (kHz)	−0.0586	−0.06870 (30)	−0.06785 (30)	−0.06785[e]	−0.05088 (84)
H_{JK} (kHz)	0.00150	0.001043 (35)	0.000957 (31)	0.000957[e]	0.000957[e]
H_{KJ} (kHz)	1.714	−0.24223 (29)	…	−1.447 (19)	1.075 (31)
H_K (kHz)	3.0975	2.516 (28)	2.1782 (77)	…	2.1782[e]
L_{KKJ} (kHz)	…	−0.000983 (37)	…	…	−0.00690 (20)
				$\eta_{12}{}^{ac}$ (MHz) = 491.7 (49)	$\eta_8{}^{ab}$ (MHz) = 705.0 (64)
				$G_{12,8}{}^{a}$ (MHz) = 306320. (450)	
				$G_{12,8}{}^{ak}$ (MHz) = −100.6 (33)	
				$F_{12,8}{}^{bc}$ (MHz) = 1.943 (47)	
J (max)		54	54	49	54
K_a (max)		8	10	7	7
Number trans.		5675[f]	5761[f]	666	1359
rms$_{dev}$		0.872		0.877	

[a]A, B, C, D, and d parameters determined by B3LYP/cc-pVTZ GAMESS (Ref. 17 calculation and VIBCA (Ref. 18). H parameters determined by GAUSSIAN (Ref. 19) calculation at same level of theory.
[b]Effective G.S. parameters for the fit to the unperturbed levels (up to K_a(GS) = 8).
[c]G.S. fitted by combined treatment with ν_8 and ν_{12}.
[d]Figures in parentheses are one standard deviation according to the least squares fit in units of the least significant figure quoted.
[e]Parameter forced during the fit to be equal to the G.S. value.
[f]The set of G.S. transitions includes 29 published microwave transitions, 126 far-IR rotational transitions and combination differences from the ν_8, ν_{12}, and ν_7 bands. Note that $\eta_{12}{}^{ac}$ has the same form as $F_{12}{}^{ac}$.
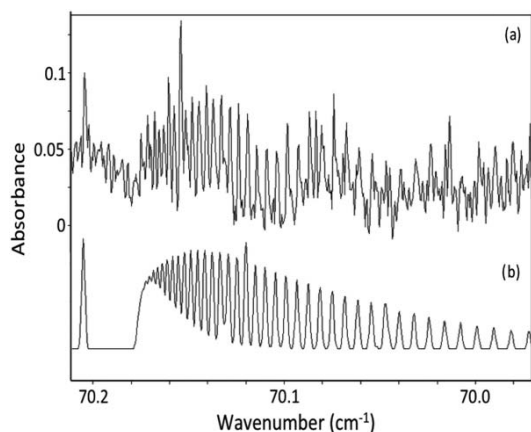
FIG. 3. (a) A section of the recorded far-IR spectrum containing the weak $K_a = 5$–6 Q-branch transitions and (b) simulation based on parameters presented in Table I. The simulation also contains an accurate prediction of the $20_{5,15} \leftarrow 19_{4,15}$ R-branch rotational transition, which is not explicitly fitted, centered about 70.204 cm^{-1} whilst extra transitions in the experimental spectrum attributed to impurities (probably water, ammonia, or methyl cyanide), which do not appear in the simulation.

FIG. 4. Calculated energies of the $J = 10$ level for K_a up to 10 for the lowest energy modes of ketenimine. ν_7 and $2\nu_{12}$ energies calculated from parameters in Table II. G.S., ν_{12}, and ν_8 energies calculated from the parameters in Table I. Some symmetry allowed Coriolis interactions between states are indicated (note: observed *Cor-a* interactions between ν_{12} and ν_8 continue to high K_a). Solid and dashed lines represent observed and predicted levels and interactions, respectively.

accuracy some weak, μ_c-type rotational structure attributed to ketenimine, which corresponded to the strongest features of the simulation. Three Q-branch heads with $K_a{}^{max}$(G.S.) $= 8$, which were not engulfed by noise or other structure, were assigned and included into the fit, with results shown in Table I. This fit is available in the supplementary material.[23] Figure 3 shows the excellent agreement between experiment and simulation for a section of the far-IR spectrum.

The final fit of the G.S. rotational structure of ketenimine included 29 rotational microwave transitions with varying but small uncertainties taken from the original microwave work,[3] 126 Q-branch far-IR rotational transitions with an uncertainty of 0.0002 cm^{-1}, 2025 IR ro-vibrational transitions with an uncertainty 0.0002 cm^{-1} to the ν_{12} and ν_8 modes and 5761 IR GSCD from the ν_{12}, ν_8, and ν_7 modes with an uncertainty of 0.00028 cm^{-1} and resulted in a fit with root mean square (rms) deviation $= 0.877$. It was found during fitting that one of the few b-type microwave transitions could not be fitted to acceptable accuracy and skewed the fit. This high J transition was "weighted out" by giving it an effectively infinite uncertainty of 999 MHz.

It can be seen from Table I that the fitted G.S. parameters are of comparable value to those of previous studies and to the theoretical predictions. The centrifugal distortion parameters d and the majority of the higher order H parameters for all the three states involved in this fit were constrained to be equal to each other, but allowed to vary during the fit. d_2 was calculated by DFT to be small relative to d_1 (calculated values are $d_1 = -0.0586$ kHz and $d_2 = -0.0016$ kHz for the G.S.), and was omitted from all modes since it did not significantly improve the fit and could not be determined with acceptable accuracy. During this analysis, the ν_{12} and ν_8 parameters were also improved, particularly, by the addition of an L_{KKJ} centrifugal distortion term to the parameters describing $\nu_8 = 1$. Addition of this term significantly improved the residual error of the fit to both the ν_{12} and ν_8

modes. Physically, the L_{KKJ} parameter is most likely "soaking up" very weak perturbations to the $\nu_8 = 1$ state not explicitly treated, such as the theoretically predicted (by GAMESS and VIBCA calculations) b-axis and c-axis interactions with $\nu_7 = 1$ and $\nu_{12} = 1$, respectively. The d_1 parameter associated with $\nu_8 = 1$ was allowed to vary freely since it greatly reduced error, particularly in the low K_a transitions, and did not deviate greatly from the expected value. The deviation from the G.S. values of the D_K and D_{JK} distortion parameters of the $\nu_{12} = 1$ and $\nu_8 = 1$ states is detailed in the previous study,[7] however, the inclusion of L_{KKJ} substantially reduces the magnitude of this affect.

Local, second order perturbations with both modes of the ν_{12}, ν_8 strongly Coriolis coupled system were identified and treated. The fitted parameters, η_i, can be related to the calculated value of α_i by the equation in, for example, Watson.[24]

$$\eta_i^{ab}(\text{cm}^{-1}) = -4\pi \sqrt{\frac{c}{h\varpi_i}} A_i B_i q_i \alpha_i^{ab}, \qquad (1)$$

where q_i is the normal co-ordinate of the mode i (Note Eq. (1) has been modified from that presented in Watson[24] and is presented in terms of rotational constants as opposed to rotational moments of inertia). Upon substitution of the fitted values and assuming $q_i = 1/2$ we obtain values of $\alpha_{12}^{ac} = 0.93$ u$^{1/2}$ Å and $\alpha_8^{ab} = 1.43$ u$^{1/2}$ Å which compares well to the theoretically calculated values of $\alpha_{12}^{ac} = 0.94$ u$^{1/2}$ Å and $\alpha_8^{ab} = 1.31$ u$^{1/2}$ Å. The necessity to fit these second order Coriolis interaction terms explicitly arises from the high dependence of the spacing of K_a levels on A. As seen in Fig. 4, interacting $\nu_{12} = 1$ levels draw nearer with increasing K_a. Equivalent interactions, e.g., $\nu_i \leftrightarrow \nu_i + \nu_{12}$, will affect high K_a levels of every other vibrational level in ketenimine also. In addition an effective fit which does not include any of the perturbed states was performed with results also shown in Table I.

TABLE II. Band parameters fitted to Watson's S-reduced I^r Hamiltonian for the system of coupled modes of ketenimine. Presented in frequency units for consistency with the previous work.

Constant	ν_7	$2\nu_{12}$[a]	$\nu_{12} + \nu_8$[a]	$2\nu_8$[a]
Band center (cm^{-1})	692.850020 (23)[b]	823.306 (43)	875.49079	932.90833
A (MHz)	196799.844 (91)	200358. (22)	198103	207158
B (MHz)	9652.7647 (24)	9731.177	9705.288	9679.398
C (MHz)	9480.7345 (23)	9469.615	9505.668	9514.374
D_J (kHz)	2.99730 (52)	3.12400	3.09731	3.07059
D_{JK} (kHz)	208.78 (11)	17.65	434.5	886.8
D_K (kHz)	1454.8 (42)	3585	14818	33220
d_1 (kHz)	−0.05799 (60)	−0.06786	−0.05010	−0.03234
H_{JK} (kHz)	0.000849 (30)	0.000922	0.000922	0.000922
H_{KJ} (kHz)	−0.1773 (45)	…	…	
H_K (kHz)	1.161 (45)	…	…	
L_{KKJ} (kHz)	−0.002060 (56)	…	…	
$G^b_{7,12+12}$ (MHz)	640.1 (20)			
Fermi$_{7,12+12}$ (MHz)	13708 (56)			
		$G^a_{12+12,12+8}$ (MHz) $= G^a_{12+8,8+8}$ (MHz) $= 434976$[a]		
J(max)	52			
K_a(max)	9			
Number trans.	2660			
rms$_{dev}$	0.718			

[a] Band centers determined by Eq. (1) A, B, C, D, d, and H parameters determined by Eq. (2). Coriolis interaction parameters determined by Eq. (3). Calculation based on parameters from Table I.

[b] Figures in parentheses are one standard deviation according to the least squares fit in units of the least significant figure quoted.

These parameters now more accurately describe the G.S. (as well as the ν_{12}, ν_8 system), and an accurate fit of ν_7 up to the recorded limit of K_a is now possible.

B. Fit and treatment of perturbations to $\nu_7 = 1$

The most probable candidate for an interaction with $\nu_7 = 1$ is $\nu_{12} = 2$ (~818 cm^1) since it is the closest in energy and strong Coriolis interactions with the next state up ($\nu_8 + \nu_{12}$) result in a very small effective A rotational constant for $2\nu_{12}$ compared with that of $\nu_7 = 1$. Because no $2\nu_{12}$ transitions were observed, (ν_{12} itself has a very low predicted IR intensity of 0.008 D^2 Å^{-2} amu^{-1} and the overtone would be expected to be weaker still), this state must be introduced into the fit as a dark state, and we rely purely on theory to describe it since no experimental data is available. The band centers, ω, of the overtones and the combination bands were predicted using the harmonic approximation

$$\varpi_{2\nu_8} \approx 2\varpi_{\nu_8}$$
$$\varpi_{\nu_8+\nu_{12}} \approx \varpi_{\nu_8} + \varpi_{\nu_{12}}. \qquad (2)$$

Calculations to determine anharmonic contributions to ω proved unreliable, and the harmonic approximation was considered sufficient. The rotational and centrifugal distortion parameters for overtones and combination bands can be calculated using the following approximation:

$$A_{2\nu_8} \approx -A_{GS} + 2A_{\nu_8}$$
$$A_{\nu_8+\nu_{12}} \approx -A_{GS} + A_{\nu_8} + A_{\nu_{12}}. \qquad (3)$$

$\nu_{12} = 2$ is itself strongly coupled directly to $\nu_{12} = 1 + \nu_8 = 1$ and indirectly to $\nu_8 = 2$. Equation (4) adapted from the theory presented in, for example, Nakagawa and

Morino[11] shows the parameter in the fit describing the a-axis Coriolis interaction, G_a, between these dark states can be approximated by

$$G^a_{2\nu_{12},\nu_{12}+\nu_8} = G^a_{2\nu_8,\nu_{12}+\nu_8} = \sqrt{2}G^a_{\nu_8,\nu_{12}}. \qquad (4)$$

As can be seen in Table I, the value of $G^{\nu_8,\nu_{12}}_a$ is large, and the interactions between the combination and overtone states cannot be ignored when attempting to describe these modes.

Equations (2)–(4) describe all of the parameters required to approximate the location of the energy levels of the three dark-states, from parameters presented in Table I. $2\nu_{12}$ has A′ symmetry implying Fermi and b-axis Coriolis interactions with ν_7 are symmetry allowed, and the parameters describing these were introduced to the fit. With the introduction of the dark state system and the interactions between ν_7 and $2\nu_{12}$, along with the improved G.S. parameters, a satisfactory fit was achieved, with the resultant rotational parameters shown in Table II. All parameters describing the strongly Coriolis coupled dark-states system, except the band center and the A rotational parameter of $\nu_{12} = 2$, were constrained to their values calculated using Eqs. (2), (3), and (4) during the fit. This fit is also available in the supplementary material.[23]

The ν_7 fit incorporated 2661 ro-vibrational transitions with an uncertainty of 0.0002 cm^1 and delivered a fit with rms$_{dev} = 0.748$. Again, d_2 was omitted since it did not significantly improve the fit and could not be determined with acceptable accuracy. The fitted band center of ν_7 (692.9 cm^1) compares well to the value calculated by DFT calculations in previous work[7] of 692.0 cm^1. The band center and A rotational constants of $2\nu_{12}$ were allowed to vary since this greatly reduced the rms$_{dev}$ of the fit and the values obtained did not vary greatly from the predicted values. The band center and A of $2\nu_{12}$ were fitted to ~1% and 5%, respectively, of their

theoretical values. All other rotational, centrifugal distortion, and interaction parameters associated with the dark-states were constrained to their theoretical value (except the Coriolis interaction between ν_7 and $2\nu_{12}$). Although the dark state system treats the perturbations in ν_7 well, it is a theoretical model that contains small errors, and such small deviations from calculated values are expected.

For the same reasons as outlined previously, an L_{KKJ} term associated with $\nu_7 = 1$ was introduced, which significantly reduced the $\mathrm{rms_{dev}}$ of the fit. This term "soaked up" a very small but anomalous J-dependant deviation of the residual error at $K_a = 8$, which could be attributed to a very weak b-axis Coriolis resonance with $\nu_8 = 1$ (see Fig. 4).

Figure 4 gives an insight into the complex nature of the ro-vibrational structure of ketenimine. The symmetry of the ν_7 and $2\nu_{12}$ modes implies that both Fermi and b-axis Coriolis interactions are allowed between them. b-axis Coriolis interactions primarily occur between the states with $\Delta K_a = \pm 1$, and it can be seen that the $K_a = 6$ and 7 states of $\nu_7 = 1$ are very close in energy to the $K_a = 5$ and 6 states of $\nu_{12} = 2$. Similarly, Fermi interactions primarily occur between states with $\Delta K_a = 0$, and Fig. 4 shows that the $K_a = 8$ and 9 states of $\nu_7 = 1$ are very close in energy to the $K_a = 8$ and 9 states of $\nu_{12} = 2$. It is important to note that the states with $K_a = 6$ and 7 can be satisfactorily fitted by introducing only the b-axis Coriolis interaction, implying that both interactions are local and primarily perturb only the states outlined in Fig. 4.

IV. CONCLUSION

Ro-vibrational transitions within the Coriolis coupled ν_7 mode of ketenimine have been assigned and fitted to determine rotational, centrifugal distortion, and Coriolis interaction parameters. Local b-axis Coriolis and Fermi interactions have been treated between ν_7 and the $2\nu_{12}$ dark state. Introduction of the $\nu_8 + \nu_{12}$ and $2\nu_8$ dark-states proved necessary in the theoretical model describing $2\nu_{12}$. Second, the G.S. parameters have been improved by incorporating GSCD up to $K_a(\mathrm{GS}) = 10$ in the G.S. fit. Ketenimine is one of the relatively few molecules where resonance perturbations are evident in the rotational levels of the ground vibrational state. Local perturbations at high $K_a(\mathrm{GS})$, attributed to interactions with the ν_{12}, ν_8 system of strongly coupled modes, have been accounted for. The fitted values of α_{12}^{ac} and α_8^{ab} are in agreement with B3LYP/cc-pVTZ calculations. The parameters describing ν_{12} and ν_8 have also been refined during the G.S. analysis. It can be seen from Figs. 2 and 3 that there is a good agreement between the observed and simulated spectra.

[1]E. Jacox and D. E. Milligan, J. Am. Chem. Soc. **85**, 278 (1963).

[2]M. E. Jacox, Chem. Phys. **43**, 157 (1979).

[3]M. Rodler, R. D. Brown, P. D. Godfrey, and L. M. Tack, Chem. Phys. Lett. **110**, 447 (1984).

[4]M. Rodler, R. D. Brown, P. D. Godfrey, and B. Kleibömer, J. Mol. Spectrosc. **118**, 267 (1986).

[5]H. W. Kroto, G. Y. Matti, R. J. Suffolk, J. D. Watts, M. Rittby, and R. J. Bartlett, J. Am. Chem. Soc. **112**, 3779 (1990).

[6]F. J. Lovas, J. M. Hollis, A. J. Remijan, and P. R. Jewell, Astrophys. J. **645**, L137 (2006).

[7]M. K. Bane, C. D. Thompson, E. G. Robertson, D. R. T. Appadoo, and D. McNaughton, Phys. Chem. Chem. Phys. **13**, 6793 (2011).

[8]L. Nemes, D. Luckhaus, M. Quack, and J. W. C. Johns, J. Mol. Struct. **517–518**, 217 (2000).

[9]D. McNaughton, E. G. Robertson, and L. D. Hatherley, J. Mol. Spectrosc. **175**, 377 (1996).

[10]G. Duxbury and M. L. Le Lerre, J. Mol. Spectrosc. **92**, 326 (1982).

[11]T. Nakagawa and Y. Morino, J. Mol. Spectrosc. **38**, 84 (1971).

[12]H. H. Blau and H. H. Nielsen, J. Mol. Spectrosc. **1**, 124 (1957).

[13]P. H. Turner, L. Halonen, and I. M. Mills, J. Mol. Spectrosc. **88**, 402 (1981).

[14]F. Ito and T. Nakanaga, J. Mol. Spectrosc. **264**, 100 (2010).

[15]A. Doughty, G. B. Bacskay, and J. C. Mackie, J. Phys. Chem. **98**, 13546 (1994).

[16]L. S. Rothman, I. E. Gordon, A. Barbe, D. C. Benner, P. F. Bernath, M. Birk, V. Boudon, L. R. Brown, A. Campargue, J. P. Champion, K. Chance, L. H. Coudert, V. Dana, V. M. Devi, S. Fally, J. M. Flaud, R. R. Gamache, A. Goldman, D. Jacquemart, I. Kleiner, N. Lacome, W. J. Lafferty, J. Y. Mandin, S. T. Massie, S. N. Mikhailenko, C. E. Miller, N. Moazzen-Ahmadi, O. V. Naumenko, A. V. Nikitin, J. Orphal, V. I. Perevalov, A. Perrin, A. Predoi-Cross, C. P. Rinsland, M. Rotger, M. Simecková, M. A. H. Smith, K. Sung, S. A. Tashkun, J. Tennyson, R. A. Toth, A. C. Vandaele, and J. Vander Auwera, J. Quant. Spectrosc. Radiat. Trans. **110**, 533 (2009).

[17]M. W. Schmidt, K. K. Baldridge, J. A. Boatz, S. T. Elbert, M. S. Gordon, J. H. Jensen, S. Koseki, N. Matsunaga, K. A. Nguyen, S. Su, T. L. Windus, M. Dupuis, and J. A. Montgomery, Jr., J. Comput. Chem. **14**, 1347 (1993).

[18]See http://info.ifpan.edu.pl/~kisiel/vibr/vibr.htm#vibca for information on VIBCA and FCONV.

[19]M. J. Frisch, G. W. Trucks, H. B. Schlegel *et al.*, GAUSSIAN *09, Revision A.1*, Gaussian, Inc., Wallingford, CT, 2009.

[20]H. M. Pickett, J. Mol. Spectrosc. **148**, 371 (1991).

[21]V. K. Wang and J. Overend, Spectrochim. Acta, Part A. **29**, 687 (1973).

[22]D. McNaughton, D. McGilvery, and F. Shanks, J. Mol. Spectrosc. **149**, 458 (1991).

[23]See supplementary material at http://dx.doi.org/10.1063/1.3597775 for transition lists and final least squares fits.

[24]J. K. G. Watson, in *Vibrational Spectra an Structure*, edited by J. R. Durig (Elsevier, New York, 1977), Vol. 6.

Declaration for Thesis Chapter 3.3

Declaration by candidate

In the case of Chapter 3.3, the nature and extent of my contribution to the work was the following:

Nature of contribution	Extent of contribution (%)
Initiation, key ideas, development, writing up	80

The following co-authors contributed to the work. Co-authors who are students at Monash University must also indicate the extent of their contribution in percentage terms:

Name	Nature of contribution	Extent of contribution (%) for student co-authors only
E. G. Robertson	Initiation, key ideas	
C. D. Thompson	Initiation, key ideas	
D. R. T. Appadoo	Experiment assistance	
D. McNaughton	Initiation, key ideas	

Candidate's Signature	Date

Declaration by co-authors

The undersigned hereby certify that:

(1) the above declaration correctly reflects the nature and extent of the candidate's contribution to this work, and the nature of the contribution of each of the co-authors.
(2) they meet the criteria for authorship in that they have participated in the conception, execution, or interpretation, of at least that part of the publication in their field of expertise;
(3) they take public responsibility for their part of the publication, except for the responsible author who accepts overall responsibility for the publication;
(4) there are no other authors of the publication according to these criteria;
(5) potential conflicts of interest have been disclosed to (a) granting bodies, (b) the editor or publisher of journals or other publications, and (c) the head of the responsible academic unit; and
(6) the original data are stored at the following location(s) and will be held for at least five years from the date indicated below:

Location(s)	Monash University, School of Chemistry

Signature 1		Date 20-8-12
Signature 2		
Signature 3		
Signature 4		

79

High-resolution Fourier-transform infrared spectroscopy of the ν_6 and Coriolis perturbation allowed ν_{10} modes of ketenimine

Michael K. Bane,[1] Evan G. Robertson,[2] Christopher D. Thompson,[1] Dominique R. T. Appadoo,[3] and Don McNaughton[1,a)]

[1]*School of Chemistry, Monash University, Wellington Rd., Clayton, Victoria 3800, Australia*
[2]*Department of Chemistry, La Trobe Institute for Molecular Science, La Trobe University, Bundoora, Victoria 3086, Australia*
[3]*Australian Synchrotron, 800 Blackburn Rd, Clayton, Victoria 3168, Australia*

High-resolution FTIR spectra of the short lived species ketenimine have been recorded in the region 700–1300 cm^{-1} and over 1500 transitions of the ν_{10} and ν_6 modes have been assigned. Effective rotational and centrifugal distortion parameters for the $\nu_{10} = 1$ and $\nu_6 = 1$ (excluding $K_a = 5$) states were determined by co-fitting transitions, and treating strong a- and c-axis Coriolis interactions between them. Other perturbations attributed to interactions with the $\nu_8 = 2$ and $\nu_{12} = 1 + \nu_8 = 1$ dark-states were also observed and treated. The ν_{10} transitions are predicted to be inherently very weak, but are enhanced by an intensity stealing effect with the highly IR active ν_6 mode. A mechanism for this intensity stealing in ketenimine is also detailed. © *2011 American Institute of Physics.*
[doi:10.1063/1.3664624]

I. INTRODUCTION

Due to it being a structural isomer of acetonitrile (H$_3$CC≡N), a known interstellar molecule, ketenimine (H$_2$C = C = NH, Figure 1) was predicted to be a chemical component of the interstellar medium. In 2006, it was located by Lovas *et al.*[1] in the star forming region Sagittarius B2(N) by observing microwave emissions predicted from a previous microwave study.[2]

The short lived molecule ketenimine was tentatively identified by Jacox and Milligan[3] and this initial identification was later confirmed by Jacox[4] using low resolution matrix isolation vibrational and electronic spectroscopic techniques. Ketenimine was generated and studied first in the gas phase by microwave spectroscopy[2,5] and subsequently by photoelectron spectroscopy.[6] Its gas phase infrared spectrum was later recorded and analyzed at low resolution[7] but due to the complexity of its high-resolution spectrum no further detailed analysis was undertaken.

Ketenimine has 12 vibrational modes of A′ and A″ symmetry, which are detailed in Ref. 8 and 9. The first ground state rotational constants from a microwave study performed by Rodler *et al.*[5] were subsequently revised to account for a mis-assignment in a later rotation-inversion study by Rodler *et. al.*[2] A small inversion splitting (energy difference between inverted conformations of the imino hydrogen determined to be 2.2×10^{-6} cm^{-1}) was observed in that study which cannot be resolved at the resolution of this study and hence the symmetry group is assumed to be C_s. Recent studies by Bane *et al.*[8,10] have further refined the ground state parameters by including ground state combination differences from the ν_{12}, ν_8, and ν_7 modes in the ground state analysis, increasing the

observed range of J and K_a.[8] At high K_a, perturbations to the ground state from the two lowest energy modes were also identified and treated.[10]

The vibrational modes of ketenimine, and molecules of similar structure such as ketene,[11] thioketene,[12] methyleneimine,[13] formaldehyde,[14] and thioformaldehyde[15] have been shown to exhibit a high degree of Coriolis coupling and consequently a complex ro-vibrational structure. The strongly Coriolis coupled ν_{12} and ν_8 modes of ketenimine were analyzed in a previous high-resolution FTIR study,[8] which uncovered a Coriolis interaction of such strength that the rotational constants of the effectively IR inactive ν_{12} mode were determined purely by analyzing transitions with intensities enhanced via Coriolis "intensity stealing." The ν_{10} and ν_6 system of Coriolis coupled states, which is the target of this study, is analogous to the previously studied system and the same intensity stealing effect was predicted to occur. The mechanism of intensity stealing is detailed in Sec. II.

The ν_7 mode has also been studied at high-resolution in a separate study,[10] and both Coriolis and Fermi local interactions with $2\nu_{12}$ were identified and accounted for, with $2\nu_{12}$ itself strongly Coriolis coupled to $\nu_{12} + \nu_8$ and indirectly to $2\nu_8$. Because these higher energy states are of similar energy to the modes targeted in this study, they were predicted to be an additional source of perturbations in this analysis as well.

Strong perturbations were located during a previous high-resolution (0.005 cm^{-1}) FTIR study of the ν_6 mode by Ito *et al.*,[9] however since the coupled ν_{10} mode was not included in the fitting procedure a satisfactory set of molecular constants could not be derived. In this work we present the assignment and co-analysis of the ν_{10} and ν_6 modes of ketenimine. Both these modes appear to be perturbed by the higher order dark-state vibrations $\nu_{12} + \nu_8$ and $2\nu_8$, and so they are included in the treatment. Since the ν_7 transitions are also

a)Author to whom correspondence should be addressed. Electronic mail: donald.mcnaughton@monash.edu.
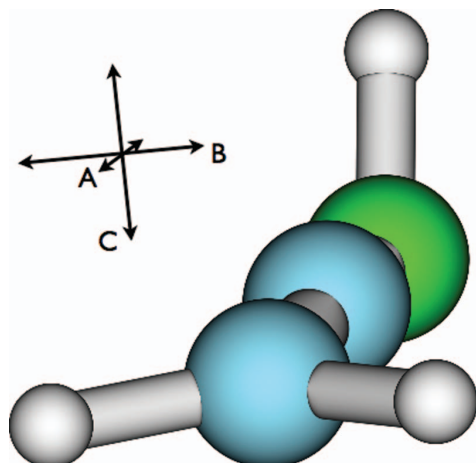
FIG. 1. Ketenimine molecule with axes labeled. Geometry optimized via DFT calculations. Note that in the I^r representation $z \equiv A$, $x \equiv B$, and $y \equiv C$.

indirectly affected by the higher order dark-states they are also co-fitted. The $K_a = 5$ sub-set of ν_6 was left out of the analysis because it was affected by a strong local perturbation that could not be satisfactorily fitted, however an in-depth discussion of a likely source of this complex, and perhaps intractable perturbation, is provided.

II. INTENSITY STEALING IN KETENIMINE

The quantum state-vectors labeled $|\nu_{10}\rangle$ and $|\nu_6\rangle$ are two unique eigenvectors of the ro-vibrational Hamiltonian of the ketenimine molecule, representing the modes ν_{10} and ν_6, respectively. $|\nu_{10}\rangle$ and $|\nu_6\rangle$ serve as an orthogonal 2D basis in which the normalized state vectors of the coupled system, $|\nu_{10}^p\rangle$ and $|\nu_6^p\rangle$, can be described. The explicit form of these is presented in Mills[16] (there is a sign error in these equations in Ref. 16) and adapted in our work as

$$\left|\nu_{10}^p\right\rangle = a_k |\nu_{10}\rangle + i\sigma b_k |\nu_6\rangle, \tag{1a}$$

$$\left|\nu_6^p\right\rangle = a_k |\nu_6\rangle - i\sigma b_k |\nu_{10}\rangle, \tag{1b}$$

where

$$a_k = [(\Delta_k + \delta)/2\Delta_k]^{1/2}, \tag{2a}$$

$$b_k = [(\Delta_k - \delta)/2\Delta_k]^{1/2}, \tag{2b}$$

$$\Delta_k^2 = \delta^2 + 16A_e^2 k^2 \zeta_{10,6}^2 \Omega_{10,6}^2, \tag{2c}$$

$$\Omega_{10,6} = (\omega_{10} + \omega_6)(\omega_{10}\omega_6)^{-1/2}, \tag{2d}$$

$$\delta = \omega_6 - \omega_{10}. \tag{2e}$$

A_e and ζ are the rotational constant and the dimensionless Coriolis coupling parameter respectively about the axis of the interaction, k is the quantum number associated with the z-projection of angular momentum, ω_x is the band centre of
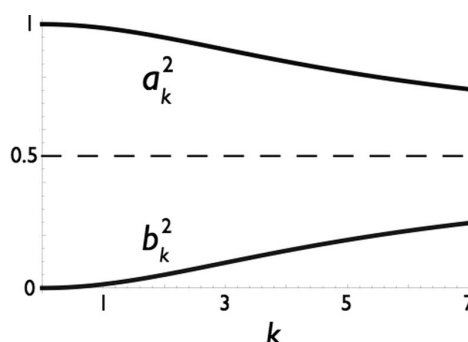

FIG. 2. Variation of a_k^2 and b_k^2 with quantum number k for the a-axis interaction between ν_6 and ν_{10} of ketenimine. Plot calculated using values from Table I.

mode x and $\sigma^2 = 1$. When $\Delta_k \gg \delta$, $a_k \approx b_k \approx 1/\sqrt{2}$ and the wavefunctions become heavily mixed. Figure 2 shows the variation of a_k and b_k as a function of k for the a-axis Coriolis interaction between the ν_{10} and ν_6 modes of ketenimine. As a consequence of the large A rotational constant of ketenimine, a large Coriolis coupling constant and a small energy gap, these modes become significantly mixed, even at low k.

Physically, the Coriolis interaction acts to make the mode of vibration in-deterministic, as summarized by the following equations:

$$\left|\langle\nu_{10} \mid \nu_{10}^p\rangle\right|^2 = \left|\langle\nu_6 \mid \nu_6^p\rangle\right|^2 = a_k^2, \tag{3a}$$

$$\left|\langle\nu_6 \mid \nu_{10}^p\rangle\right|^2 = \left|\langle\nu_{10} \mid \nu_6^p\rangle\right|^2 = b_k^2. \tag{3b}$$

The transition probability of such perturbed systems can also be evaluated. ν_{10} and ν_6 are b- and a-type modes, respectively, and the non-zero transition probabilities of $|\nu_{10}^p\rangle$ and $|\nu_6^p\rangle$ are

$$\langle GS| \mu_a \left|\nu_6^p\right\rangle = a_k \langle GS| \mu_a |\nu_6\rangle, \tag{4a}$$

$$\langle GS| \mu_b \left|\nu_6^p\right\rangle = -i\sigma b_k \langle GS| \mu_b |\nu_{10}\rangle, \tag{4b}$$

$$\langle GS| \mu_a \left|\nu_{10}^p\right\rangle = i\sigma b_k \langle GS| \mu_a |\nu_6\rangle, \tag{4c}$$

$$\langle GS| \mu_b \left|\nu_{10}^p\right\rangle = a_k \langle GS| \mu_b |\nu_{10}\rangle, \tag{4d}$$

where "GS" denotes the vibrational ground state. This result shows that as a mode couples to another via the Coriolis interaction, it acquires a non-zero transition probability in the direction of the mode it is coupled to, effectively making the resultant band similar to a hybrid band. The b-type ν_{10} mode is predicted by DFT calculations to be very weak, and the quantity $\langle GS|\mu_b|\nu_{10}\rangle$ is approximately equal to zero. We come to the final result for the intensity, I, of the coupled modes,

$$I \propto \left|\langle GS| \mu_a \left|\nu_6^p\right\rangle\right|^2 = a_k^2 |\langle GS| \mu_a |\nu_6\rangle|^2, \tag{5a}$$

$$I \propto \left|\langle GS| \mu_a \left|\nu_{10}^p\right\rangle\right|^2 = b_k^2 |\langle GS| \mu_a |\nu_6\rangle|^2. \tag{5b}$$

Hence, the intensity of both bands arises from the a-type dipole moment of ν_6 and in a sense, intensity is stolen by ν_{10}

from ν_6. The "stealing" is also k dependant, and intensity is shifted to transitions of higher k than would be expected from conventional line-strength factors. Since b_k^2 is significant even at low k for these two modes of ketenimine and the quantity $|\langle GS|\mu_a|\nu_6\rangle|^2$ is predicted to be very large (the ν_6 mode is the second most intense) it is likely that only those ν_{10} transitions enhanced by the intensity stealing mechanism will be observed.

III. EXPERIMENTAL

The transient species ketenimine was generated by flow pyrolysis of 3-hydroxypropionitrile as described in Refs. 8 and 10. Under the experimental conditions formaldehyde, hydrogen cyanide, carbon monoxide, and acetonitrile are also present in varying concentrations depending on the precise experimental conditions. Acetonitrile is present from the rapid tautomerization of ketenimine, a reaction studied theoretically by Doughty *et al.*,[17] whilst the other species are side products of the pyrolysis. From the microwave studies, the half-life of ketenimine in the microwave absorption cell was <1 s and our flow experiments are consistent with a similar half-life. The optimum experimental conditions were found to be an oven temperature of ~1100° C, to ensure the precursor was completely decomposed, whilst pumping the products through the multi-pass White cell at a rate high enough to ensure that the amount of the more stable acetonitrile isomer was minimized.

The experiments were performed at the Australian synchrotron, using a Bruker IFS 125HR spectrometer capable of achieving a nominal resolution of 0.001 cm^{-1}. An internal globar source with a 1.5 mm aperture was used for the region of the spectrum between 1300 and 700 cm^{-1}. The signal/noise ratio obtainable with the internal source was considered to be equal or greater than that of the synchrotron source for most of this region, consequently, the spectrum was recorded during a beam shut-off period. A KBr beam-splitter and mercury cadmium telluride (MCT) detector were used. The pressure within the cell was maintained at approximately 0.3 mbar with an optical path-length of 24 m and the temperature in the cell was ambient, assumed to be 300 K for simulations. Eighteen interferograms were recorded at 0.002 cm^{-1}, averaged

then Fourier transformed using a 4P apodization function and a post-zero fill factor of 8. All spectra were calibrated using water line positions from the HITRAN database.[18]

Density functional theoretical (DFT) calculations were performed using GAMESS (Ref. 19) at the B3LYP/cc-pVTZ level of theory, and were input into the harmonic force-field analysis program VIBCA (Ref. 20) as described in Refs. 8 and 10. These calculations allowed us to determine theoretical values for the a-axis, b-axis, and c-axis Coriolis coupling constants, ζ, between all fundamental modes, which were used to assist in the initial fitting process and for comparison with eventual fitted parameters.

Assigned lines were fitted with Pickett's SPFIT (Ref. 21) and spectral simulation data were achieved by inputting the parameters obtained from the fits into Pickett's prediction software SPCAT (Ref. 21). The resulting calculated transitions were then convolved with a Gaussian line shape with appropriate FWHM (~0.002 cm^{-1}) to produce a simulated spectrum.

IV. RESULTS

The spectrum was recorded between 1300 and 700 cm^{-1}, and the region containing the ν_{10} and ν_6 transitions is shown in Figure 3(a). Under the experimental conditions the concentration of acetonitrile was minimal since the ν_7 band[22] at 1040.8 cm^{-1} was not observed in the spectrum. According to the DFT calculations, the ν_{10} mode is inherently very weak, with an IR intensity of 0.003 D^2 Å^{-2} amu^{-1} that is 3 orders of magnitude smaller than that of ν_6 (5.055 D^2 Å^{-2} amu^{-1}).

ν_6, a CNH bend, has A' symmetry corresponding to an a-/c-hybrid mode, however no c-type transitions were observed implying the dipole derivative along this direction is negligible. The observed a-type transitions thus have selection rules of $eo \leftrightarrow ee$ and $oe \leftrightarrow oo$ ($\Delta K_a = 0, \pm 2, \ldots, \Delta K_c = \pm 1, \pm 3, \ldots$). The ν_6 spectrum was peak-picked and presented in the Loomis-Wood format using MacLoomis,[23] which groups regularly spaced lines, such as those differing in J but sharing constant K_a, into approximately vertical series of constant K_a. Presenting the spectra in this way allowed the series between $K_a = 0$ and 6 to be assigned, with J(max) = 57.
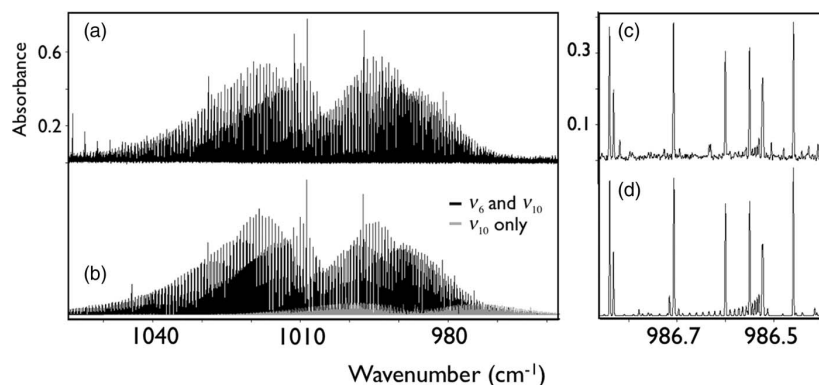

FIG. 3. (a) Experimental survey spectrum of ν_{10} and ν_6 and (b) corresponding simulation. The expanded experimental (c) and simulated (d) sections illustrate the agreement between the two. The expanded section contains both intense P and R transitions to the ν_6 mode and the weaker $K_a = 5$ Q-branch structure of the ν_{10} mode originating at approximately 986.54 cm^{-1}. Weak hot-band structure appears in (c) which does not appear in the simulation.

TABLE I. Band parameters for the global fit to Watson's S-reduced I^r. Presented in frequency units for consistency with previous work.

Constant	G. S.[a]	ν_{12}[a]	ν_8[a]	ν_7[b]	$2\nu_{12}$[a]
Band centre (cm^{-1})		409.036 624 (63)[c]	466.454 164 (23)	692.850 020 (23)	823.306 (43)
A (MHz)	201 445.279 (28)	195 260. (160)	204 290. (160)	196 799.918 (91)	200 158 (26)
B (MHz)	9663.1593 (10)	9697.170 (79)	9671.280 (12)	9652.7684 (24)	9731.177
C (MHz)	9470.1547 (10)	9483.557 (85)	9492.265 (12)	9480.7345 (23)	9469.615
D_J (kHz)	2.98672 (66)	3.0558 (17)	3.02893 (88)	2.99751 (52)	3.12400
D_{JK} (kHz)	130.52 (60)	56.3 (18)	508.8 (16)	208.74 (11)	17.65
D_K (kHz)	10 218.0 (11)	3290. (290)	21 750. (290)	1446.7 (42)	3585
d_1 (kHz)	−0.06 785 (30)	−0.06785[d]	−0.05088 (84)	−0.05 805 (60)	−0.06786
H_{JK} (kHz)	0.000 957 (31)	0.000 957[d]	0.000 957[d]	0.000 866 (30)	0.000 922
H_{KJ} (kHz)	...	−1.447 (19)	1.075 (31)	−0.1763 (45)	...
H_K (kHz)	2.1782 (77)	...	2.1782[d]	1.254 (45)	...
L_{KKJ} (kHz)	...	...	−0.00690 (20)	−0.002 091 (56)	...

$\eta_{12}{}^{ac}$ (MHz) = 491.7 (49)[a]
$\eta_8{}^{ab}$ (MHz) = 705.0 (64)[a]
$G_{12,8}{}^a$ (MHz) = 306 320. (450)[a] $G^b{}_{7,12+12}$ (MHz) = 654.0 (19)[a]
$G_{12,8}{}^{ak}$ (MHz) = −100.6 (33)[a] $Fermi_{7,12+12}$ (MHz) = 13514 (57)[a]
$F_{12,8}{}^{bc}$ (MHz) = 1.943 (47)[a]

Constant	G. S.	ν_{12}	ν_8	ν_7	$2\nu_{12}$
J (max)	54	49	54	52	...
K_a (max)	10	7	7	9	...
Number trans.	5761	666	1359	2660	...

Constant	$\nu_{12}+\nu_8$[a]	$2\nu_8$[a]	ν_{10}[b]	ν_6[b]
Band centre (cm^{-1})	873.335 (40)	940.201 (19)	983.13 107 (25)	1000.236 609 (24)
A (MHz)	198 103	207 158	212 178.6 (34)	213 554.3 (40)
B (MHz)	9705.288	9679.398	9672.302 (19)	9645.853 (64)
C (MHz)	9505.668	9514.374	9482.438 (19)	9496.737 (64)
D_J (kHz)	3.09731	3.07059	2.8290 (39)	3.16211 (93)
D_{JK} (kHz)	434.5	886.8	298.84 (79)	370.32 (21)
D_K (kHz)	14 818	33 220	3763 (24)	58 538 (14)
d_1 (kHz)	−0.05 010	−0.03 234	...	...
H_{JK} (kHz)	0.000 922	0.000 922	...	...
L_{KKJ} (kHz)	...	...	−0.15 845 (68)	0.09 034 (44)

$G^a{}_{6,10}$ (MHz) = 65 184 (16)[b]
$F^a{}_{6,10}$ (MHz) = 9.370 (55)[b]
$G^a{}_{12+12,12+8}$ (MHz) = $G^a{}_{12+8,8+8}$ (MHz) = 43 497[a] $G^c{}_{6,10}$ (MHz) = 564.9 (41)[b]
$G^a{}_{10,8+8}$ (MHz) = 19 248.7 (46)[b] $G^b{}_{8,8}$ (MHz) = −4896(13)[b]
$G^c{}_{10,8+8}$ (MHz) = −2404.2 (17)[b] $\eta_j{}^b{}_{6,8+8}$ (MHz) = 0.03273(23)[b]
$G^c{}_{6,8+12}$ (MHz) = 5466(22)[b]

Constant	$\nu_{12}+\nu_8$	$2\nu_8$	ν_{10}	ν_6
J(max)			40	57
K_a(max)			7	6
Number trans.			441	1065

[a] Parameters fixed to those presented in Ref. 10 excluding ω of $2\nu_{12}$, $\nu_{12}+\nu_8$, and $2\nu_8$ and A of $2\nu_{12}$.

[b] ν_7, ν_{10}, and ν_6 transitions co-fit with RMS of 1.40.

[c] Figures in brackets are 1 sd according to the least squares fit in units of the least significant figure quoted.

[d] Constrained to ground state value.

Overall 1195 P, Q, and R ro-vibrational transitions were assigned from this mode, and given uncertainty 0.0002 cm^{-1} (10% of the FWHM of the peak) in the fitting procedure. These assignments were confirmed by comparison with ground state combination differences generated from the known ground state constants.

The CH$_2$ rock mode, ν_{10}, has A$''$ symmetry corresponding to a b-type band with selection rules $eo \leftrightarrow oe$ and $ee \leftrightarrow oo$ ($\Delta K_a = \pm 1, \pm 3, \ldots, \Delta K_c = \pm 1, \pm 3, \ldots$). However, these conventional b-type transitions could not be detected because they are far weaker than the observed lines due to the intensity stealing effect. The selection rules for an a-type transition moment being shared via an a-axis Coriolis interaction are $ee \leftrightarrow ee$ and $oo \leftrightarrow oo$ ($\Delta K_a = 0, \pm 2, \ldots, \Delta K_c = 0, \pm 2,$

$\ldots$) and upper state quantum numbers were assigned based on this. The assignments of the measured lines were again confirmed by comparison with the ground state combination differences. Overall 441 P and R ro-vibrational transitions between $K_a = 3$ and 7 with J(max) $= 40$ were assigned from this mode, and given uncertainty of 0.0002 cm^{-1}. Low K_a transitions are too weak to be observed due to the k dependence of intensity stealing as shown in Figure 2.

The assigned ν_6 and ν_{10} transitions were least-squares fitted simultaneously to Watson's S-reduced rotor Hamiltonian in the I^r representation using Pickett's SPFIT.[21] Both a-axis and c-axis Coriolis interactions are symmetry allowed between these modes and parameters describing these were introduced to the fit. From the resultant high residual errors
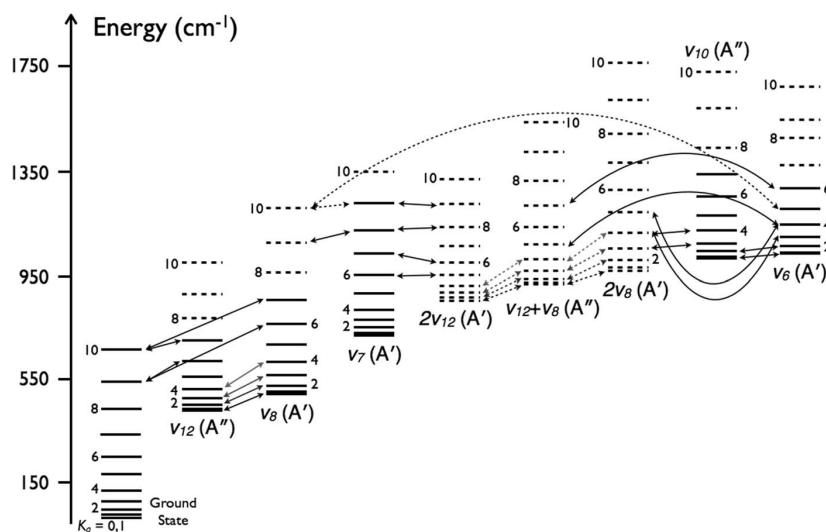
FIG. 4. Calculated energies of the $J = 10$ levels for K_a up to 10 for the analyzed modes of ketenimine. Energies calculated from parameters in Table I. A sample of the symmetry allowed Coriolis interactions between states are indicated. Solid lines represent observed levels and interactions whereas dashed lines indicate predicted quantities.

it was apparent that the system contained additional perturbations, which could not be described by the parameters already contained in the fit.

The most likely sources of these added perturbations are the 2nd order vibrations $\nu_{12} + \nu_8$ (873 cm^{-1}, A$''$) and $2\nu_8$ (940 cm^{-1}, A$'$), since they are the closest in energy to ν_{10} and ν_6. Since transitions of these modes are not observed, the energy levels associated with these modes must be introduced into the fit as dark-states, and we rely purely on theory to describe them, as detailed in Ref. 10. The theoretically derived molecular parameters for the dark-states are shown in Table I (they are identical, apart from the precise band centers, to the previous study). Since the ν_7 transitions are also indirectly affected by $\nu_{12} + \nu_8$ and $2\nu_8$ they were also introduced into the fit and co-fitted with the ν_{10} and ν_6 transitions. These extra states were added to the fit along with symmetry allowed interaction parameters and an acceptable fit was achieved for all transitions apart from those of ν_6 with $K_a = 5$. This subset of transitions was excluded by giving them an effectively infinite uncertainty of 999 cm^{-1} in the fit. The fitted parameters are shown in Table I and a simulated spectrum from these parameters is shown in Figure 3. It can be seen from Figure 3 that there is good agreement between the observed and simulated spectra. The integrated intensity of the simulations of both ν_6 and ν_{10} ($I^i_{10,6}$) and that of just ν_{10} (I^i_{10}) were compared, and their ratio was found to be $I^i_{10}/I^i_{10,6} \approx 0.20$. This implies that approximately 20% of the intensity of the ν_6 mode is stolen by ν_{10}. The final fit is available as supplementary material.[24]

V. DISCUSSION

The final fit incorporated 4296 ro-vibrational transitions attributed to ν_{10}, ν_6, and ν_7 with an uncertainty of 0.0002 cm^{-1} and delivered a fit with RMS error of 1.404. It was found that the fit was not sensitive to the higher order d

and H parameters of either ν_{10} or ν_6 and they were omitted. The addition of the L_{KKJ} parameter however greatly reduces the RMS error of the fit and was included, as it has been in previous analyses. Physically, this parameter is most likely accounting for weak perturbations to the ν_{10} and ν_6 modes which are not explicitly treated. The band centers of the dark-states were allowed to vary since this reduced the RMS error of the fit and the fitted value did not vary greatly from theoretical predictions. The ν_7 parameters which were also included in the fit did not vary by more than 1 standard deviation from those in the previous study.[10] The fitted band centers of ν_6 (1000.2 cm^{-1}) and ν_{10} (983.1 cm^{-1}) are approximately 1%–2% higher than the values obtained from DFT calculations of 993.3 cm^{-1} and 967.0 cm^{-1}, respectively, however the ν_6 band centre is in agreement with the previous study.[9] The fit also determined the value of $\alpha_6 = A_{GS} - A_{\nu6}$ to be -0.40391 cm^{-1} (s.d. $= 0.00013$ cm^{-1}) which differs substantially from the value presented in the previous ν_6 study[9] of $\alpha_6 = -0.6684$ cm^{-1}. However, the value obtained in this study is close to the sum of the harmonic, anharmonic, and large amplitude motion contributions to α_6 calculated from DFT predictions in Ref. 9 as -0.36 cm^{-1}. The contribution to α_6 from Coriolis interactions can be neglected since the most significant ones are now treated explicitly and should not affect the fitted value of $A_{\nu6}$.

The a- and c-axis Coriolis interaction parameters, $\zeta^a_{10,6}$ and $\zeta^c_{10,6}$, which are a measure of the strength of the Coriolis interaction can be calculated from the $G^a_{10,6}$ and $G^c_{10,6}$ fitted parameters as 0.162 and 0.029, respectively (using $G^a_{10,6} \approx 2A\zeta^a_{10,6}$). This compares favorably with the values calculated by GAMESS and VIBCA of $\zeta^a_{10,6} = 0.164$ and $\zeta^c_{10,6} = 0.032$. Additionally, the inclusion of a higher order Coriolis interaction parameter F^a was found to be critical in lowering the RMS error of the fit to an acceptable level. The magnitude of the interactions between the fundamentals and the dark-states could not be accurately determined and thus their fitted

values cannot be verified. Because of this, the determined parameters can only be considered to be effective, although all values that can be verified are in agreement with predicted values. Perhaps one indication of the validity of the interaction parameter associated with the dark-states is that their band centers are fitted to within 1% of the theoretical values, despite the fact they are able to freely vary in the fit.

An analysis of the energy levels of the states involved in the fit (see Figure 4) gives an insight into the complex and interconnected ro-vibrational structure of the ν_{10}, ν_6 system and of ketenimine as a whole. It is of note that the $K_a = 5$ levels of ν_6 are almost equal in energy to the $K_a = 10$ levels of ν_8. The energies of these two levels are within ± 0.5 cm^{-1} for the majority of the recorded range of J. Since ν_6 and ν_8 are both A$'$ symmetry, the Coriolis interactions that can occur directly between their energy levels are about the b-axis. Theoretical calculations predict the $\zeta^b_{8,6}$ to be very small, and the interaction is between levels with $\Delta K_a = 5$, so a direct interaction between these modes is unlikely to cause observable perturbations. It is conceivable however that an interaction could be facilitated via an intermediate state. A likely candidate for this is the currently unstudied A$''$ symmetry mode ν_{11} since very strong a- and c-axis perturbations are predicted between both ν_8 and ν_{11} ($\zeta^a_{8,11} = 0.11$, $\zeta^c_{8,11} = 0.27$) and also ν_{11} and ν_6 ($\zeta^a_{11,6} = 0.45$, $\zeta^c_{11,6} = 0.61$). The precise location of the energy levels of ν_{11} are not well known, however they can be crudely approximated (rotational parameters restricted to those of the *G. S.*, theoretically calculated band centre, no perturbations). Under this approximation, the $K_a = 7$ levels of ν_{11} are closest in energy to $K_a = 5$ of ν_6 and $K_a = 10$ of ν_8 which indicates they are the most likely to bridge the $\Delta K_a = 5$ b-axis interaction via a $\Delta K_a = 2$ a-axis interaction and a $\Delta K_a = 3$ c-axis interaction. It is also possible for the bridging to occur via the $K_a = 8$ levels of ν_{11} and there is likely to be a contribution from both mechanisms. Explicit treatment of this type of interaction was considered to be an intractable problem, given the sheer number of coupled vibrational levels and possible interactions. Even the ground state is not independent, coupled in to the system via both ν_8 and ν_{12} states.

VI. CONCLUSION

Ro-vibrational transitions within the Coriolis coupled doublet ν_{10} and ν_6 have been assigned, and rotational, centrifugal distortion and Coriolis interaction parameters determined. The fitted values of $\zeta^a_{10,6}$ and $\zeta^c_{10,6}$ are in agreement with DFT calculations. Perturbations to these observed states from dark-states have also been treated. A probable source of the perturbation to $K_a = 5$ of ν_6 has been proposed; however due to its complexity it has not been fitted. These coupled

modes have again demonstrated the capacity of ketenimine to exhibit strong intensity stealing effects in coupled systems.

[1] F. J. Lovas, J. M. Hollis, A. J. Remijan, and P. R. Jewell, Astrophys. J. **645**, L137 (2006).

[2] M. Rodler, R. D. Brown, P. D. Godfrey, and B. Kleibömer, J. Mol. Spectrosc. **118**, 267 (1986).

[3] E. Jacox and D. E. Milligan, J. Am. Chem. Soc. **85**, 278 (1963).

[4] M. E. Jacox, Chem. Phys. **43**, 157 (1979).

[5] M. Rodler, R. D. Brown, P. D. Godfrey, and L. M. Tack, Chem. Phys. Lett. **110**, 447 (1984).

[6] H. W. Kroto, G. Y. Matti, R. J. Suffolk, J. D. Watts, M. Rittby, and R. J. Bartlett, J. Am. Chem. Soc. **112**, 3779 (1990).

[7] J. August, Ph.D. dissertation, Sussex University, 1986.

[8] M. K. Bane, C. D. Thompson, E. G. Robertson, D. R. T. Appadoo, and D. McNaughton, Phys. Chem. Chem. Phys. **13**, 6793 (2011).

[9] F. Ito and T. Nakanaga, J. Mol. Spectrosc. **264**, 100 (2010).

[10] M. K. Bane, E. G. Robertson, C. D. Thompson, C. Medcraft, D. R. T. Appadoo, and D. McNaughton, J. Chem. Phys. **134**, 234306 (2011).

[11] L. Nemes, D. Luckhaus, M. Quack, and J. W. C. Johns, J. Mol. Struct. **517–518**, 217 (2000).

[12] D. McNaughton, E. G. Robertson, and L. D. Hatherley, J. Mol. Spectrosc. **175**, 377 (1996).

[13] G. Duxbury and M. L. Le Lerre, J. Mol. Spectrosc. **92**, 326 (1982).

[14] H. H. Blau and H. H. Nielsen, J. Mol. Spectrosc. **1**, 124 (1957).

[15] P. H. Turner, L. Halonen, and I. M. Mills, J. Mol. Spectrosc. **88**, 402 (1981).

[16] I. M. Mills, Pure Appl. Chem. **11**, 325 (1965).

[17] A. Doughty, G. B. Bacskay, and J. C. Mackie, J. Phys. Chem. **98**, 13546 (1994).

[18] L. S. Rothman, I. E. Gordon, A. Barbe, D. C. Benner, P. F. Bernath, M. Birk, V. Boudon, L. R. Brown, A. Campargue, J. P. Champion, K. Chance, L. H. Coudert, V. Dana, V. M. Devi, S. Fally, J. M. Flaud, R. R. Gamache, A. Goldman, D. Jacquemart, I. Kleiner, N. Lacome, W. J. Lafferty, J. Y. Mandin, S. T. Massie, S. N. Mikhailenko, C. E. Miller, N. Moazzen-Ahmadi, O. V. Naumenko, A. V. Nikitin, I. Orphal, V. I. Perevalov, A. Perrin, A. Predoi-Cross, C. P. Rinsland, M. Rotger, M. Simecková, M. A. H. Smith, K. Sung, S. A. Tashkun, J. Tennyson, R. A. Toth, A. C. Vandaele, and J. Vander Auwera, J. Quant. Spectrosc. Radiat. Transf. **110**, 533 (2009).

[19] M. W. Schmidt, K. K. Baldridge, J. A. Boatz, S. T. Elbert, M. S. Gordon, J. H. Jensen, S. Koseki, N. Matsunaga, K. A. Nguyen, S. Su, T. L. Windus, M. Dupuis, and J. A. Montgomery, Jr., J. Comput. Chem. **14**, 1347 (1993).

[20] See http://info.ifpan.edu.pl/~kisiel/vibr/vibr.htm#vibca for information for vibca and fconv .

[21] H. M. Pickett, J. Mol. Spectrosc. **148**, 371 (1991).

[22] T. Shimanouchi, *Tables of Molecular Vibrational Frequencies,* Consolidated Volume 1 (National Bureau of Standards, Washington, DC, 1972).

[23] D. McNaughton, D. McGilvery, and F. Shanks, J. Mol. Spectrosc. **149**, 458 (1991).

[24] See supplementary material at http://dx.doi.org/10.1063/1.3664624 for transition lists and final least squares fits.

Declaration for Thesis Chapter 3.4

Declaration by candidate

In the case of Chapter 3.4, the nature and extent of my contribution to the work was the following:

Nature of contribution	Extent of contribution (%)
Initiation, key ideas, development, writing up	80

The following co-authors contributed to the work. Co-authors who are students at Monash University must also indicate the extent of their contribution in percentage terms:

Name	Nature of contribution	Extent of contribution (%) for student co-authors only
C. Jones	Molecule synthesis	
S. L. Choong	Molecule synthesis	
C. D. Thompson	Initiation, key ideas	
P. D. Godfrey	key ideas	
D. R. T. Appadoo	Experiment assistance	
D. McNaughton	Initiation, key ideas	

Candidate's Signature		Date

Declaration by co-authors

The undersigned hereby certify that:

(1) the above declaration correctly reflects the nature and extent of the candidate's contribution to this work, and the nature of the contribution of each of the co-authors.
(2) they meet the criteria for authorship in that they have participated in the conception, execution, or interpretation, of at least that part of the publication in their field of expertise;
(3) they take public responsibility for their part of the publication, except for the responsible author who accepts overall responsibility for the publication;
(4) there are no other authors of the publication according to these criteria;
(5) potential conflicts of interest have been disclosed to (a) granting bodies, (b) the editor or publisher of journals or other publications, and (c) the head of the responsible academic unit; and
(6) the original data are stored at the following location(s) and will be held for at least five years from the date indicated below:

Location(s)	**Monash University, School of Chemistry**

Signature 1		Date
Signature 2		
Signature 3		
Signature 4		
Signature 5		

Signiture 6

High-resolution FTIR spectroscopy of the v_7 and v_8 bands of 1-phosphapropyne

Michael K. Bane [a], Cameron Jones [a], Sam L. Choong [a], Christopher D. Thompson [a], Peter D. Godfrey [a], Dominique R.T. Appadoo [b], Don McNaughton [a,*]

[a] School of Chemistry, Monash University, Wellington Rd., Clayton, Victoria 3800, Australia
[b] Australian Synchrotron, 800 Blackburn Rd., Clayton, Victoria 3168, Australia

ARTICLE INFO

ABSTRACT

1-Phosphapropyne has been prepared and high-resolution (0.001 cm^{-1}) spectra have been recorded on the far-infrared beamline at the Australian synchrotron between 1500–700 cm^{-1} and 400–50 cm^{-1}. Ro-vibrational transitions of the v_8 (308 cm^{-1}) and v_7 (1006 cm^{-1}) fundamentals as well as the $2v_8^{\pm2} \leftarrow v_8^{\pm1}$ and $2v_8^0 \leftarrow v_8^{\pm1}$ hot-bands have been assigned, and rotational, centrifugal distortion and Coriolis interaction parameters determined. The $2v_8^{\pm2} \leftarrow v_8^{\pm1}$ hot-band is an example of a particularly complex $E \leftarrow E$ transition, for which both states are strongly Coriolis and $l(2,2)$ coupled.

© 2012 Elsevier Inc. All rights reserved.

1. Introduction

It has only been recently that the development of a gram scale synthesis of the unhindered 1-phosphapropyne [1] (CH$_3$C≡P, see Table 1), has allowed its chemistry to be investigated and compared to that of bulkier systems. These studies of this P-analogue of propyne and acetonitrile, have revealed that the reactivity of CH$_3$C≡P can be significantly different to that of more hindered phosphaalkynes, and that the compound is a versatile synthon in both organophosphorus and coordination chemistries [2–5].

CH$_3$C≡P, which is unstable at room temperature, was first generated and characterized by Hopkinson et al. [6] in a microwave spectroscopic study and subsequently investigated by Westwood et al. [7] using photoelectron spectroscopy. The rotational structure of both the ground and v_8 = 1, 2 and 3 vibrational states were studied in a microwave study by Kroto et al. [8], however due to the limited number and range of transitions, the determined parameters only accurately described the rotational and ro-vibrational structure with low J and K quantum numbers. A more recent microwave spectroscopic study by Bizzocchi et al. [9] improved the ground state (G.S.) molecular parameters by including higher J and K rotational transitions, which allowed a more accurate determination of higher order centrifugal distortion parameters.

CH$_3$C≡P has C_{3v} symmetry and thus has eight vibrational modes belonging to A_1 (non-degenerate) and E (degenerate) symmetry. A medium-resolution (0.08 cm^{-1}) infra-red (IR) study of the modes lying between 4000 and 400 cm^{-1}, including v_7, is provided by Ohno et al. [10]. The regions of the spectrum containing the v_2, v_6 and v_8 modes have also been the target of more focused medium-resolution ($\geqslant 0.01$ cm^{-1}) studies by Ohno et al. [11–14]. Unresolved q-branch structure of v_8 and v_7 was analyzed in these previous studies.

This study is concerned with assignment and analysis of the regions containing v_8 (308 cm^{-1}) and v_7 (1006 cm^{-1}) transitions. The analysis has resulted in improved molecular parameters for the previously studied (at lower resolution or with a lower range of J and K) v_8 and $2v_8^0 \leftarrow v_8^{\pm1}$ modes. The $2v_8^{\pm2} \leftarrow v_8^{\pm1}$ component of the hot-band was also studied, and an analysis of this previously unobserved, complex $E \leftarrow E$ mode has been included. An analysis of the v_7 mode is also presented, and a significant mis-assignment in the previous study [10] has been corrected.

2. Experimental

2.1. Synthesis

CH$_3$C≡P was prepared by a variation of the literature procedure [1], which involved the dehydrochlorination of the primary phosphine, CH$_3$C(Cl)$_2$PH$_2$, with the strong base 1,8-diazabicyclo(5.4.0)undec-7-ene (DBU) in diglyme as shown in Eq. 1. The phosphaalkyne was purified by distilling all volatiles from the reaction mixture and passing them through two traps at −40 °C and −120 °C. The phosphaalkyne was recovered from the colder trap and was shown to have a purity in the liquid phase of >99% by ^{1}H NMR spectroscopy.

* Corresponding author. Fax: +61 399054597.
  E-mail address: donald.mcnaughton@monash.edu (D. McNaughton).

$$\begin{array}{c}\text{Me} \\ \big\backslash \\ \text{Cl}^{\text{\tiny{////}}}\text{C}-\text{P}^{\text{\tiny{\\\\}}}\text{H} \\ \big/ \qquad \big| \\ \text{Cl} \qquad \text{H}\end{array} \xrightarrow[\text{-DBU.HCl}]{\text{2 DBU}} \text{Me}-\text{C}\equiv\text{P}$$
(1)
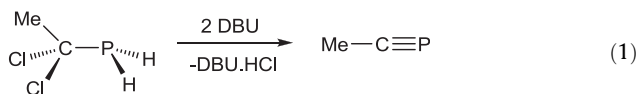
2.2. Theoretical predictions

Geometry optimizations and subsequent frequency calculations were performed at the B3LYP/cc-pVTZ level using Gaussian09 [15]. In order to determine the energy of various structural configurations and so determine whether spectra from other isomers may be present, geometry optimizations of the structures shown in Table 1 were carried out. These calculations also determined structural parameters such as rotational, centrifugal distortion, Coriolis coupling parameters and dipole moments which were used as a comparison to fitted values.

2.3. Spectroscopy

The experiments were performed at the far-IR beam-line at the Australian synchrotron, and two regions of the spectrum were recorded between 400–50 cm^{-1} (region 1) and 1550–700 cm^{-1} (region 2). The liquid sample is unstable at room temperature and was maintained at dry-ice temperature ($\sim$195 K) throughout the experiment. Sample vapor was released into a multi-pass White cell equipped with polyethylene windows coupled to a Bruker IFS 125HR spectrometer capable of achieving a nominal resolution of 0.00096 cm^{-1}. The sample vapor was found to be sufficiently stable at low concentrations in the cell for spectra to be recorded before degradation. The high far-IR flux of the synchrotron source ensured sufficient sensitivity in region 1. Region 2 was recorded using an internal Globar source, since it was expected to give equal or better signal/noise at 1004 cm^{-1} (synchrotron S/N advantage extends to approx 1000 cm^{-1}). The spectrum in region 1 was recorded with a 6.3 mm aperture (effectively open since the synchrotron radiation focused beam is ca 200 μm), a 6-μm mylar beam splitter and a

Table 1
CH$_3$C$\equiv$P isomers optimized energy at the B3LYP/cc-pVTZ level of theory.

Isomer	Structure	Relative energy (kcal mol^{-1})
1-Phosphaprop-1-yne		0
1-Phosphapropadiene		14.7[a]
1-Phosphaprop-2-yne		20.8
2-Phosphaprop-1-yne		68.9
1H-phosphirene		26.1
2H-phosphirene		20.7
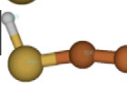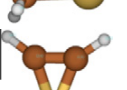
[a] Zero point energies have not been accounted for.

silicon bolometer operating at 4.2 K, equipped with an 800 cm^{-1} far-infrared cut-on type cold filter (consisting of a 13 μm polyethylene film overlaid with 4–8 μm diamond scatter layer) at a scan rate of 40 kHz. The 40 kHz scan rate was used to ensure the detector was not saturated and to take data as rapidly as possible. Region 2 was recorded with a 0.8 mm aperture, a KBr beam splitter and a mercury cadmium telluride (MCT) detector at a scan rate of 40 kHz. The pressure within the cell was maintained at approximately 0.2 mbar, with an optical path-length of 24 m and the temperature in the cell was ambient, assumed to be 300 K for spectral simulations. Overall 84 (region 1) and 149 (region 2) interferograms were recorded at 0.00096 cm^{-1}, averaged then Fourier transformed using a 4P apodization function and a post-zero fill factor of 8. All spectra were calibrated using water line positions from the HITRAN database [16].

Assigned lines were fitted with Pickett's SPFIT [17] and spectral simulation data were achieved by inputting the parameters obtained from the fits into Pickett's prediction software SPCAT [17]. The resulting calculated transitions were then convolved with a Gaussian line shape, with appropriate FWHM ($\sim$0.002 cm^{-1}) to produce a simulated spectrum.

3. Results and discussion

3.1. v_8 and v_7 fundamental modes

The Hamiltonian used to describe the energy levels of the symmetric rotor is as follows:

$$H = v_0 + BJ(J+1) + (A-B)K^2 - 2\zeta Akl - D_J[J(J+1)]^2 - D_{JK}J(J+1)K^2 - D_K K^4 + H_J[J(J+1)]^3 + H_{JK}[J(J+1)]^2 K^2 + H_{kJ}[J(J+1)]K^4 + H_K K^6 + \cdots$$
(2)

where v_0 is the vibrational energy associated with the fundamental transition and J, k and l are the quantum numbers associated with the total, the z-projection and orbital angular momentum respectively. It can be seen from Eq. (2) that the energy levels of the degenerate vibrational levels will, in general, be split via a Coriolis mechanism based on the magnitude and sign of the product kl.

The second observable source of perturbations is $l(2,2)$ coupling, which acts to split levels with $A_1 + A_2$ rotational symmetry via coupling with levels of $\Delta l = \Delta k = 2$. This condition is always satisfied in the fundamentals for the $K = 1$, $kl = \pm 1$ resulting in splitting of these levels. This splitting, to first order, is governed by the matrix element,

$$\langle v_8 = 1, J, k, l = \mp 1 | H | v_8 = 1, J, k \pm 2, l = \pm 1 \rangle$$
$$= -q/2[J(J+1) - k(k\pm 1)]^{1/2}[J(J+1) - (k\pm 1)(k\pm 2)]^{1/2}$$
(3)

The selection rules for a molecule with C_{3v} symmetry follow the Amat rule, $\Delta k - \Delta l = 3n$, where n is an integer. Since the G.S. has A_1 symmetry it follows that the first order selection rules for fundamental modes with E symmetry are $\Delta k = \Delta l = \pm 1$ ($\Delta K = 1$ transitions are to states where $kl > 0$ and $\Delta K = -1$ transitions are to states where $kl < 0$. $K \equiv |k|$).

The v_8 CCP bending mode has E symmetry and is predicted to exhibit high intensity absorption (IR intensity theoretically calculated as 13.03 km mol^{-1}). The spectral region containing the v_8 ro-vibrational transitions is shown in Fig. 1a. Transitions in the spectrum were selected and presented in the Loomis–Wood format using MacLoomis [18], which groups regularly spaced transitions, such as those differing in J but sharing constant K, into approximately vertical series of constant K. Presenting the spectra in this way allowed the series between $K = 1$ and 8 of the v_8^{+1} component (from $\Delta K = 1$ transitions) and $K = 0$ and 5 of the v_8^{-1} component (from $\Delta K = -1$ transitions) to be assigned, with $J(\text{max}) = 70$. Overall
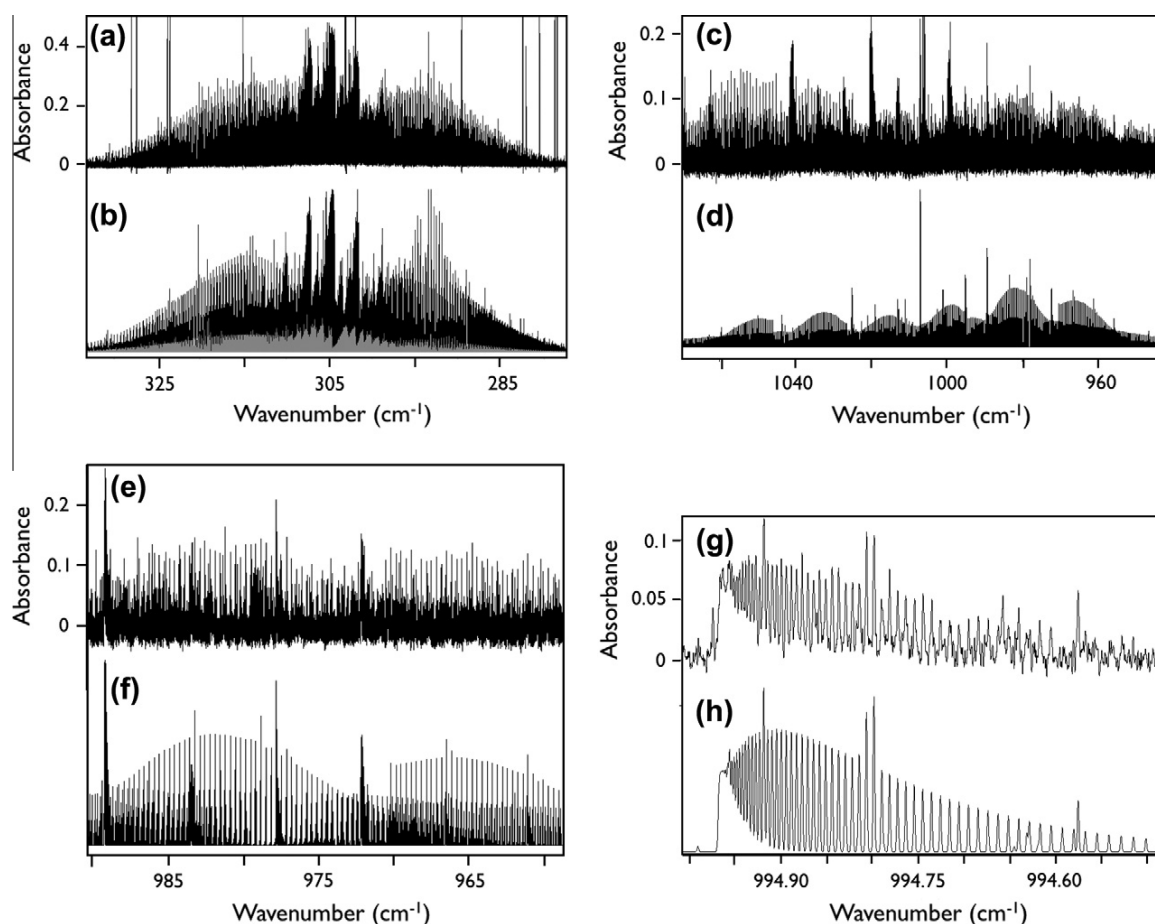
Fig. 1. Experimental survey spectra in (a) regions 1 and (c) region 2, (b) corresponding simulations of the v_8 fundamental (black) and $2v_8^{\pm2} \leftarrow v_8^{\pm1}$ and hot-band (gray) and (d) corresponding simulation of the v_7 fundamental. The expanded experimental, (e and g), and simulated (f and h), sections illustrate the agreement between the two. All experimental spectra contain intense transitions attributed to the v_6 (also a CH_3 rock) mode [21] of the contaminant molecule CH_3Cl centered about 1017 cm^{-1} which do not appear in the simulations. Further additional lines are due to residual water.

1553 ro-vibrational transitions were assigned from this mode, and given uncertainty 0.0002 cm^{-1} (10% of the FWHM of the peak) in the fitting procedure. These assignments were confirmed by comparison with ground state combination differences generated from the known G.S. constants [9].

These assigned v_8 transitions, as well as 13 pure rotational transitions associated with this mode determined by the previous microwave study [8] were least-squares fit simultaneously to the symmetric rotor Hamiltonian (Eq. (2)) using Pickett's SPFIT [17]. The final fit derived the ro-vibrational parameters shown in Table 2, with an RMS deviation of 0.69. One of the microwave transitions could not be fitted with acceptable error and was removed from the fit by giving it effectively infinite uncertainty (999 MHz). From the fit the value of the Coriolis coupling constant was determined (using $G_{88} \approx 2A\zeta_{88}$) to be $\zeta_{88} = 0.878$, which compares well to the theoretically calculated value of $\zeta_{88} = 0.876$ as well as those presented in previous studies [8,14]. The value of q is also consistent with the microwave study [8]. The H_{JK} term was allowed to vary from the G.S. value since this significantly reduces the RMS error of the fit and is justified since it is well determined and does not deviate greatly from the G.S. value. Fig. 1 shows there is good agreement between observed and simulated spectra.

The spectrum between 1500 and 700 cm^{-1} was recorded and the region containing the v_7 ro-vibrational transitions is shown in Fig. 1c. This region contains a large number of intense transitions

from a species other then $CH_3C\equiv P$ and alternative structural isomers of $CH_3C\equiv P$ were explored using *ab initio* calculations with the relative energies of the species shown in Table 1. Cheng et al. [19] carried out a study of these isomers at the B3LYP/6-311++G** level of theory exploring transition states and reaction pathways and concluded that 1-phosphaprop-2-yne, $HCCPH_2$ is the only other isomer likely to be experimentally accessible. In our calculations 1-phosphapropadiene, $CH_2C\equiv PH$ is the next lowest energy structural isomer, which is more consistent with earlier work by Berger et al. [20], and both it and the two cyclic structures are low enough in energy to be considered as possible species for detection. No evidence for the presence of any of these species was found in our spectra and the contaminant transitions were eventually attributed to the v_6 mode [21] of methyl chloride (CH_3Cl) at 1017 cm^{-1}. CH_3Cl appears as an undesired remnant of the synthesis, and since it has a greater volatility than $CH_3C\equiv P$, it is expected to be present in higher concentrations in the gas phase than determined in the liquid phase. Intense CH_3Cl transitions were also found in the 732 cm^{-1} spectral region (attributed to the v_3 CCl stretch mode [21]), however this mode had sufficient strength to completely mask the weak CC stretch mode, v_4, of $CH_3C\equiv P$ which was expected to be of similar energy (from solid state spectra [10] and B3LYP/cc-pVTZ calculations).

The v_7 CH_3 rocking mode is the second lowest energy E symmetry mode and is predicted to have much weaker absorption (IR

Table 2
Band parameters fitted to Watson's S-reduced I^r Hamiltonian for the G.S., v_8, $2v_8^0 \leftarrow v_8^{\pm1}$, $2v_8^{\pm2} \leftarrow v_8^{\pm1}$ and v_7 modes of $CH_3C\equiv P$.

Constant	G.S.[a]	G.S.[b]	v_8	$2v_8^{\pm2}$	$2v_8^0$	v_7
Band centre (cm^{-1})			308.286266 (11)[c]	625.110927 (17)	602.47376 (60)	1005.836092 (19)
A (MHz)	158827	155072	155025.153 (28)	154979.067 (83)	155080.16 (31)	155970.358 (40)
B (MHz)	5009.027	4991.342947	5003.65518 (41)	5015.83664 (82)	5014.875451 (20)	4988.24486 (83)
D_J (kHz)	0.951667	0.996783	1.01807 (13)	1.05656 (37)	0.93060 (33)	0.99765 (26)
D_{JK} (kHz)	63.164	66.237	66.730 (32)	62.71 (15)	67.85 (11)	67.944 (27)
H_{JK} (Hz)	0.13823	0.19781	0.1440 (99)	0.19781[d]	0.19781[d]	0.19781[d]
H_{KJ} (Hz)	−701.14	1.7613	1.7613[d]	1.7613[d]	1.7613[d]	1.7613[d]
$G_a = 2\zeta A_{GS}$ (MHz)			272310.93 (12)	544665.31 (28)		123526.94 (22)
η_J (kHz)			110.550 (62)	244.43 (24)		68.07 (11)
η_{JK} (kHz)			–	−1.983 (28)		–
η_K (kHz)			−854.8 (38)	–		−5427 (14)
η_{KK} (kHz)			–	–		15.72 (17)
			q^{88} (MHz) = 3.15834 (53)	$q^{8+8(2),8+8(0)}$ (MHz) = −4.5272 (53)		q^{77} (MHz) = 1.57189 (34)
			q_J^{88} (Hz)=−4.42 (17)	$q_K^{8+8(2),8+8(0)}$ (kHz) = 97.3 (16)		
				$q_{KK}^{8+8(2),8+8(0)}$ (kHz) = −6.720 (79)		
J(max)			70	59	67	63
K_a(max)			8	5	3	8
Number trans.			1566[e]	626[e]	48[e]	1053
RMS deviation			0.69	1.60		1.50

[a] Determined from calculations at the B3LYP/cc-pVTZ level of theory. The value of H_{KJ} is in clear disagreement with experiment.
[b] G.S. Parameters determined by a previous study [9].
[c] Figures in brackets are one standard deviation according to the least squares fit in units of the least significant figure quoted.
[d] Parameter forced during the fit to be equal to the G. S. value.
[e] Includes 13, 10 and 7 previously published [8] microwave transitions of v_8, $2v_8^{\pm2}$ and $2v_8^0$ respectively.

intensity theoretically calculated as 0.02 km mol^{-1}). The spectrum was peak-picked in the same way as detailed above and series between $K = 1$ and 4 of the v_7^{+1} component (from $\Delta K = 1$ transitions) and $K = 0$ and 8 of the v_7^{-1} component (from $\Delta K = -1$ transitions) assigned, with J(max) = 63. The higher resolution of this study allowed us to identify a significant mis-assignment in the previous study [10]. This was confirmed by comparison of G.S. combination differences with those generated from the known G.S. constants, as well as the observation of the affects of $l(2,2)$ doubling which only occurs at specific values of K. Only q-branches with $K = 3n$ in the G.S. were observed in the previous study (since these are enhanced due to spin-statistics in C_{3v} molecules) and a mis-assignment of one unit in this scheme results in the true K assignment being incorrect by 3. These same spin-statistics were also very clearly observed in the spectra associated with this work and were an assistance to correct assignment of the lines. Overall 1053 ro-vibrational transitions from this mode were correctly assigned, and given uncertainty 0.0002 cm^{-1} in the fitting procedure.

These assigned v_7 transitions were least-squares fitted to the symmetric rotor Hamiltonian (Eq. (2)), and the derived parameters are shown in Table 2 with RMS deviation of 1.50. From the fit the value of the Coriolis coupling constant can be determined as $\zeta_{77} = 0.396$, which is in agreement with the calculated value of $\zeta_{77} = 0.412$. Fig. 1 shows there is good agreement between observed and simulated spectra.

3.2. v_8 Hot-bands

Eq. (2) also accurately describes the structure of the two components of the overtone. For the $2v_8^{\pm2}$ component which has E symmetry, $l = \pm2$ and the splitting should be approximately double that of the fundamental. For the $2v_8^0$ component which has A_1 symmetry, $l = 0$ and thus the splitting term in the Hamiltonian vanishes.

It follows from the Amat rule that the selection rules for these types hot-bands are $\Delta k = \Delta l = \pm1$ as for the fundamental. For the $2v_8^{\pm2} \leftarrow v_8^{\pm1}$ component, this can be summarized by stating that $\Delta K = 1$ transitions both originate from and transition to states where $kl > 0$ and $\Delta K = -1$ transitions both originate from and transition to states where $kl < 0$. For the $2v_8^0 \leftarrow v_8^{\pm1}$ component, it is summarized by the statement that $\Delta K = 1$ transitions originate

from states where $kl < 0$ and $\Delta K = -1$ transitions originate from states where $kl > 0$.

In the same manner as for the fundamental, the $l(2,2)$ coupling was considered. This only differs from the case of the fundamental in that the interaction is now between the two different components of the overtone, which in general will have different band-centers and an interaction only occurs if symmetry allowed interacting levels are close in energy. Since the $K = 2$, $kl = 4$ rotational levels are the first with $A_1 + A_2$ rotational symmetry these are the most likely to be split by this mechanism.

The majority of transitions observed, which were assigned to the hot-band, were for the $2v_8^{\pm2} \leftarrow v_8^{\pm1}$ component and this analysis was attempted first. Using the same process as was previously detailed, the series between $K = 1$ and 5 of the $2v_8^{+2}$ component (from $\Delta K = 1$ transitions) and $K = 0$ and 2 of the $2v_8^{-2}$ component (from $\Delta K = -1$ transitions) were assigned, with J(max) = 59. Overall 617 ro-vibrational transitions were assigned from this mode, and given uncertainty 0.0002 cm^{-1} in the fitting procedure. These assignments were confirmed by comparison with lower state combination differences, which are generated from the parameters determined in the fit to the fundamental. Attempts to satisfactorily fit the $2v_8^{\pm2} \leftarrow v_8^{\pm1}$ transitions alone were not successful. From the high residual error it was clear that this component of the overtone was perturbed, most likely by the $2v_8^0$ component. These two components would need to be analyzed and co-fit together for an acceptable fit to be achieved.

The precise location of the q-branch structure of the $2v_8^0 \leftarrow v_8^{\pm1}$ component of the hot-band in the spectrum is well documented in a previous study [14] and the search for these transitions was purely based on this. Only two useful series were found due to the low intensity of these transitions and the congestion of the spectrum. These were the p- and r-branch of the $K = 0 \leftarrow 1$ series and the q-branch of the $K = 3 \leftarrow 2$ series, which both have enhanced intensity (see Graner [22]). These assignments were confirmed by comparison with the lower state combination differences.

These assigned $2v_8^{\pm2} \leftarrow v_8^{\pm1}$ and $2v_8^0 \leftarrow v_8^{\pm1}$ transitions, as well as 17 pure rotational transitions associated with these modes determined by the previous microwave study [8] were least-squares fitted simultaneously to the symmetric rotor Hamiltonian (Eq. (2)). The final fit derived the ro-vibrational parameters shown
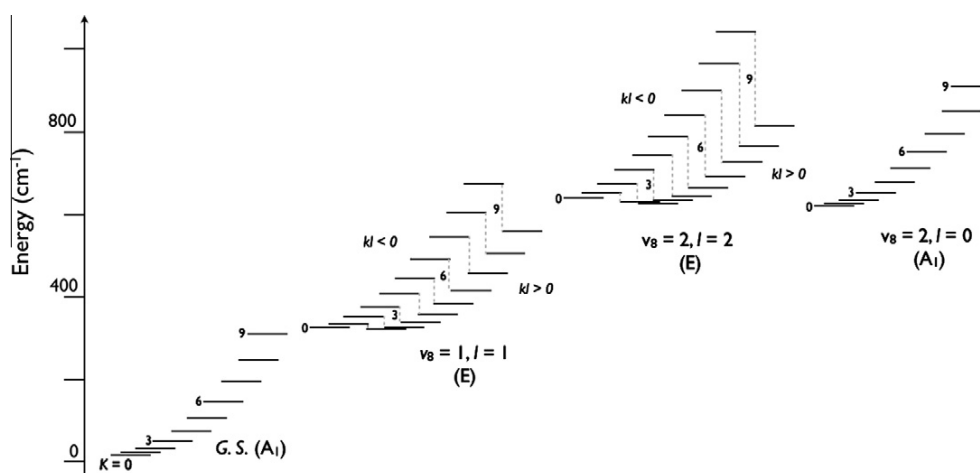
Fig. 2. Calculated energies of the $J = 10$ level for K up to 9 for the lowest energy modes of $CH_3C{\equiv}P$. All energies calculated from parameters in Table 2.

in Table 2, with an RMS error of 1.60. The RMS error of the fit to the hot-bands is expected to be larger than that of the fundamental, since errors in the lower state will contribute to the overall RMS error of the fit. Two of the microwave transitions could not be fitted with acceptable error and were removed by giving them effectively infinite uncertainty. Although there are a limited number of observed transitions involving the $2v_8^0$ component of the overtone, the parameters determined for this state are consistent with previous work [8,14], are well determined and do not differ greatly from expected values. It appears that the dataset is sufficient to describe the mode, at least at low K, allowing us to model the interactions between the two components of the overtone sufficiently. Subsequently this allows us to achieve an acceptable fit for the $2v_8^{\pm2}$ component, for which there are a large number of observed transitions. Fig. 1 shows there is good agreement between observed and simulated spectra for the $2v_8^{\pm2} \leftarrow v_8^{\pm1}$ component. The $2v_8^0 \leftarrow v_8^{\pm1}$ component is not simulated since there are an insufficient number of observable transitions for a meaningful comparison. All fits are available as Supplementary material.

Fig. 2 shows the particularly large splitting due to the Coriolis coupling in both the fundamental and hot-band (since both A and ζ are large), which is so large that for some $kl > 0$ levels of low K there is actually a decrease in energy with increasing K. Because of this the low K levels of the $2v_8^0$ overtone have energies which are similar to those of $2v_8^{\pm2}$ where the product $kl > 0$, and an $l(2,2)$ interaction is likely to be significant (as observed).

As a final note, the combination differences from all modes were co-fitted with the microwave transitions from previous work [8,9], however due to the extent and quality of the most recent mmwave work, it had negligible effect on the G.S. parameters and is thus not presented.

4. Conclusion

Ro-vibrational transitions of the v_7 and v_8 fundamentals as well as the $2v_8^{\pm2} \leftarrow v_8^{\pm1}$ and $2v_8^0 \leftarrow v_8^{\pm1}$ hot-bands have been assigned, and rotational, centrifugal distortion and Coriolis interaction parameters determined. The fitted values of ζ_{88}, ζ_{77} and q_{88} are in good agreement with B3LYP/cc-pVTZ calculations and with values presented in previous studies [8,10,14]. The $2v_8^{\pm2} \leftarrow v_8^{\pm1}$ hot-band is an example, of which there are few for C_{3v} molecules (see Graner [22]), of a complex $E \leftarrow E$ transition, for which both states are strongly Coriolis and $l(2,2)$ coupled.

Appendix A. Supplementary material

Supplementary data associated with this article can be found, in the online version, at http://dx.doi.org/10.1016/j.jms.2012.04.005.

References

[1] J.-C. Guillemin, T. Janati, J.-M. Denis, J. Org. Chem. 66 (2001) 7864–7868.
[2] S.L. Choong, C. Jones, A. Stasch, Dalton Trans. 39 (2010) 5774–5776.
[3] C. Jones, C. Schulten, A. Stasch, Inorg. Chem. 47 (2008) 1273–1278.
[4] C. Jones, C. Schulten, A. Stasch, Dalton Trans. (2007) 1929–1933.
[5] C. Jones, C. Schulten, A. Stasch, Dalton Trans. (2006) 3733–3735.
[6] M.J. Hopkinson, H.W. Kroto, J.F. Nixon, N.P.C. Simmons, Chem. Phys. Lett. 42 (1976) 460–461.
[7] N.P.C. Westwood, H.W. Kroto, J.F. Nixon, N.P.C. Simmons, J. Chem. Soc., Dalton Trans. (1979) 1405–1408.
[8] H.W. Kroto, J.F. Nixon, N.P.C. Simmons, J. Mol. Spec. 77 (1979) 270–285.
[9] L. Bizzocchi, L. Cludi, C. Degli Esposti, J. Mol. Spec. 218 (2003) 53–57.
[10] K. Ohno, H. Matsuura, D. McNaughton, H.W. Kroto, J. Mol. Spec. 111 (1985) 415–424.
[11] K. Ohno, Y. Yamamoto, H. Matsuura, H. Murata, Chem. Lett. (1984) 413–414.
[12] K. Ohno, H. Matsuura, D. McNaughton, H.W. Kroto, J. Mol. Spec. 124 (1987) 82–91.
[13] K. Ohno, H. Matsuura, D. McNaugton, H.W. Kroto, J. Mol. Spec. 126 (1987) 245–254.
[14] K. Ohno, H. Matsuura, Bull. Chem. Soc. Jpn. 60 (1987) 2265–2267.
[15] M.J. Frisch, G.W. Trucks, H.B. Schlegel, G.E. Scuseria, M.A. Robb, J.R. Cheeseman, G. Scalmani, V. Barone, B. Mennucci, G.A. Petersson, H. Nakatsuji, M. Caricato, X. Li, H.P. Hratchian, A.F. Izmaylov, J.Z. Bloino, G. Zheng, J.L. Sonnenberg, M. Hada, M. Ehara, K. Toyota, R. Fukuda, J. Hasegawa, M. Ishida, T. Nakajima, Y. Honda, O. Kitao, H. Nakai, T. Vreven, J. Montgomery, J.A. Montgomery, J.E. Peralta, F. Ogliaro, M. Bearpark, J.J. Heyd, E. Brothers, K.N. Kudin, V.N. Staroverov, R. Kobayashi, J. Normand, K. Raghavachari, A. Rendell, J.C. Burant, S.S. Iyengar, J. Tomasi, M. Cossi, N. Rega, N.J. Millam, M. Klene, J.E. Knox, J.B. Cross, V. Bakken, C. Adamo, J. Jaramillo, R. Gomperts, R.E. Stratmann, O. Yazyev, A.J. Austin, R. Cammi, C. Pomelli, J.W. Ochterski, R.L. Martin, K. Morokuma, V.G. Zakrzewski, G.A. Voth, P. Salvador, J.J. Dannenberg, S. Dapprich, A.D. Daniels, Ö. Farkas, J.B. Foresman, J.V. Ortiz, J. Cioslowski, D.J. Fox, Gaussian, Inc., Wallingford, CT, 2009.
[16] L.S. Rothman, I.E. Gordon, A. Barbe, D.C. Benner, P.F. Bernath, M. Birk, V. Boudon, L.R. Brown, A. Campargue, J.P. Champion, K. Chance, L.H. Coudert, V. Dana, V.M. Devi, S. Fally, J.M. Flaud, R.R. Gamache, A. Goldman, D. Jacquemart, I. Kleiner, N. Lacome, W.J. Lafferty, J.Y. Mandin, S.T. Massie, S.N. Mikhailenko, C.E. Miller, N. Moazzen-Ahmadi, O.V. Naumenko, A.V. Nikitin, J. Orphal, V.I. Perevalov, A. Perrin, A. Predoi-Cross, C.P. Rinsland, M. Rotger, M. Simecková,

M.A.H. Smith, K. Sung, S.A. Tashkun, J. Tennyson, R.A. Toth, A.C. Vandaele, J. Vander Auwera, J. Quant. Spectrosc. Radiat. Transfer 110 (2009) 533–572.

[17] H.M. Pickett, J. Mol. Spec. 148 (1991) 371–377.

[18] D. McNaughton, D. McGilvery, F. Shanks, J. Mol. Spec. 149 (1991) 458–473.

[19] X. Cheng, Y. Zhao, L. Li, X. Tao, J. Mol. Struct. (THEOCHEM) 682 (2004) 137–143.

[20] D.J. Berger, P.P. Gaspar, P. LeFloch, F. Mathey, R.S. Grev, Organometallics 15 (1996) 4904–4915.

[21] T. Shimanouchi, Tables of Molecular Vibrational Frequencies. National Bureau of Standards, 1972.

[22] G. Graner, J. Mol. Spec. 161 (1993) 58–79.

Declaration for Thesis Chapter 3.5

Declaration by candidate

In the case of Chapter 3.5, the nature and extent of my contribution to the work was the following:

Nature of contribution	Extent of contribution (%)
Initiation, key ideas, development, writing up	80

The following co-authors contributed to the work. Co-authors who are students at Monash University must also indicate the extent of their contribution in percentage terms:

Name	Nature of contribution	Extent of contribution (%) for student co-authors only
C. D. Thompson	Initiation, key ideas	
D. R. T. Appadoo	Experiment assistance	
D. McNaughton	Initiation, key ideas	

Candidate's Signature		Date

Declaration by co-authors

The undersigned hereby certify that:

(1) the above declaration correctly reflects the nature and extent of the candidate's contribution to this work, and the nature of the contribution of each of the co-authors.
(2) they meet the criteria for authorship in that they have participated in the conception, execution, or interpretation, of at least that part of the publication in their field of expertise;
(3) they take public responsibility for their part of the publication, except for the responsible author who accepts overall responsibility for the publication;
(4) there are no other authors of the publication according to these criteria;
(5) potential conflicts of interest have been disclosed to (a) granting bodies, (b) the editor or publisher of journals or other publications, and (c) the head of the responsible academic unit; and
(6) the original data are stored at the following location(s) and will be held for at least five years from the date indicated below:

Location(s)	**Monash University, School of Chemistry**

Signature 1		Date
Signature 2		
Signature 3		

The proceeding article has been accepted for publication and is in the final proof stage. Some minor formatting issues have been rectified and the article is presented in this state for the sake of consistency with the other work presented in this thesis. Some amendments to the references are required.

- Reference 14 should read "W. D. Allen, J. E. Bertie, M. V. Falk, J. B. A. Hess, G. B. Mast, D. A. Othen, L. J. Schaad, and H. F. Schaefer, J. Chem. Phys. **84**(8), 4211 (1986)".
- Reference 17 should read "M. J. Frisch, G. W. Trucks, H. B. Schlegel *et al.*, GAUSSIAN *09, Revision A.1*, Gaussian, Inc., Wallingford, CT, 2009".

Synchrotron far infrared spectroscopy of the ground, ν_5, and ν_{15} states of thiirane

Michael K. Bane,[1] Christopher D. Thompson,[1] Dominique R. T. Appadoo,[2] and Don McNaughton[1,a)]

[1]*School of Chemistry, Monash University, Wellington Rd., Clayton, Victoria 3800, Australia*
[2]*Australian Synchrotron, 800 Blackburn Rd., Clayton, Victoria 3168, Australia*

The high-resolution (0.001 cm^{-1}) spectrum of thiirane has been recorded at the far-infrared beamline at the Australian synchrotron between 760–400 cm^{-1} and 170–10 cm^{-1}. Ro-vibrational transitions of the highly Coriolis coupled ν_5 (628.1 cm^{-1}) and ν_{15} (669.7 cm^{-1}) fundamentals, as well as pure rotational far-IR transitions have been assigned, and rotational, centrifugal distortion, and Coriolis interaction parameters determined. ν_{15} gains the vast majority of its intensity from an interesting Coriolis intensity stealing mechanism, which is also outlined. © *2012 American Institute of Physics.* [http://dx.doi.org/10.1063/1.4747191]

INTRODUCTION

Oxirane (c-C_2H_4O), the oxygen analogue of thiirane (ethylene sulfide, c-C_2H_4S, Figure 1), has been shown to be of astrophysical importance, and has been located in the interstellar medium by multiple surveys.[1,2] One of the more probable routes for the synthesis of this molecule in interstellar systems is via a spontaneous addition of excited atomic oxygen with ethylene.[1,3] Atomic sulfur has been implicated as both a reactant and product in interstellar chemistry (see, for example, Oppenheimer and Dalgarno[4]), and is known to be produced by photolysis of interstellar species such as H_2S,[5] SO_2,[6] and OCS.[7] Recently, Leonori *et al.*[8] have shown the reaction with ethylene is also spontaneous with excited sulfur atoms, thus opening up the tantalizing prospect of thiirane production in the interstellar medium. Thiirane has also been implicated in the formation of important prebiotic organosulfur compounds, as summarized by Balucani.[9] Due to its interstellar importance the high-resolution far-IR spectrum of oxirane has very recently been studied extensively;[10] however, the equivalent thiirane spectroscopy has been largely neglected.

The thiirane molecule is of C_{2V} symmetry and thus has 15 modes with A_1, A_2, B_1, and B_2 symmetry and should exhibit nuclear spin statistics as outlined in Table I. The rotational structure of the ground state (G. S.) of thiirane has been studied by microwave spectroscopy, first by Okiye *et al.*[11] and more recently by Hirao *et al.*[12] and accurate molecular parameters have been determined from transitions up to ~12 cm^{-1}. The rotational spectrum of thiirane in excited vibrational states was also studied by Hirose *et al.*[13] using microwave spectroscopy, and molecular parameters have been determined for some low energy modes, including ν_5 and ν_{15}. To our knowledge no high resolution IR studies have been carried out to date; however, Allen *et al.*[14] presents an extensive list (excluding ν_{15}) of mode assignments determined from low resolution (~1 cm^{-1}) IR and Raman spectra.

This study thus aims first to increase the range and quality of the fits to the rotational data by including pure rotational far-IR transitions of higher energy into the analysis. Additionally, the ro-vibrational structure of thiirane has also been recorded and an analysis of the ν_5 and ν_{15} modes, which are the lowest in energy and most likely to be populated in astrophysical systems, is presented. Intensity stealing facilitated by Coriolis coupling has been shown in previous studies[15] to be of sufficient strength that IR inactive (or inactive enough to not be observable given noise) modes can become observable. These modes are predicted to be coupled via a strong c-axis Coriolis interaction, which is treated, and a novel intensity stealing effect which occurs as a result of this coupling is also elucidated.

EXPERIMENT

The experiments were performed at the far-IR beamline at the Australian synchrotron, with two regions of the spectrum recorded between 170–10 cm^{-1} (region 1) and 760–400 cm^{-1} (region 2). Sample vapor of thiirane (98%, Sigma-Aldrich, Australia) was released into a multi-pass White cell equipped with polyethylene windows and coupled to a Bruker IFS 125HR spectrometer capable of achieving a nominal resolution of 0.001 cm^{-1}. The high far-IR flux of the synchrotron source ensured sufficient sensitivity in both regions. The spectrum in region 1 was recorded with a 12.5 mm aperture, effectively open since the synchrotron can be considered a point source emission (electron beam diameter ~350 μm) which results in a highly collimated beam, a 75–μm mylar beam splitter, scan rate of 40 kHz, and a silicon bolometer operating at 4.2 K. Region 2 was recorded with a 5 mm aperture, a KBr beam splitter, scan rate of 80 kHz, and silicon bolometer detector. Spectra were taken with the sample pressure within the cell maintained at 200 and 600 mTorr in region 1 and 3 and 75 mTorr in region 2. The cell had an optical pathlength of 24 m and was at ambient temperature throughout the

a)Author to whom correspondence should be addressed. Electronic mail: donald.mcnaughton@monash.edu. Tel.: 61399054525. FAX: 61 399054597.
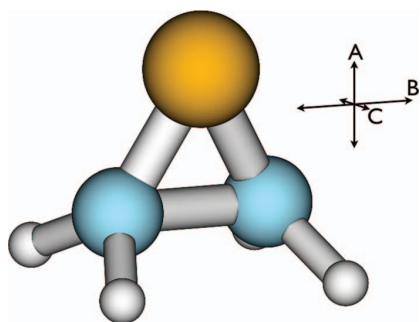
FIG. 1. Thiirane molecule with rotational axes labeled. Structure optimized by DFT calculations.

experiment (assumed to be 300 K for spectral simulations). Overall 73 (region 1, 200 mTorr), 53 (region 1, 600 mTorr), 116 (region 2, 3 mTorr), and 139 (region 2, 75 mTorr) interferograms were recorded at 0.001 cm^{-1}, each set averaged then Fourier transformed using a 4P apodization function and a post-zero fill factor of 8. All spectra were calibrated using water line positions from the HITRAN database.[16]

Geometry optimizations and subsequent frequency calculations were performed at the B3LYP/cc-pVTZ level of theory using GAUSSIAN09.[17] These calculations determined structural parameters such as rotational, centrifugal distortion (see Table II), and Coriolis coupling constants, as well as and IR intensities (proportional to the square of the transition dipole moment) and vibrational energies. Assigned lines were fitted with Pickett's SPFIT (Ref. 18) and spectral simulation data were achieved by inputting the parameters obtained from the fits into Pickett's prediction software SPCAT.[18] The resulting calculated transitions were then convolved with a Gaussian line-shape to produce a simulated spectrum. The FWHM line-width chosen was 0.002 cm^{-1}, which corresponded to the observed spectra.

RESULTS AND DISCUSSION

The spectra containing the pure rotational, ν_5, and ν_{15} transitions are shown in Figures 2–4, respectively. According to DFT calculations, the ν_{15} mode is predicted to be substantially weaker than the ν_5 mode, with IR intensities of 0.89 km mol^{-1} and 28.36 km mol^{-1}, respectively.

Fitting procedure

The far-IR pure rotational data was analyzed first, since the parameters derived would be used in the fitting of the

TABLE I. Statistical weights of the thiirane transitions.

K_a	K_c	Weight
Even	Even	5
Even	Odd	3
Odd	Even	3
Odd	Odd	5

ro-vibrational spectra. The spectrum was peak-picked and presented in the Loomis-Wood format using MacLoomis,[19] which groups regularly spaced lines, such as those differing in J but sharing constant K_a, into approximately vertical series of constant K_a. The permanent dipole moment is along the A-axis, and ground state rotational transitions followed a-type selection rules, $eo \leftrightarrow ee$ and $oe \leftrightarrow oo$ ($\Delta K_a = 0, \pm2\ldots,$ $\Delta K_c = \pm1, \pm3\ldots$). Overall, 576 far-IR rotational transitions of $J(\max) = 75$ and $K_a(\max) = 12$ were assigned and given an uncertainty of 10% of the FWHM of the peaks (0.0002 cm^{-1}). These were added to the 241 previously recorded microwave transitions which had varying uncertainty as detailed in the previous study. These transitions were co-fitted to Watsons s-reduced Hamiltonian[20] in the I^r representation using Pickett's SPFIT,[18] and the derived molecular parameters are shown in Table II. The parameters derived in the previous study utilized the a-reduced Hamiltonian, however, using the s-reduction allowed for a higher quality fit. This fit is available as supplementary material.[21] The S/N of the spectrum precluded observation of the rotational spectra of excited vibrational states and the ^{34}S isotopologue.

The resulting fit was determined with a RMS deviation of 1.15. The inclusion of the observed far-IR transitions and the use of the s-reduced Hamiltonian marginally improved the quality of the ground state parameters and extended the range of J for which the fit is known to be valid. Since this improvement is modest, the ground state combination differences generated from the ro-vibrational analysis were not included, since their range and certainty is poorer than the observed transitions, and they had negligible effect on the fit. Four of the microwave transitions could not be fitted with sufficient accuracy and skewed the fit. These transitions were omitted by giving them effectively infinite uncertainty (999 MHz). The derived parameters were used to describe the ground state in the fit to the ro-vibrational spectra.

ν_5, a symmetric ring-deformation mode centered about 628.1 cm^{-1}, has A_1 symmetry corresponding to an a-type mode. The observed transitions thus have selection rules of $eo \leftrightarrow ee$ and $oe \leftrightarrow oo$ ($\Delta K_a = 0, \pm2\ldots, \Delta K_c = \pm1, \pm3\ldots$). The ν_5 spectrum was peak-picked and presented in the Loomis-Wood format and this allowed series between $K_a = 0$ and 18 to be assigned with $J(\max) = 61$. It is of note that the nuclear spin statistics described in Table I were observed, as a clear intensity alternation in those transitions which were non-degenerate. An asymmetry in intensity was observed, particularly at high K_a values, which meant that the observed range of K_a in the P-branch was much higher than that of the R-branch. The Q-branch transitions for this mode were too congested to be accurately assigned and were not included in the analysis, which is justifiable since they contain the same information as the P- and R-branch transitions which are well resolved. Overall, 1505 P- and R-branch ro-vibrational transitions were assigned from this mode, and given an uncertainty of 0.0002 cm^{-1} in the fitting procedure. These assignments were confirmed by comparison with ground state combination differences generated from the known ground state constants. Thirty-five microwave transitions recorded in a previous study[13] within the ν_5 mode were also included in the fitting procedure, and given an uncertainty of 0.1 MHz.

TABLE II. Band parameters fitted to Watson's *s*-reduced I^r Hamiltonian for the G. S., ν_5, and ν_{15} modes of thiirane.

Constant	G. S.[a]	G. S.	ν_5	ν_{15}
Band centre (cm^{-1})			628.1401285 (21)[b]	669.7400253 (32)
A (MHz)	22 007.73	21 973.63602 (60)	21 949.8564 (94)	22 042.3402 (17)
B (MHz)	10 563.87	10 824.89267 (24)	10 782.6653 (16)	10 745.5237 (42)
C (MHz)	7891.04	8026.24761 (20)	7976.76 (33)	7986.57 (33)
D_J (kHz)	6.68135	7.05245 (40)	6.86967 (91)	7.3328 (25)
D_{JK} (kHz)	14.4998	13.7696 (15)	13.184 (12)	13.90 (10)
D_K (kHz)	14.2400	16.5063 (73)	17.870 (35)	16.65 (46)
d_1 (kHz)	−2.035601	−2.192477 (64)	−2.35577(50)	−2.07342 (66)
d_2 (kHz)	−0.399670	−0.428793 (48)	−0.497619 (58)	−0.3722 (12)
H_J (mHz)	3.005	2.34 (14)	2.34[c]	2.34[c]
H_{JK} (Hz)	−0.1844	−0.2056 (12)	−0.2056[c]	−0.2056[c]
H_{KJ} (Hz)	0.6396	0.6402 (90)	0.6402[c]	0.6402[c]
h_1 (mHz)	1.155	1.184 (50)	1.184[c]	1.184[c]
h_2 (mHz)	−0.439	−0.514 (41)	−0.514[c]	−0.514[c]
h_3 (mHz)	0.534	0.612 (11)	0.612[c]	0.612[c]
$G^c \approx -2\zeta\, C_{GS}$ (MHz)			−10863 (19)	
F^c (MHz)			−75.48 (15)	
J (max)		75	61	63
K_a (max)		19	18	7
No. trans.		817[d]	1505[d]	596[d]
RMS deviation		1.15	0.75	

[a]Determined by DFT calculation.
[b]Figures in brackets are one standard deviation according to the least squares fit in units of the least significant figure quoted.
[c]Parameter forced during the fit to be equal to the G. S. value.
[d]Includes 241, 35, and 47 previously published[12,13] microwave transitions for the G. S., ν_5, and ν_{15} modes, respectively.

It is also worth noting that some weak Q-branch transitions were observed for the ν_5 mode of the ^{34}S isotopologue of thiirane (see Figure 5), which are predicted to exhibit ~4% of the absorbance of the ^{32}S isotopologue, reflecting their natural abundance. DFT calculations predicted a relatively large shift in the band centre compared with ^{32}S of 8.2 cm^{-1}, which guided the search for these transitions. Since only a limited number of Q-branch transitions were observed, any to attempt to fit these transitions would not have significant physical meaning, especially since this mode is strongly Coriolis coupled to the much weaker ν_{15} mode. A tentative assignment of some ^{34}S lines was made based on comparison with the Q-branch of the ^{32}S isotopologue, and this led to an approximate observed band centre of 620.8 cm^{-1}. This corresponds to a shift of 7.3 cm^{-1} from the ^{32}S isotopologue which compares well to the calculated value.

ν_{15}, an asymmetric ring-deformation mode centered about 669.7 cm^{-1}, has B_2 symmetry corresponding to a b-type mode. The observed transitions thus have selection rules of $eo \leftrightarrow oe$ and $oe \leftrightarrow eo$ ($\Delta K_a = \pm 1, \pm 3 \ldots$, $\Delta K_c = \pm 1, \pm 3 \ldots$). The spectrum was also peak-picked and presented in the Loomis-Wood format, however, initially assignment was
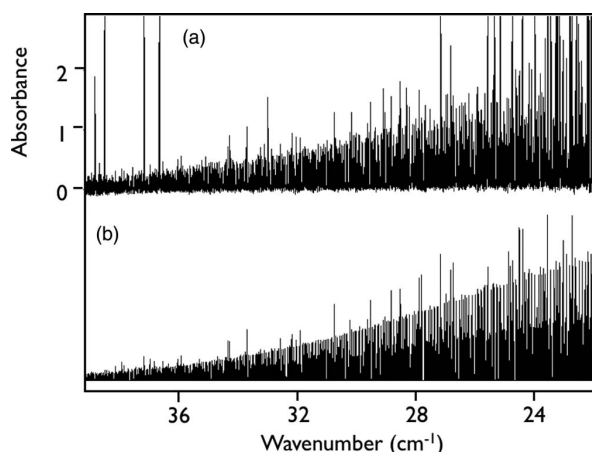

FIG. 2. Experimental survey spectrum of (a) pure rotational spectrum at 200 mTorr and (b) corresponding simulation. All experimental spectra (Figures 2–5) contain contamination (particularly from H_2O and the CO_2 bending mode at 667 cm^{-1}) which does not appear in the simulations.
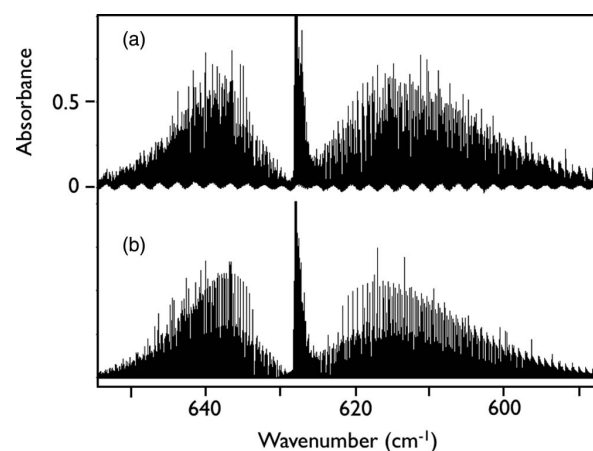

FIG. 3. (a) Experimental survey spectrum of ν_5 at 3 mTorr and (b) corresponding simulation.
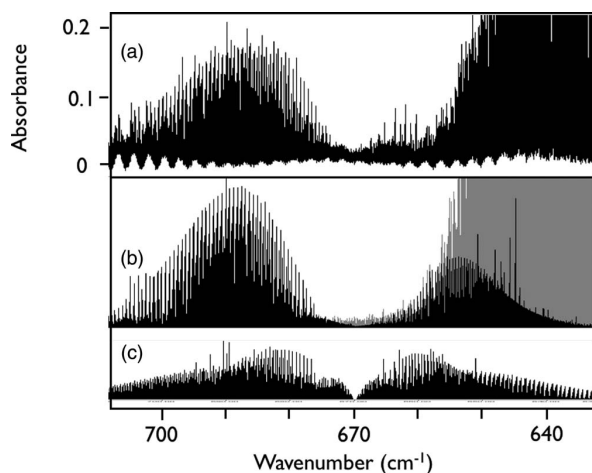
FIG. 4. (a) Experimental survey spectrum of ν_{15} at 75 mTorr and (b) corresponding simulation. A baseline oscillation, the result of a multi-reflections in the cell widows, has been partially removed in (a) by subtraction of an appropriate oscillatory function. (b) Shows simulation of ν_{15} (black) under the assumption that the majority of intensity is sourced via intensity stealing with $M_5^2/M_{12}^2 \approx 31$. Grey lines are attributed to ν_5 and included as a reference. (c) Shows the intensity distribution of ν_{15} if a normal b-type character is assumed.

hampered by the unexpected lack of any observed P-branch transitions (or the Q-branch transitions expected for a b-type mode). The observed R-branch transitions were eventually assigned from the magnitude of the low-J splitting between states of $J = K_a + K_c$ and $J = K_a + K_c - 1$. This splitting is dependent on the rotational parameters, and is predicted with reasonable certainty by assuming ground state parameters. Overall, 549 R-branch ro-vibrational transitions with $J(\max) = 63$ and $K_a(\max) = 7$ were assigned from this mode, and given uncertainty 0.0002 cm^{-1} in the fitting procedure. Forty-seven microwave transitions with uncertainty of 0.1 MHz recorded in a previous study[13] within the ν_{15} mode were also included in the fitting procedure.

Since a strong c-axis interaction between ν_5 and ν_{15} is predicted, the two modes must be co-fit, and parame-
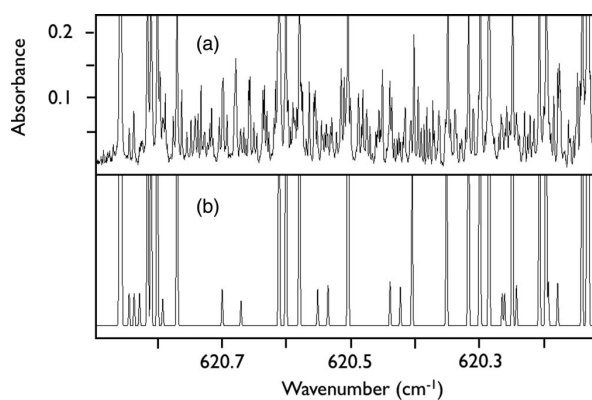

FIG. 5. (a) Expanded section and (b) corresponding simulation. (a) contains Q-branch transitions from the S^{34} isotopologue not present in the simulation. This figure also serves as an example of the agreement between experiment and simulation for the S^{32} isotopologue transitions.

ters describing the interaction must be included. Overall, 82 microwave pure rotational transitions and 2054 far-IR ro-vibrational transitions were co-fit to Watson's s-reduced Hamiltonian[20] in the I^r representation, with the derived parameters presented in Table II. The resulting fit was determined with a RMS deviation of 0.75. During the fitting procedure, the higher order H and h distortion parameters were held at the ground state values, while the D and d parameters were allowed to vary since they were well determined and did not vary greatly from the ground state values. This fit is also available as supplementary material.[21]

The Coriolis interaction parameter, $\zeta_{5,12}^c$, can be calculated from the fit as 0.68, which is in excellent agreement with theoretical prediction from DFT calculations which predict a value of $\zeta_{5,12}^c = 0.72$. This value is $\sim$10% lower than that from the theoretical work quoted in the previous study;[13] however, our theoretical and fitted values are more compatible with each other. The higher order Coriolis interaction parameter, F_{ab}, was introduced into the fit since it significantly reduced the error and was well determined.

Simulation

When attempts were made to simulate the spectra using the derived parameters, the intensity distribution of the ν_{15} spectra could not be accurately reproduced. If a normal b-type structure was assumed during the simulations (see Figure 4), intense transitions close to the band centre are predicted where none are actually observed. Second, the P- and R-branch transitions were predicted to have the same intensity, which was also not observed experimentally. Both of these features can be explained if a strong intensity stealing mechanism is proposed.

Mills[22] derives an expression for the line-strengths of Coriolis coupled modes which for the case of ν_5 and ν_{15} is summarized in Eqs. (1a)–(1g):

$$S_{5'} = a_k^2 M_5^2 + b_k^2 M_{12}^2 \pm 2a_k b_k M_5 M_{12}, \tag{1a}$$

$$S_{12'} = a_k^2 M_{12}^2 + b_k^2 M_5^2 \mp 2a_k b_k M_5 M_{12}, \tag{1b}$$

$$a_k^2 = (\Delta_k + \delta)/2\Delta_k, \tag{1c}$$

$$b_k^2 = (\Delta_k - \delta)/2\Delta_k, \tag{1d}$$

$$\Delta_k^2 = \delta^2 + 16C_e^2 k^2 \zeta_{5,12}^2 \Omega_{5,12}^2, \tag{1e}$$

$$\Omega_{X,Y} = (\omega_5 + \omega_{12})(\omega_5 \omega_{12})^{-1/2}, \tag{1f}$$

$$\delta = \omega_{12} - \omega_5, \tag{1g}$$

where M is the transition dipole moment, ω is the band centre, and the sign of the cross term in Eqs. (1a) and (1b) depends on whether R- or P-branch transitions are considered.
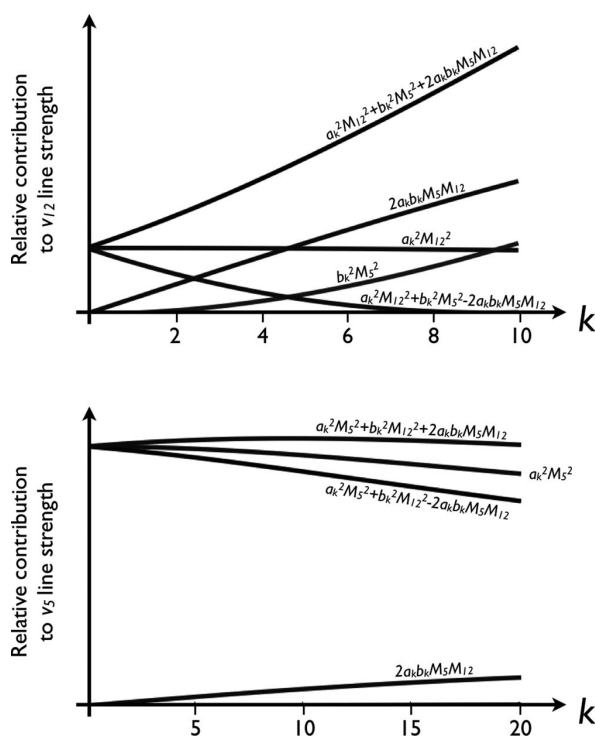
FIG. 6. Relative magnitudes of the contributions (from Eq. (1)) to the line-strength of the ν_{15} and ν_5 modes. The figure is based on theoretically calculated ratio of $M_5^2/M_{12}^2 = 31$ determined by DFT calculation. The quantity $b_k^2 M_{12}^2$ is too small to be viewable on the presented scale.

As is shown in Figure 6, the relative contributions from all terms in Eq. (1) can be plotted as a function of the k quantum number. This shows that the $b_k^2 M_5^2$ and $2a_k b_k M_5 M_{12}$ terms, which provide intensity to ν_{15}, are only significant at higher k. High k transitions are located away from the band centre, and thus intensity is shifted away from this region, giving rise to the unusual intensity distribution observed in the experimental spectrum. Second, the asymmetric contribution from the $2a_k b_k M_5 M_{12}$ term to the P- and R-branch transitions explains the asymmetry in intensity observed between these two branches. This observation shows that although M_{12} may be negligible, the product $M_5 M_{12}$ is not, which allows ν_{15} to be observed. The selection rules, as determined by symmetry and used by the SPCAT simulation, for this mode are $eo \leftrightarrow oe$ and $oe \leftrightarrow eo$ ($\Delta K_a = \pm 1, \pm 3 \ldots, \Delta K_c = \pm 1, \pm 3 \ldots$), which are identical to those of a b-type mode. Since the selection rules for both stealing and natural mechanisms are identical, there is no way of knowing about the intensity perturbation when only the energies are considered (as is the case during fitting).

A similar argument can be made for the intensity distribution of the high K_a transitions of ν_5 although the effect is not as dramatic. The reversed sign of the cross term in Eq. (1a) implies that the opposite ($P-$) branch of ν_5 should be enhanced in this case, which is observed. Since the natural transitions dipole moment ($a_k^2 M_5^2$ term) is the strongest contributor to intensity in this case, the effect is only noticeable at much higher K_a when the natural transitions are weaker

and the magnitude of intensity stealing is at its greatest. The selection rules, as determined by symmetry, for the high K_a transitions which are only observed in the P-branch are $eo \leftrightarrow ee$ and $oe \leftrightarrow oo$ ($\Delta K_a = 0, \pm 2 \ldots, \Delta K_c = \pm 1, \pm 3 \ldots$), which are the same as those of a normal a-type mode. This effect is illustrated in Figure 6.

SPCAT simulates the intensity stealing mechanic well and supports these hypotheses. It can be seen from Figures 3 and 4 that there is now good agreement between observed and simulated spectra.

CONCLUSION

Ro-vibrational transitions within the Coriolis coupled ν_5 and ν_{15} modes of thiirane have been assigned, and fitted to determine rotational, centrifugal distortion, and Coriolis interaction parameters. Strong c-axis Coriolis interactions have been treated, with the fitted value of $\zeta_{5,12}^c$ in agreement with theoretical predictions from DFT calculations. A novel intensity stealing effect in the ν_{15} mode has been observed and characterized. The G. S. parameters have also been improved, and their range of predictive usefulness extended, by the inclusion of observed far-IR pure rotational transitions to the extensive list of microwave transitions.

[1] J. E. Dickens, W. M. Irvine, M. Ohishi, M. Ikeda, S. Ishikawa, A. Nummelin, and A. Hjalmarson, Astrophys. J. **489**(2), 753 (1997).
[2] A. Nummelin, J. E. Dickens, P. Bergman, A. Hjalmarson, W. M. Irvine, M. Ikeda, and M. Ohishi, A&A **337**(1), 275 (1998); M. Ikeda, M. Ohishi, A. Nummelin, J. E. Dickens, P. A. H. Bergman, and W. M. Irvine, Astrophys. J. **560**, 792 (2001); M. A. Requena-Torres, J. Martín-Pintado, S. Martín, and M. R. Morris, *ibid.* **672**, 352 (2008).
[3] C. Patrice, B. Jean-Michel, N. Rafael, and R. Franacois, Astrophys. J. **598**(1), 700 (2003).
[4] M. Oppenheimer and A. Dalgarno, Astrophys. J. **187**, 231 (1974).
[5] J. Steadman and T. Baer, J. Chem. Phys. **89**(9), 5507 (1988).
[6] J. R. Appling, M. R. Harbol, R. A. Edgington, and A. C. Goren, J. Chem. Phys. **97**(6), 4041 (1992).
[7] S. T. Pratt, Phys. Rev. A **38**(3), 1270 (1988).
[8] F. Leonori, R. Petrucci, N. Balucani, P. Casavecchia, M. Rosi, D. Skouteris, C. Berteloite, S. B. D. Le Picard, A. Canosa, and I. R. Sims, J. Phys. Chem. A **113**(52), 15328 (2009).
[9] N. Balucani, Int. J. Mol. Sci. **10**(5), 2304 (2009).
[10] J. M. Flaud, W. J. Lafferty, F. K. Tchana, A. Perrin, and X. Landsheere, J. Mol. Spectrosc. **271**(1), 38 (2012); C. Medcraft, C. D. Thompson, E. G. Robertson, D. R. T. Appadoo, and D. McNaughton, Astrophys. J. **753**(1), 18 (2012).
[11] K. Okiye, C. Hirose, D. G. Lister, and J. Sheridan, Chem. Phys. Lett. **24**(1), 111 (1974).
[12] T. Hirao, T. Okabayashi, and M. Tanimoto, J. Mol. Spectrosc. **208**(1), 148 (2001).

[13] C. Hirose, K. Okiye, and S. Maeda, Bull. Chem. Soc. Jpn. **49**(4), 916 (1976).

[14] W. D. Allen, J. E. Bertie, M. V. Falk, J. B. A. Hess, G. B. Mast, D. A. Othen, L. J. Schaad, and H. F. S. III, J. Chem. Phys. **84**(8), 4211 (1986).

[15] M. K. Bane, C. D. Thompson, E. G. Robertson, D. R. T. Appadoo, and D. McNaughton, Phys. Chem. Chem. Phys. **13**, 6793 (2011); J. Chem. Phys. **135**(22), 224306 (2011).

[16] L. S. Rothman, I. E. Gordon, A. Barbe, D. C. Benner, P. F. Bernath, M. Birk, V. Boudon, L. R. Brown, A. Campargue, J. P. Champion, K. Chance, L. H. Coudert, V. Dana, V. M. Devi, S. Fally, J. M. Flaud, R. R. Gamache, A. Goldman, D. Jacquemart, I. Kleiner, N. Lacome, W. J. Lafferty, J. Y. Mandin, S. T. Massie, S. N. Mikhailenko, C. E. Miller, N. Moazzen-Ahmadi, O. V. Naumenko, A. V. Nikitin, J. Orphal, V. I. Perevalov, A. Perrin, A. Predoi-Cross, C. P. Rinsland, M. Rotger, M. Simecková, M. A. H. Smith, K. Sung, S. A. Tashkun, J. Tennyson, R. A. Toth, A. C. Vandaele, and J. Vander Auwera, J. Quant. Spectrosc. Radiat. Transfer **110**(9-10), 533 (2009).

[17] M. J. Frisch, G. W. Trucks, H. B. Schlegel *et al.* GAUSSIAN09, ■, Gaussian, Inc., Wallingford, CT, 2009.

[18] H. M. Pickett, J. Mol. Spectrosc. **148**(2), 371 (1991).

[19] D. McNaughton, D. McGilvery, and F. Shanks, J. Mol. Spectrosc. **149**(2), 458 (1991).

[20] J. K. G. Watson, in *Vibrational Spectra an Structure*, edited by J. R. Durig (Elsevier Scientific, 1977), vol. 6.

[21] See supplementary material at http://dx.doi.org/10.1063/1.4747191 for transition lists and final least squares fits.

[22] I. M. Mills, Pure Appl. Chem. **11**(3-4), 325 (1965).

Declaration for Thesis Chapter 3.6

Declaration by candidate

In the case of Chapter 3.6, the nature and extent of my contribution to the work was the following:

Nature of contribution	Extent of contribution (%)
key ideas, development	15

The following co-authors contributed to the work. Co-authors who are students at Monash University must also indicate the extent of their contribution in percentage terms:

Name	Nature of contribution	Extent of contribution (%) for authors only
D. McNaughton	Initiation, key ideas, development, writing up	
E. G. Robertson	Initiation, key ideas	
C. D. Thompson	Initiation, key ideas,	
T. Chimdi	Initiation, key ideas,	15
D. R. T. Appadoo	Experimental assistance	

Candidate's Signature		Date

Declaration by co-authors

The undersigned hereby certify that:

(1) the above declaration correctly reflects the nature and extent of the candidate's contribution to this work, and the nature of the contribution of each of the co-authors.
(2) they meet the criteria for authorship in that they have participated in the conception, execution, or interpretation, of at least that part of the publication in their field of expertise;
(3) they take public responsibility for their part of the publication, except for the responsible author who accepts overall responsibility for the publication;
(4) there are no other authors of the publication according to these criteria;
(5) potential conflicts of interest have been disclosed to (a) granting bodies, (b) the editor or publisher of journals or other publications, and (c) the head of the responsible academic unit; and
(6) the original data are stored at the following location(s) and will be held for at least five years from the date indicated below:

Location(s)	Monash University, School of Chemistry

Signature 1		Date
Signature 2		
Signature 3		
Signature 4		
Signature 5		

Overview of High-Resolution Infrared Measurement and Analysis for Atmospheric Monitoring of Halocarbons[†]

Don McNaughton,[*,‡] **Evan G. Robertson,**[§] **Christopher D. Thompson,**[‡] **Tarekegn Chimdi,**[‡]
Michael K. Bane,[‡] **and Dominique Appadoo**[||]

School of Chemistry, Monash University, Wellington Road, Clayton, Victoria 3800, Australia, La Trobe University, Department of Chemistry, Bundoora, Victoria 3086, Australia, and Australian Synchrotron, Blackburn Road, Clayton, Victoria 3168, Australia

The current state of the art in recording and analyzing rotationally resolved vibration−rotation bands of atmospheric pollutant halocarbon species is reviewed. It is shown that in order to obtain molecular constants of sufficient accuracy to simulate the vibration−rotation structure over the range of atmospheric temperatures, it is necessary to obtain spectra at a range of temperatures using static cooling cells, supersonic jet expansions, and collisional cooling devices; employ sophisticated pattern recognition and analysis software; assign and fit spectral perturbations; and use spectral simulation and digital spectral subtraction (SASSI) to further simplify spectral bands for analysis. To demonstrate the techniques, an analysis of the ν_5 band of $CH^{37}ClF_2$ in natural abundance is presented.

Infrared (IR) spectroscopy is an ideal technique for characterizing, monitoring, and quantifying atmospheric molecules, be it for baseline determination of small atmospheric species or for exotic atmospheric pollutants. It thus has a significant role in environmental monitoring and is used in a variety of roles including in ground, airborne, and satellite based systems. For tropospheric measurements, the majority of work is carried out using medium resolution instruments because pressure and collisional line broadening limits direct atmospheric observations to resolutions >0.1 cm^{-1}. For such work, quantification relies on using model spectra simulated from well determined molecular constants or on spectral libraries. Spectral libraries are usually generated using Fourier transform-IR (FT-IR) techniques and unless carefully and systematically compiled are not easily transferable to different instruments or for different applications and few useful libraries are available. Sharpe and co-workers at the Pacific Northwestern National Laboratory (PNNL) have been building a comprehensive library of spectra specifically for general use in tropospheric

monitoring to fill this gap.[1] For upper atmosphere monitoring, where the spectral linewidths are much reduced, medium and high-resolution techniques are required and the determinations are usually carried out using spectra "synthesized" from carefully compiled databases of line positions calculated from accurate molecular constants, together with transition cross sections and appropriate line shape parameters. A clear advantage of this approach is its ready application to samples at any temperature, pressure, or continuously varying set of these that may occur within a column profile. The high-resolution transmission molecular absorption database (HITRAN), under constant compilation at the Air Force Cambridge Research Laboratories (AFCRL), is the best known and most widely used such database and its progress has been outlined recently by Rothman et al.[2] The database provides the basis for many applications in terrestrial and atmospheric remote sensing, open path monitoring, laboratory based studies, and process monitoring.

The many spectrometer based satellite systems now in operation require new and more accurate data for an increasing number of molecules that require monitoring, and this information comes from fundamental laboratory based experiments optimized to provide data of sufficient accuracy. One extremely important group of molecules where the essential molecular parameters are required are the ozone depleting halocarbon molecules and their replacements such as hydrofluorocarbons, most of which have significant global warming potential. Such large molecules often with numerous isotopomers, heavily populated low vibrational states, and complications arising from interacting energy states have extremely rich high-resolution infrared spectra. Measurement, assignment, and fitting these spectra presents a challenge to even the most hardened molecular spectroscopist. In order to provide sufficient accuracy for line position and intensity prediction

(1) Sharpe, S. W.; Johnson, T. J.; Sams, R. L.; Chu, P. M.; Rhoderick, G. C.; Johnson, P. A. *Appl. Spectrosc.* **2004,** *58,* 1452–1461.

(2) Rothman, L. S.; Gordon, I. E.; Barbe, A.; Benner, D. C.; Bernath, P. F.; Birk, M.; Boudon, V.; Brown, L. R.; Campargue, A.; Champion, J.-P.; Chance, K.; Coudert, L. H.; Dana, V.; Devi, V. M.; Fally, S.; Flaud, J.-M.; Gamache, R. R.; Goldman, A.; Jacquemart, D.; Kleiner, I.; Lacome, N.; Lafferty, W. J.; Mandin, J.-Y.; Massie, S. T.; Mikhailenko, S. N.; Miller, C. E.; Moazzen-Ahmadi, N.; Naumenko, O. V.; Nikitin, A. V.; Orphal, J.; Perevalov, V. I.; Perrin, A.; Predoi-Cross, A.; Rinsland, C. P.; Rotger, M.; Šimečková, M.; Smith, M. A. H.; Sung, K.; Tashkun, S. A.; Tennyson, J.; Toth, R. A.; Vandaele, A. C.; Vander Auwera, J. *J. Quant. Spec. Rad. Transfer* **2009,** *110,* 533–572.

Table 1. Fluorocarbon-Related Species Studied by High-Resolution Infrared Spectroscopy

molecular formula	name	refs
CH_2F_2	HFC-32	4
CH_2ClF	HCFC-31	5–9
CH_2BrF	CFC-31B1	10–15
CF_3Cl	CFC-13	16–24
CF_3Br	Halon 1301	25–29
$CHClF_2$	HCFC-22	30–40
$CHBrF_2$	Halon 1201	a
$CHBrClF$	FC21B1	41
CF_2ClBr	Halon 1211	42, 43
CF_2Cl_2	CFC-12	44–46
CF_2Br_2	Halon 1202	a
CHF_3	HFC-23	47–49
$CHCl_2F$	HFC-21	50, 51
$CHBr_2F$	Halon1102	a
$CFCl_3$	CFC-11	52, 53
CF_3I	Freon13T1	54, 55
CH_3CH_2F	HFC-161	a
CH_3CHF_2	HFC 152a	56–60
CH_3CF_3	HFC 143a	61, 62
CF_3CHF_2	HFC 125	63, 64
CF_3CH_2F	HFC134a	65–68
C_2F_6	FC-116	69
C_2F_4	tetrafluoroethylene	70
CH_3CF_2Cl	HCFC-142b	71–75
CF_3CHFCF_3	HFC-227ea	76
$(CH_3)_3CF$	*tert*-butyl fluoride	77

a Species with no available high-resolution data to date.

(and even accurate band shapes for low-resolution work) over the complete range of atmospheric temperatures, it is necessary to assign and fit the full range of isotopomers and their hot bands together with all perturbing states, including often "dark" states where there are no observed transitions. Recent analysis of satellite measurements of halocarbons and hydrohalocarbons[3] by the Atmospheric Trace Molecular Spectroscopy Experiment (ATMOS) and the Interferometric Monitor for Greenhouse gases (IMG) led to the conclusion that "The reliability of the existing spectroscopic parameters has been examined, and it was found that only laboratory parameters measured at high resolution reproduce the satellite observations well".

This paper reviews the high-resolution studies carried out to date for halocarbon and hydrohalocarbons and the techniques necessary to provide accurate data for the prediction of their line positions. A new analysis of the ν_5 band of chlorodifluoromethane (HCFC-22) utilizing some of these techniques is also presented.

EXPERIMENTAL SECTION

R22 ($CHClF_2$) (99% commercial grade, BOC gases Australia) was transferred to an evacuated glass multipass cell, set to a path length of 4 m. High-resolution spectra over the range $150–600$ cm^{-1} were recorded with an unapodized resolution of 0.000 96 cm^{-1} on a Bruker IFS 125HR at the Australian Synchrotron using the infrared synchrotron edge radiation continuum source. The FT-IR spectrometer was equipped with a multilayer Mylar beam splitter and a liquid helium-cooled external Si:B bolometer. Over 200 scans were coadded at a sample pressure of 500 mTorr and post zero-filled with a factor of 8. Calibration was carried out by 67 H_2O and CO_2 lines in

the spectra from residual traces in the interferometer compartment, using measured line positions from the HITRAN database[2] in the spectral region of $420–680$ cm^{-1}.

REVIEW OF HIGH-RESOLUTION STUDIES

Apart from methyl fluoride, a low molecular weight symmetric top molecule with a relatively simple structure that was thoroughly studied at high resolution in the early days of infrared spectroscopy, most fluorocarbon species required the development of modern FT-IR and laser based spectrometer systems to provide assignable high-resolution data. Most work has been carried out since the advent of these systems in the 1980s with the majority of studies taking place after the realization of the ozone depleting potential of the halon containing species and the high greenhouse warming potential of many of the fluorocarbons. Table 1 at left lists the majority of the fluorocarbon-related molecules with some or all bands now characterized at high resolution to produce reliable molecular constants together with references to the work. The chloro and bromo substituted fluoroethylenes, although not considered to have major roles in atmospheric chemistry, have also been extensively studied by the groups of Gambi and Stoppa with a recent paper[78] on a band of *cis*-chlorofluoroethylene pointing to progress with these species.

(3) Coheur, P. F.; Clerbaux, C.; Colin, R. *J. Geophys. Res. (Atmos.)* **2003**, *108*, 4130.

(4) Smith, K. M.; Duxbury, G.; Newnham, D. A.; Ballard, J. *J. Mol. Spectrosc.* **1999**, *193*, 166–173.

(5) Baldacci, A.; Stoppa, P.; Giorgianni, S.; Visinoni, R.; Ghersetti, S. *J. Mol. Spectrosc.* **1993**, *159*, 481–93.

(6) Baldacci, A.; Stoppa, P.; Giorgianni, S.; Ghersetti, S. *J. Mol. Spectrosc.* **1999**, *194*, 73–78.

(7) Baldacci, A.; Stoppa, P.; Giorgianni, S.; Visinoni, R.; Baldan, A. *J. Mol. Spectrosc.* **1997**, *183*, 388–397.

(8) Baldacci, A.; Stoppa, P.; Giorgianni, S.; Visinoni, R. *J. Mol. Spectrosc.* **1996**, *177*, 106–114.

(9) Baldacci, A.; Stoppa, P.; Giorgianni, S.; Visinoni, R.; Ghersetti, S. *J. Mol. Spectrosc.* **1994**, *166*, 264–72.

(10) Stoppa, P.; Baldacci, A.; Visinoni, R.; Giorgianni, S. *Mol. Phys.* **2006**, *104*, 3187–3192.

(11) Baldacci, A.; Stoppa, P.; Giorgianni, S.; Wugt Larsen, R. *J. Mol. Spectrosc.* **2008**, *251*, 123–128.

(12) Baldacci, A.; Stoppa, P.; Pietropolli Charmet, A.; Giorgianni, S.; Cazzoli, G.; Cludi, L.; Puzzarini, C.; Wugt Larsen, R. *J. Mol. Spectrosc.* **2007**, *246*, 126–132.

(13) Baldacci, A.; Stoppa, P.; Pietropolli Charmet, A.; Giorgianni, S.; Cazzoli, G.; Puzzarini, C.; Wugt Larsen, R. *J. Phys. Chem. A* **2007**, *111*, 7090–7097.

(14) Baldacci, A.; Stoppa, P.; Pietropolli Charmet, A.; Giorgianni, S. *J. Mol. Spectrosc.* **2003**, *220*, 7–12.

(15) Baldacci, A.; Stoppa, P.; Gambi, A. *J. Mol. Spectrosc.* **2000**, *201*, 280–284.

(16) Amrein, A.; Hollenstein, H.; Locher, P.; Quack, M.; Schmitt, U.; Bürger, H. *Chem. Phys. Lett.* **1987**, *139*, 82–88.

(17) Nencini, L.; Snels, M.; Hollenstein, H.; Quack, M. *Mol. Phys.* **1989**, *67*, 989–1009.

(18) Baldacchini, G.; Bizzarri, A.; Nencini, L.; Snels, M.; Giorgianni, S.; Ghersetti, S. *J. Mol. Spectrosc.* **1988**, *130*, 337–43.

(19) Pietropolli Charmet, A.; Stoppa, P.; Toninello, P.; Giorgianni, S.; Ghersetti, S. *Phys. Chem. Chem. Phys.* **2003**, *5*, 3595–3599.

(20) Giorgianni, S.; Stoppa, P.; De Lorenzi, A.; Ghersetti, S. *J. Mol. Spectrosc.* **1992**, *154*, 265–76.

(21) Giorgianni, S.; Stoppa, P.; Baldacci, A.; Gambi, A.; Ghersetti, S. *J. Mol. Spectrosc.* **1991**, *150*, 184–94.

(22) Hollenstein, H.; Quack, M. *Mol. Phys.* **1989**, *68*, 759–764.

(23) Stoppa, P.; Gambi, A. *J. Mol. Struct.* **2000**, *517*, 209–216.

(24) Kelly, J. F.; Maki, A.; Blake, T. A.; Sams, R. L. *J. Mol. Spectrosc.* **2008**, *252*, 81–89.

(25) Bürger, H.; Burczyk, K.; Hollenstein, H.; Quack, M. *Mol. Phys.* **1985**, *55*, 255–275.

(26) Pietropolli Charmet, A.; Tasinato, N.; Stoppa, P.; Baldacci, A.; Giorgianni, S. *Mol. Phys.* **2008**, *106*, 1171–1179.

(27) Pietropolli Charmet, A.; Stoppa, P.; Toninello, P.; Baldacci, A.; Giorgianni, S. *Phys. Chem. Chem. Phys.* **2006**, *8*, 2491–2498.

REVIEW OF EXPERIMENTAL TECHNIQUES

The majority of laboratory based spectroscopy of the halocarbon and hydrohalocarbon species has been carried out using broad band FT-IR spectrometers at spectral resolutions between 0.000 96 and 0.005 cm^{-1} depending on the spectral region, instrument capabilities, and experimental line widths, with fewer studies using either tunable diode laser absorption spectroscopy (TDLAS) at similar resolution to FT-IR or CO$_2$ sideband laser systems with restricted wavenumber coverage

Figure 1. (a) Room temperature spectrum of CBrClF$_2$ at 0.01 cm^{-1} resolution; (b) jet-cooled spectrum of CBrClF$_2$ at an effective resolution of 0.005 cm^{-1}. The rotational temperature is ~40 K.

but extremely high resolution.[79] For all but the smallest molecular species, the spectra at room temperature are highly congested with many thousands of individual vibration−rotation lines from the set of isotopomers and heavily populated low vibrational states. BCF, bromochlorodifluoromethane, CBrClF$_2$, for example, has four main isotopomers and low wavenumber modes for each of these. For example, the ^{79}Br^{35}Cl isotopomer has modes at 214.5, 307, 337.7, 408.4, and 443.3 cm^{-1}.[43] The room temperature spectrum in Figure 1(a) has absorption bands that are wide due to population of states with high rotational quantum numbers and congested due to overlapping features from

(28) (a) Visinoni, R.; Baldacci, A.; Giorgianni, S.; Stoppa, P.; Ghersetti, S. *J. Mol. Spectrosc.* **1990**, *140*, 162–9. (b) Amrein, A.; Locher, P.; QuackM.; Schmitt, U. *COMET* **1987**, *10*, 9−11.

(29) Amrein, A.; Hollenstein, H.; Quack, M.; Schmitt, U. *Infrared Phys.* **1989**, *29*, 561–574.

(30) Albert, S.; Hollenstein, H.; Quack, M.; Willeke, M. *Mol. Phys.* **2006**, *104*, 2719–2735.

(31) Gambi, A.; Stoppa, P.; Giorgianni, S.; De Lorenzi, A.; Visinoni, R.; Ghersetti, S. *J. Mol. Spectrosc.* **1991**, *145*, 29–40.

(32) Albert, S.; Hollenstein, H.; Quack, M.; Willeke, M. *Mol. Phys.* **2004**, *102*, 1671–1686.

(33) Snels, M.; D'Amico, G. *J. Mol. Spectrosc.* **2001**, *209*, 1–10.

(34) Luckhaus, D.; Quack, M. *Mol. Phys.* **1989**, *68*, 745–758.

(35) Ross, J.; Amrein, A.; Luckhaus, D.; Quack, M. *Mol. Phys.* **1989**, *66*, 1273–1277.

(36) Klatt, G.; Graner, G.; Klee, S.; Mellau, G.; Kisiel, Z.; Pszczolkowski, L.; Alonso, J. L.; Lopez, J. C. *J. Mol. Spectrosc.* **1996**, *178*, 108–112.

(37) Kisiel, Z.; Alonso, J. L.; Blanco, S.; Cazzoli, G.; Colmont, J. M.; Cotti, G.; Graner, G.; Lopez, J. C.; Merke, I.; Pszczolkowski, L. *J. Mol. Spectrosc.* **1997**, *184*, 150–155.

(38) Thompson, C. D.; Robertson, E. G.; McNaughton, D. *Chem. Phys.* **2002**, *279*, 239–248.

(39) Thompson, C. D.; Robertson, E. G.; McNaughton, D. *Phys. Chem. Chem. Phys.* **2003**, *5*, 1996–2000.

(40) Thompson, C. D.; Robertson, E. G.; McNaughton, D. *Mol. Phys.* **2004**, *102*, 1687–1695.

(41) Bauder, A.; Beil, A.; Luckhaus, D.; Müller, F.; Quack, M. *J. Chem. Phys.* **1997**, *106*, 7558–7570.

(42) McNaughton, D.; McGilvery, D.; Robertson, E. G. *J. Mol. Struct.* **1995**, *348*, 1–4.

(43) McNaughton, D.; Robertson, E. G.; Shanks, F. *Chem. Phys.* **1996**, *206*, 161–171.

(44) D'Amico, G.; Snels, M.; Hollenstein, H.; Quack, M. *Phys. Chem. Chem. Phys.* **2002**, *4*, 1531–1536.

(45) Giorgianni, S.; Gambi, A.; Baldacci, A.; De Lorenzi, A.; Ghersetti, S. *J. Mol. Spectrosc.* **1990**, *144*, 230–238.

(46) McNaughton, D.; McGilvery, D.; Robertson, E. G. *J. Chem. Soc. Faraday Trans.* **1994**, *90*, 1055–1071.

(47) Smith, K. M.; Duxbury, G.; Newnham, D. A.; Ballard, J. *J. Mol. Spectrosc.* **2002**, *212*, 6–16.

(48) Amrein, A.; Quack, M.; Schmitt, U. *Mol. Phys.* **1987**, *60*, 237–248.

(49) Dübal, H. R.; Quack, M. *Chem. Phys. Lett.* **1981**, *80*, 439–444.

(50) Albert, S.; Bauerecker, S.; Quack, M.; Steinlin, A. *Mol. Phys.* **2007**, *105*, 541–558.

(51) Albert, S.; Albert, K. K.; Quack, M. *J. Mol. Struct.* **2004**, *695−696*, 385–394.

(52) Snels, M.; Beil, A.; Hollenstein, H.; Quack, M.; Schmitt, U.; D'Amato, F. *J. Chem. Phys.* **1995**, *103*, 8846–53.

(53) Snels, M.; D'Amico, G.; Piccarreta, L.; Hollenstein, H.; Quack, M. *J. Mol. Spectrosc.* **2001**, *205*, 102–109.

(54) Hollenstein, H.; Quack, M.; Richard, E. *Chem. Phys. Lett.* **1994**, *222*, 176–184.

(55) Baldacci, A.; Giorgianni, S.; Stoppa, P.; De Lorenzi, A.; Ghersetti, S. *J. Mol. Spectrosc.* **1991**, *147*, 208–14.

(56) Chimdi, T.; Robertson, E. G.; Puskar, L.; Thompson, C. D.; Tobin, M. J.; McNaughton, D. *Chem. Phys. Lett.* **2008**, *465*, 203–206.

(57) Chimdi, T.; Robertson, E. G.; Puskar, L.; Thompson, C. D.; Tobin, M. J.; McNaughton, D. *J. Mol. Spectrosc.* **2008**, *251*, 256–260.

(58) Appadoo, D. T.; Robertson, E. G.; McNaughton, D. *J. Mol. Spectrosc.* **2003**, *217*, 96–104.

(59) McNaughton, D.; Robertson, E. G.; Evans, C. *Mikrochim. Acta* **1997**, *S14*, 543–546.

(60) McNaughton, D.; Evans, C. *J. Mol. Spectrosc.* **1997**, *182*, 342–349.

(61) Duxbury, G.; McPhail, M. J. W.; Smith, K. W.; Nivellini, G.; Tullini, F.; Celli, A. *J. Mol. Spectrosc.* **2000**, *199*, 13–17.

(62) Duxbury, G.; McPhail, M. J. W.; Smith, K. M.; et al. *J. Mol. Spectrosc.* **2000**, *199*, 13–17.

(63) Thompson, C. D.; Robertson, E. G.; Aleksic, I.; McNaughton, D. *J. Mol. Spectrosc.* **2005**, *230*, 133–138.

(64) McNaughton, D.; Aleksic, I.; Appadoo, D. T.; Thompson, C. D.; Robertson, E. G. *Vib. Spectrosc.* **2004**, *36*, 123–128.

(65) Thompson, C. D.; Robertson, E. G.; Evans, C.; McNaughton, D. *J. Mol. Spectrosc.* **2003**, *218*, 48–52.

(66) McNaughton, D.; Evans, C.; Robertson, E. G. *J. Chem. Soc. Faraday Trans.* **1995**, *91*, 1723–1728.

(67) Snels, M.; D'Amico, G. *J. Mol. Spectrosc.* **2003**, *221*, 156–162.

(68) Xu, L. H.; Andrews, A. M.; Cavanagh, R. R.; et al. *J. Phys. Chem. A* **1997**, *101*, 2288–2297.

(69) Ward, K. M.; Duxbury, G.; Lorono, M.; Henze, W.; Davies, P. B.; Newnham, D. A. *J. Mol. Spectrosc.* **2000**, *204*, 268–274.

(70) Robertson, E. G.; Thompson, C. D.; Appadoo, D. T.; McNaughton, D. *Phys. Chem. Chem. Phys.* **2002**, *4*, 4849–4854.

(71) McNaughton, D.; Evans, C. *J. Phys. Chem.* **1996**, *100*, 8660–8664.

(72) di Lauro, C.; D'Amico, G.; Snels, M. *J. Mol. Spectrosc.* **2009**, *254*, 108–118.

(73) D'Amico, G.; Snels, M. *J. Mol. Spectrosc.* **2003**, *217*, 72–78.

(74) Snels, M.; D'Amico, G. *Eur. Phys. J., D* **2002**, *21*, 137–142.

(75) Baskakov, O. I.; Ilyushin, V. V.; Alekseev, E. A.; Bürger, H.; Pawelke, G. *J. Mol. Spectrosc.* **2000**, *202*, 285–292.

(76) McNaughton, D.; Evans, C. *Spectrochim. Acta* **1999**, *55*, 1177–1183.

(77) Hollenstein, H.; Quack, M.; Thöne, H. *J. Mol. Phys.* **1985**, *56*, 463–477.

(78) Gambi, A.; Stoppa, P.; Tamassia, F. *J. Mol. Spectrosc.* **2008**, *252*, 47–51.

(79) Stone, S. C.; Miller, C. C.; Philips, L. A.; Andrews, A. M.; Fraser, G. T.; Pate, B. H.; Xu, L. H. *J. Mol. Spectrosc.* **1995**, *174*, 297–318.

hot bands. Stoppa has simplified such spectra by synthesizing pure [81]Br and [79]Br isotopomers for CH_2BrF (see references in Table 1), thus removing one source of overlap in room temperature spectra. In order to reduce the congestion resulting from vibrational hot bands and the highly populated rotational levels, it is necessary to cool the sample as much as possible. Some of the early TDLAS was done by simply cooling an absorption cell.[18] The restriction of course is that the lowest possible temperature is near the freezing point of the gas under study and so simple cooling is often of limited use. By far the most popular methodology is to cool the sample via supersonic expansion in the manner first used by Smalley[80] and so achieve temperatures as low as a few degrees Kelvin for small molecules, depending on the carrier gas, backing pressure, expansion nozzle diameter, and pumping capacity. Herman et al. reviewed the whole field of high-resolution FT-IR spectroscopy of jet-cooled molecules in 2000[81] and some of the early studies on halocarbons and hydrohalocarbons and the instrumentation developed for the work is described in that review. Most FT-IR based work has been carried out by Quack's group, expanding the gases through a pinhole nozzle into a diffusion pumped vacuum chamber to intersect a single pass of the IR beam from a Bomem004 FT-IR system,[82] and by McNaughton's group, using a pinhole nozzle and cryopumped vacuum system containing an 11-pass optical arrangement connected to a Bruker HR120 system.[46] These systems typically achieve rotational temperatures of 20–50 K depending on the size of the molecule under study, with vibrational degrees of freedom also cooled but to a lesser extent. Figure 1(b) is of jet cooled $CBrClF_2$,[42] where a temperature of ∼40 K is achieved with significant reduction of structure in the wings of the transitions and no significant hot bands apparent in the spectrum. The group of Stoppa have recently coupled a pulsed slit jet expansion system to their diode laser systems and achieved temperatures of around 50 K for CF_3Br[26,27] and CF_3Cl.[19] With the recent developments in tunable quantum cascade lasers (QCL) for high-resolution spectroscopy, reviewed by Curl,[83] their usage is growing. Kelly et al.[24] have coupled a supersonic free jet system to a QCL in a recent study on CF_3Cl.

Although jet cooling provides exceedingly simplified spectra amenable to analysis, the restricted rotational quantum number range of observed transitions results in molecular constants that cannot necessarily simulate the spectrum at the higher temperatures of the atmosphere and the normal laboratory. A case in point is the ν_1 band of $C^{35}Cl_2F_2$. Giorgianni et al.[45] used a diode laser to record a spectrum of a natural abundance sample cooled to 200 K in order to simplify the structure and assigned a set of transitions that were strong at this temperature. In order to obtain a fit, they removed transitions that appeared heavily perturbed by Coriolis resonances. The subsequent fit provided a set of rotational constants that could correctly simulate only part of the spectrum at 200 K. We carried out a jet cooled study at 40 K[46] and assigned a set of low J transitions
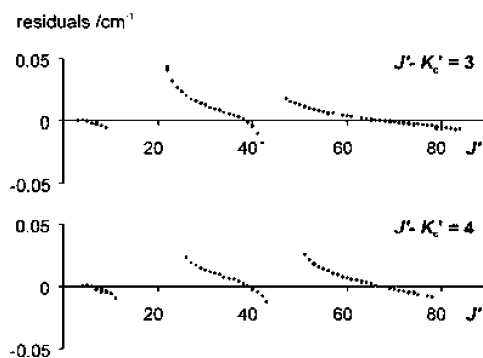

Figure 2. Residuals (observed − calculated) versus rotational quantum numbers for an effective fit without Coriolis interactions of ν_1 fundamental transitions in $C^{35}Cl_2F_2$ (from unpublished analysis in progress).

containing none of those measured by Giorgianni et al. but less affected by resonances. This data could only simulate the spectrum correctly at very low temperatures. Figure 2, showing some data for this band from an analysis that is in progress, illustrates the problem caused by the Coriolis perturbations. The first part of the range (up to $J = 20$) covers the transitions assigned from the jet-cooled spectrum. The second part ($J = 25-45$) corresponds to those transitions from the diode laser spectrum included in the first analysis. The final set of transitions ($J > 45$) were excluded from both reported fits and hence neither study could achieve the desired outcome. The use of molecular constants from incomplete analyses such as these would result in inaccurate simulations at typical atmospheric temperatures and thereby compromise the ability to determine atmospheric concentrations.

Such problems require greater control over the range of experimental temperatures than that provided by static cooling cells or jet expansions, and such a cell has been developed by Bauerecker et al.[84] and coupled to a TDLAS system and FT-IR spectrometer. Bauerecker's multipass cell allows for enclosive flow cooling or collisional cooling at temperatures between 4 and 400 K and in enclosive flow mode allows for cooling below the normal freezing point of samples. We built a simple dual pass system of similar design and used it to simplify the spectra of a range of halocarbons.[38–40,56,58,64–66] Figure 3 shows one such example, CF_3CH_2F, and illustrates the benefits of being able to analyze spectra measured at a range of different temperatures to maximize the set of assignable transitions. More recently we have, in collaboration with Bauerecker, built a full multipass system and have coupled it to the high-resolution Bruker HR125 spectrometer on the infrared beamline of the Australian synchrotron. The group of Quack have also coupled a Bauerecker cell to a high-resolution FT-IR instrument and have used it recently to obtain spectra of $CHCl_2F$.[50]

REVIEW OF ANALYSIS TECHNIQUES

For molecules such as the fluorocarbons where successful simulation of the spectrum from molecular constants is desired, it is essential to assign and fit all the features in a spectrum, recognizing and treating all perturbations. The many thousands of individual rotational lines in a single vibrational band present

(80) Smalley, R. E.; Wharton, L.; Levy, D. H. *Acc. Chem. Res.* **1977**, *10*, 139–145.
(81) Herman, M.; Georges, R.; Hepp, M.; Hurtmans, D. *Int. Rev. Phys. Chem.* **2000**, *19*, 277–325.
(82) Èbal, H. R.; Quack, M.; Schmitt, U. *Chimia* **1984**, *38*, 438.
(83) Curl, R. F.; Capasso, F.; Gmachl, C.; Kosterev, A. A.; McManus, B.; Lewicki, R.; Pusharsky, M.; Wysocki, G.; Tittel, F. K. *Chem. Phys. Lett.* **2010**, *487*, 1–18.
(84) Bauerecker, S.; Taraschewski, M.; Weitkamp, C.; Cammenga, H. K. *Rev. Sci. Instrum.* **2001**, *72*, 3946–3955.
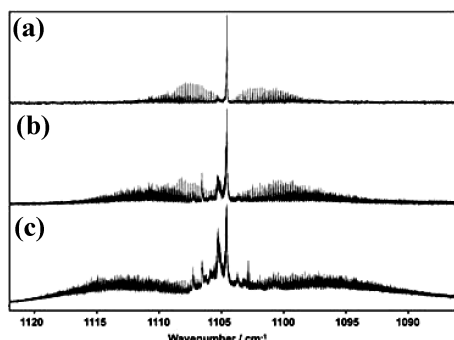
Figure 3. (a) Jet cooled spectrum of CF_3CH_2F at ~65 K; (b) collisional cooled spectrum of CF_3CH_2F ~150 K; (c) room temperature spectrum of CF_3CH_2F. Reproduced with permission from ref 65. Copyright 2003 Elsevier.

a challenge in initial assignment and this is achieved by utilizing computer assisted methods based primarily on Loomis−Wood plots.[85] In its original graphical interface mode on either a PC[86] or Mac,[87] the Loomis−Wood technique treated the spectrum as that of a linear molecule where the line spacings of the P and R branches are approximately 2 times the rotational constant B and the line positions can be fitted by a polynomial expansion of a running variable that is related to the rotational angular quantum number J, where the coefficients are related to the molecular constants. The technique uses a peaklist, containing position and intensity information, generated from the spectrum and replots the spectrum in rows of adjacent sections one under another where the successive section widths are a function of the polynomial coefficients. For a hypothetical linear molecule with the B rotational constant the same in the upper and lower energy states and no centrifugal distortion, each section would be $2B$ wide and the related transitions would appear as a perfect vertical line on the plot. Peaks can then be selected, ground state combination differences automatically calculated to check assignments, and the assigned lines fitted with an appropriate Hamiltonian. Any perturbations in the spectrum (such as those in Figure 2) are readily recognized in the Loomis plots and the technique is readily adapted to symmetric tops. Even asymmetric tops have branches of lines with almost equivalent line spacings that slowly change with quantum number so the original programs are also useful for the assignment of asymmetric top molecules, as shown in Figure 4a where a MacLoomis plot of the P branch of the ν_2 band of $CHClF_2$ in natural abundance is shown. Intense K_a subbands are easily observed. Recently, new versions[88−90] have appeared with extended capabilities that are designed to allow the assignment of almost any molecule and provide direct input into fitting and simulation programs such as Pickett's SPFIT and SPCAT.[91]

Figure 4. Macloomis plots of (a) the observed ν_2 spectrum of $CHClF_2$ with cold sub-bands of the $CH^{35}ClF_2$ species highlighted and (b) the resultant spectrum after SASSI of the cold bands of both isotopic species showing features. Lines associated with the $2_0^1 9_1^1$ and $2_0^1 6_1^1$ hotbands can mostly be seen in (b) the resultant spectrum. Reproduced with permission from ref 39. Copyright 2003 Royal Society of Chemistry.

The Loomis plot allows the assignment of regularly spaced series of transitions based on visual pattern recognition through a graphical interface and is extremely useful for assigning well resolved and/or prominent spectral transitions. However, with the reduction of the spectrum to a list of peaks, some information is invariably lost, e.g., when shoulder or coincident peaks are not detected as separate features and numerous weak peaks from hot bands or low-abundance isotopomers become essentially a noisy background in the graphical plot. When a weak band is obscured or overlapped by a stronger one, the reduction in distinct peaks associated with the weaker band in the graphical plot may also prevent recognition of the pattern of its regularly spaced lines and reduce the possibility of successful rovibrational assignments. The information extracted from high-resolution IR spectra may be enhanced by digitally subtracting contributions from one or more components, obtained through simulation of their rovibrational structure, an approach we have named spectral assignment by simulated spectral intensities (SASSI). With a simple molecule like ClSN,[92] SASSI allowed seven different spectral contributions from three different isotopomers and four hot bands to be extracted and assigned. Its application to the ν_2 (1313.1 cm^{-1}) and ν_7 (1351.7 cm^{-1}) bands of $CHClF_2$[39] led to rovibrational line assignments for less intense and overlapping features. The number of transitions assigned to the fundamental bands of the two chlorine isotopomers increased from 9 217 to 15 695 with a greater range of rotational quantum numbers than found in a previous study, and three hotbands otherwise completely obscured in the observed spectrum were assigned. Figure 5c shows a section of the spectrum that results from subtracting a

(85) Loomis, F. W.; Wood, R. W. *Phys. Rev.* **1928**, *32*, 223.
(86) Winnewisser, B. P.; Reinstaedtler, J.; Yamada, K. M. T.; Behrend, J. *J. Mol. Spectrosc.* **1989**, *136*, 12–16.
(87) McNaughton, D.; McGilvery, D.; Shanks, F. *J. Mol. Spectrosc.* **1991**, *149*, 458–73.
(88) Medvedev, I. R.; Winnewisser, M.; Winnewisser, B. P.; De Lucia, F. C.; Herbst, E. *J. Mol. Struct.* **2005**, *742*, 229–236.
(89) Lodyga, W.; Kreglewski, M.; Pracna, P.; Urban, S. *J. Mol. Spectrosc.* **2007**, *243*, 182–188.
(90) Tasinato, N.; Pietropolli Charmet, A.; Stoppa, P. *J. Mol. Spectrosc.* **2007**, *243*, 148–154.
(91) Pickett, H. M. *J. Mol. Spectrosc.* **1991**, *148*, 371–377.

(92) Robertson, E. G.; McNaughton, D. *J. Mol. Spectrosc.* **2006**, *238*, 56–63.
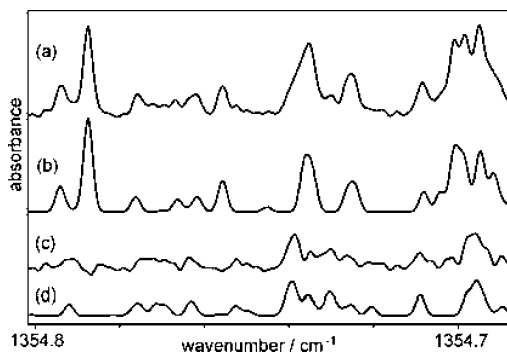
Figure 5. (a) Expanded high-resolution FT-IR spectrum of the ν_7 band of CHClF$_2$, together with (b) a simulation of the dominant CH^{35}ClF$_2$ component, (c) the resultant spectrum after the CH^{35}ClF$_2$ component has been subtracted, and (d) a CH^{37}ClF$_2$ simulation. Simulations are based on experimentally derived spectroscopic parameters from ref 39.

simulated CH^{35}ClF$_2$ spectrum (Figure 5b) from the original (Figure 5a). Comparison of the resultant spectrum (Figure 5c) with a simulated CH^{37}ClF$_2$ spectrum (Figure 5d) reveals how the CH^{37}ClF$_2$ peaks that were completely obscured in the raw experimental spectrum are effectively exposed. Subsequent subtraction of the CH^{37}ClF$_2$ features allowed us to assign the remaining structure belonging to hot bands and eventually simulate successfully both full bands. The MacLoomis plot of Figure 4 shows the power of the SASSI approach where in Figure 4b the strong lines of ν_2 for both chlorine isotopes of CHClF$_2$ have been subtracted out prior to peak-picking and subsequent analysis. The lines that now emerge are due to hot bands that comprise some 17% of the total intensity of the band. The low K_a structure of one of the 3 hot bands assigned, $2_0^1 9_1^1$, is highlighted.

Successful simulation and indeed SASSI analysis of a whole spectral band depends also on ascertaining and fitting all Coriolis and anharmonic (e.g., Fermi) resonances. These may cause local avoided crossings such as those evident in Figure 2 as well as more global perturbations. Work on the Coriolis coupled ν_3 and ν_8 band system of CHClF$_2$[40] provides an excellent example of how the full gamut of MacLoomis, collisional cooled spectra (150 K), room temperature spectra, and SASSI are required to reach a successful assignment and simulation. In order to assign, fit, and simulate the complete band, it was necessary to include two "dark" states that perturb three different parts of the spectrum in the procedure. Dark states are those for which no transitions would normally be observable and are usually weak combination bands. After final SASSI subtraction, the interacting states and resonances shown in Figure 6 were all understood and assigned. A number of lines associated with the "dark" $3\nu_9$ state that appear with sufficient borrowed intensity were correctly simulated and assigned.

ANALYSIS OF R22 (CH^{37}ClF$_2$) ν_5

Chlorodifluoromethane (also known as HCFC-22, R22, Genetron 22, or Freon 22) is used in air conditioning applications as an alternative to the ozone depleting CFC-11 and CFC-12 molecules. R22 itself has an ozone depletion potential of 0.05 and a
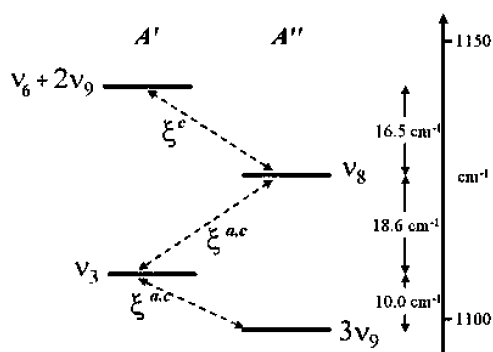

Figure 6. Energy level diagram showing the Coriolis resonance interactions between vibrational states of CH^{35}ClF$_2$.
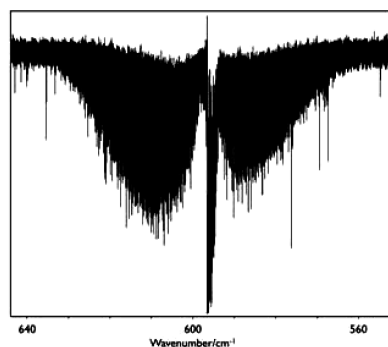

**Figure 7.** High-resolution FT-IR spectrum of the ν_5 band of CHClF$_2$.
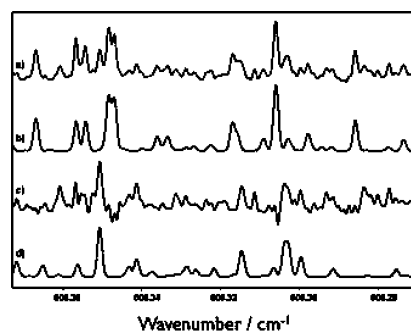
Figure 8. (a) Expanded spectrum of the ν_5 band of CHClF$_2$, together with (b) a CH^{35}ClF$_2$ simulation, (c) the resultant spectrum after the CH^{35}ClF$_2$ component has been subtracted, and (d) a CH^{37}ClF$_2$ simulation. Simulations are based on the spectroscopic parameters in Table 2, with μ_a^2/μ_c^2 of 0.38:1, the Herman Wallis factor = −0.004 (coded 50013 in the Pickett program) for the ^{35}Cl species, T_{rot} = 300 K, and a Gaussian full width half-maximum line width of 0.0014 cm^{-1}.

global warming potential (GWP) of 1780[93] and as a consequence has been phased out in 2010. R22 is a near-prolate asymmetric top, which belongs to the C_s symmetry point group and has six vibrational modes with symmetry species of A' (A/C-type bands) and 3 modes of symmetry A'' (B-type bands). All nine bands have been extensively studied. Both experimental and *ab initio* vibrational assignments for R22 are summarized in the

(93) *Intergovernmental Panel on Climate Change/Technology and Economic Assessment Panel. Special Report on Safeguarding the Ozone Layer and the Global Climate System; Issues Related to Hydrofluorocarbons and Perfluorocarbons*; Cambridge University Press: Cambridge, U.K., 2006.

Table 2. Fitted Spectroscopic Constants (cm⁻¹) in Watson's *A*-Reduced *Iʳ* Hamiltonian for the ν_5 Band of CH³⁷ClF₂

constant	ground state, CH³⁷ClF₂[a]	ν_5, CH³⁵ClF₂[b,c]	ν_5, CH³⁷ClF₂[c]
band center		596.371 399 (5)	595.480 336 (19)
A	0.341 364 817	0.340 451 710 7(70)	0.340 418 743 (43)
B	0.157 347 146	0.162 142 8 (11)	0.157 344 03 (10)
C	0.114 474 126	0.116 983 64 (31)	0.114 465 388 (21)
$\Delta_J \times 10^6$	0.049 588 272	0.052 365 7 (23)	0.049 762 (38)
$\Delta_{JK} \times 10^6$	0.148 145 488	0.152 653 6 (70)	0.146 94 (13)
$\Delta_K \times 10^6$	0.171 658 755	0.161 257 (11)	0.169 396 (94)
$\delta_J \times 10^6$	0.013 769 993	0.014 741 86 (80)	0.013 802 (19)
$\delta_K \times 10^6$	0.162 488 411	0.166 429 (17)	0.161 83 (21)
$\Phi_J \times 10^{12}$	0.021 664 2	0.021 04 (47)	0.021 664 2[d]
$\Phi_{JK} \times 10^{12}$	0.347 106 3	0.376 (11)	0.347 106 3[d]
$\Phi_{KJ} \times 10^{12}$	−0.103 572 0	−0.178 (33)	−0.103 572 0[d]
$\Phi_K \times 10^{12}$	0.174 120 6	0.196 (23)	0.174 120 6[d]
$\varphi_J \times 10^{12}$	0.010 170 3	0.01050 (17)	0.010 170 3[d]
$\varphi_{JK} \times 10^{12}$	0.187 062 7	0.1961 (63)	0.187 062 7[d]
$\varphi_K \times 10^{12}$	3.148 177 2	3.152 (56)	3.148 177 2[d]
J_{max}		78	94
number trans.		7996[b]	3804
rms deviation/cm⁻¹			0.000 441
σ_{dev}			1.0996

[a] Ground state constants from ref 37. [b] ν_5, CH³⁵ClF₂ constants from ref 36 obtained from the fit to 7788 IR lines and 208 microwave lines. [c] The numbers in parentheses are 1 standard deviation according to the least-squares fit in units of the least significant figure quoted. [d] Sextic constants have been constrained to the ground state values.

works of Thompson et al.[38,39] and Gambi et al.[31] For the ν_5 (*A/C*-type band), Gambi et al.[31] and Klatt et al.[36] performed high-resolution FT-IR and microwave spectroscopic studies, respectively, of the dominant isotope, CH³⁵ClF₂. Gambi et al. reported that the large density of lines in the spectrum and the overlap with stronger absorptions coming from CH³⁵ClF₂ made the analysis of CH³⁷ClF₂ very difficult so that an assignment and analysis was not achieved. We have now succeeded in analyzing the CH³⁷ClF₂ band using the SASSI approach.

The experimental spectrum of the ν_5 band of CHClF₂ is shown in Figure 7, and a small section of this experimental spectrum is shown in Figure 8a. The excellent sets of constants provided for ν_5 of the ³⁵Cl species by Klatt et al.[36] and for the ground state by Kisiel et al.[37] were used to first predict line intensities and positions of the ³⁵Cl ν_5 band using SPCAT,[91] which were then convolved using a Gaussian line shape function of appropriate full width half height to simulate the spectrum, a small part of which is shown in Figure 8b. This spectrum was then subtracted from the experimental spectrum to obtain the new spectrum shown in Figure 8c where the ³⁷Cl species dominates. The optimum subtraction was achieved in an iterative fashion to determine the correct ratio of *A* and *C*-type components for subtraction and to determine the Herman Wallis factors[94] that severely affected the relative intensities of the *C*-type component. The resultant spectrum (a small section is shown in Figure 8c) was then peak picked and the data analyzed using MacLoomis.[87] The ground state constants of CH³⁷ClF₂[37] were used to calculate ground state combination differences and confirm the assignment and the assigned lines then fitted with Pickett's SPFIT program to obtain the constants of Table 2. There was no evidence of local avoided crossings or other resonance perturbations, and the derived constants are well determined and comparable in magnitude and sign with those of the ³⁵Cl species. The higher order centrifugal distortion constants were held to those of the ground state in the fit. Simulation of

the CH³⁷ClF₂ spectrum, shown in Figure 8d, shows much of the spectrum in Figure 8c is due to the CH³⁷ClF₂ fundamental. The remaining spectral features are due to hot bands. From the spectral simulations the dipole derivate ratio μ_a^2/μ_c^2 is 0.38:1 and the Herman Wallis factor = −0.004 for the ³⁵Cl species. No standard deviations are given because these parameters are merely those that result in the optimum spectral subtraction, and given the complex overlapping spectral bands that constitute the spectrum, such an exercise can only produce approximate answers. Now that both isotopic species have been assigned and simulated, a complete analysis of the intensities to derive accurate Herman Wallis factors should be possible leading to analysis of the more intense hot band structure.

CONCLUSIONS

The experimental and analysis techniques required to obtain molecular constants of sufficient accuracy to provide simulated spectra of use in the quantification of atmospheric pollutant species using high-resolution infrared spectroscopy have been reviewed. Such constants, together with line intensity parameters, also provide an accurate basis for the prediction of band profiles for low-resolution atmospheric identification and quantification. The ν_5 band of chlorodifluoromethane in natural abundance has been recorded at an unapodized resolution of 0.000 96 cm⁻¹, analyzed using a Loomis−Wood based program and spectral assignment by simulated spectral intensities (SASSI) and fitted to produce a set of accurate molecular constants for CH³⁷ClF₂.

(94) Herman, R.; Wallis, R. F. *J. Chem. Phys.* **1955**, *23*, 637–646.

Chapter 4

Future Work

One major focus of future work in FIR high-resolution spectroscopy is expected to be centered around the development of new radiation sources. For the specific case of synchrotron based studies, the development of CSR techniques and traditional FIR edge emission will allow for the recording of pure rotational transitions in the THz region, which have traditionally been difficult to access. Since this region has only quite recently started to become more accessible, a wide range of molecules are still yet to be studied in this region. The recording of high J and K pure rotational transitions has been shown to be particularly important for studies involving perturbations to the ground state, such as that presented in the ketenimine publications.

While progress is always being made in terms of the interstellar identification of molecules, there are still vast catalogues of observed emissions which have yet to be assigned to specific molecular transitions. Not only is the hypothesizing of new molecules important, but the recording of their spectra is of course crucial in filling these gaps. The flow through, and enclosive flow cooling setups currently under development at the AS should allow for the recording of spectra of molecules which may only exist for very short lifetimes under terrestrial conditions. This is important since under interstellar conditions the same molecule may be stable and observable.

In terms of the ro-vibrational work presented in this thesis, the higher energy modes of ketenimine, 1-phosphapropyne and thiirane are mostly uncharacterized at high resolution. The characterization of the lowest energy modes of these molecules serves as a stepping stone, which will make the analysis of higher energy modes more certain, empirically

based and potentially simpler. The hot-bands and combination modes of the lowest energy modes affect the analysis of higher energy modes via their very presence and through Coriolis interactions, and a high accuracy set of molecular parameters of these based on experiment will allow these interactions to be more accurately modeled (as was shown in the ketenimine analysis). It is the author's belief that the complexity and interesting dynamics displayed, particularly in the interacting vibrational modes of ketenimine warrants further analysis, and that this investigation may lead to even more interesting and novel physics. This is only achievable through a detailed characterization of the lowest energy modes, and accurate modeling of their respective overtones should now be achievable.

Finally, this thesis lays a foundation for describing modes which are made observable purely by intensity stealing mechanics. The frequency of this effect appearing in the analyses presented here suggests that this mechanic may be important in accurately describing the ro-vibrational structure of other molecules which exhibit a high degree of Coriolis coupling. The effect the intensity stealing mechanic has on the observed spectra is subtle, and the identification and characterization presented in this thesis may be important in future ro-vibrational spectroscopic studies of a wide variety of molecules.